SYNTHESIS OF ZINC OXIDE FILMS AND NANOWIRES FOR NANOELECTRONICS APPLICATIONS

ONG WEI LI
(B.Eng.(Hons.), NUS)

A THESIS SUBMITTED

FOR THE DEGREE OF DOCTOR OF PHILOSOPHY

DEPARTMENT OF ELECTRICAL AND COMPUTER ENGINEERING

NATIONAL UNIVERSITY OF SINGAPORE

2012

DECLARATION

I hereby declare that this thesis is my original work and it has been written by me in its entirety. I have duly acknowledged all the sources of information which have been used in the thesis.

This thesis has also not been submitted for any degree in any university previously

Ong Wei Li
12 November 2012

Acknowledgements

First of all, I would like to express my deepest appreciation to Dr Ho Ghim Wei for giving me the chance to carry out my PhD studies under her supervision. She has been an excellent mentor who has displayed great patience and foresight, and her invaluable guidance and insightful suggestions has helped me a great deal during the course of my work.

I would also like to thank Mr Thomas Ang, the lab officer in charge of our lab. His high standards of lab safety and logistics have enabled me to carry out my work smoothly without any serious logistics issues.

My sincere thankfulness also goes out to my fellow colleagues: Dr Shweta, Kevin, Connor, Gah Hung, Franco, Ben and Minmin. You guys have made the time spent in lab enjoyable and also gave me a lot of ideas and insight during the many discussions that we had.

I would also like to thank Dr Andrew Wong and Dr Goutam from IMRE for their help and guidance in several of the characterisation needed in my work. I also wish to thank Prof Sow Chorng Haur from the Physics Department for giving me access to some of his equipment, Mr Chen for many of his logistical help and the numerous equipment parts I have borrowed from him, Sharon for her guidance and advice on the field emission studies, Zhihan for his insightful perspective of things and many interesting ideas for experiments, and Minrui for his valuable inputs during discussions with him and his help in several of my experiments carried out in Physics.

I would also like to thank some of the staff and students from CICFAR: Mrs Ho, Mr Koo, Linn Linn, Dr Huang Jinquan and Pi Can who have helped me greatly with regards to logistics and equipment issues, and also giving me advice and help during my PhD studies.

Finally, and most importantly, my profound gratitude goes to my family especially my wife for her patience and the immense love she has for me. Without her constant support, motivation and love, I would not have been able to finish this work. Thank you for everything.

Table of contents

Summary

Zinc oxide (ZnO) nanomaterials have received broad attention due to their excellent performance in electronics, optics and photonics. The synthesis of ZnO thin films has been an active field since the 1960s due to applications as sensors, transducers and catalysts. In the last few decades, the study of one-dimensional (1D) materials has attracted much interest due to the novel electrical, mechanical, chemical and optical properties introduced by surface and quantum confinement effects. However, to maximize the potential of ZnO in nanoelectronics applications, it is important to have control over the physical, chemical and electrical properties of ZnO nanostructures. Several issues regarding the development of ZnO for nanoelectronics have also arisen over the years.

The increasing emphasis on environmental protection has brought about a demand for a synthesis method that is environmentally friendly, requires low energy input, highly scalable and has low manufacturing costs. The doping of ZnO is also an issue that has received much attention. While a number of research groups have reported achieving p-type ZnO, there are still problems concerning the reproducibility of the results and the stability of the p-type conductivity. The development of high performance transparent and conformal electronic devices has become an important research focus in recent years owing to the demand for portable display, communication and various state-of-the-art electronics products. The accessibility to optically transparent and mechanically flexible electronic platforms is the key to next-generation electronic devices.

In this dissertation, ZnO films and nanowires were grown on rigid (silicon and c-sapphire) and flexible (polyethylene terephthalate (PET)) substrates via the low temperature, low cost and scalable hydrothermal method. This synthesis method

negates the need for ultra high vacuum systems that involve expensive multi-stage pumps and stainless steel chambers with high maintenance demands. The influence of growth parameters such as precursor concentration, addition of surfactant and growth duration on the synthesized nanostructures were investigated.

Ammonia plasma treatment was then applied to the films and nanowires to modify the electrical properties towards p-type conductivity. The plasma treatment was carried out without any additional heating of the sample, thus allowing plastic substrates with low melting point to be used. The duration of the plasma treatment was varied to study the effect of treatment duration on the electrical properties. Devices such as hydrogen gas sensors, P-N junctions and metal-oxide-semiconductor (MOS) capacitors were then fabricated to characterize and showcase the p-type properties of the plasma treated nanowires.

Flexible hydrogen gas sensors were fabricated from pristine ZnO nanowires on PET substrates and the gas sensing performance at room temperature was investigated. The flexible sensors proved to be robust and showed little deterioration in the sensing performance even in the bent state. The sensing performance was improved by decorating the nanowires with platinum (Pt) catalyst due to the catalytic dissociation of the hydrogen gas molecules by Pt.

Field emission properties of ZnO nanowires grown on PET substrates were also studied. Laser writing on photoresist was used to pattern the growth of ZnO nanowires bundles in a periodic array. The array spacing was varied to investigate the influence of screening effect on the field emission properties. An optimal spacing with the least screening effect from neighbouring emitters was determined. The feasibility and robustness of the flexible field emitters were also demonstrated.

List of Tables

List of Figures

Chapter 1 Introduction

A brief background of zinc oxide (ZnO) is presented here together with some basic properties of the metal oxide. Various synthesis methods for ZnO are described and the hydrothermal growth mechanism is explained. The theoretical background and literature review of p-type ZnO, hydrogen sensing and field emission of ZnO nanostructures will also be discussed. The organization of the thesis will be presented at the end of the chapter.

1.1 Background

ZnO is a promising semiconductor material which has attracted a large amount of attention in recent years. It has a wide bandgap of 3.37 eV and high exciton binding energy of 60meV at room temperature[1-3] which allow efficient exciton UV emission at room temperature under low excitation energy intensity. This also makes ZnO a suitable candidate for short wavelength optoelectronic applications[4] (UV and blue spectral range), for instance, in laser development. Other applications include solar cells,[5] chemical sensors,[6] nanogenerators[7] and field emitters.[8]

ZnO have potential applications in light-emitting diodes (LEDs) and lasing. Solid state lightings which make use of LEDs will allow reduced heat generation or parasitic energy dissipation. However, the application of ZnO to the development of LEDs is still an issue due to the lack of stable p-type doping due to self-compensation by donor-like native defects, low solubility of p-type dopants, and formation of deep acceptor levels.[9] Although successful p-type doping has been reported,[10-12] its reproducibility still remains a question.

Detection of gases such as hydrogen (H_2), oxygen (O_2), nitrogen dioxide (NO_2) and ammonia (NH_3) have been demonstrated where ZnO nanowires exhibited high sensitivity.[6] Gas sensing is based on a working mechanism where oxygen vacancy

sites found on the ZnO nanowire surface act as oxidation sites via adsorption of molecules such as O_2 and NO_2. As a result of the oxidation-adsorption mechanism, electrons are withdrawn from the conduction band resulting in a reduction of conductivity, which will be read as a signal for the gas by the sensor. ZnO nanostructures with high surface-to-volume ratios have been regarded as one of the most efficient methods for fabricating high efficiency gas sensors. A glucose sensor based on ZnO nanowires has also been reported.[13]

In addition, 1D ZnO nanostructures also show potential as excellent field emission materials due to their high mechanical stability, high aspect ratio, and negative electron affinity in various vacuum environments.[14] Although carbon nanotubes (CNTs) have attracted much attention due to their low turn-on fields and large emission currents,[15] oxide emitters are more stable in harsh environment and controllable in electrical properties.[16] Therefore, ZnO-based 1D nanostructure is an appropriate alternative to CNT for field emission devices.

1.2 Properties of ZnO

ZnO is a white powder that is insoluble in water, and is widely used as an additive in numerous materials and products including plastics, ceramics, glass, cement, lubricants, paints, ointments, adhesives, sealants, pigments, foods, batteries, ferrites, fire retardants, and first aid tapes. It is usually found in the wurtzite phase because it is the most stable phase at room temperature. Some of the basic physical properties of ZnO in bulk form is shown in Table 1.1. However, as ZnO shrinks to the nanoscale, some of these properties undergo changes due to quantum size effects.

Table 1.1. Physical property of Zinc Oxide

Property (Lattice parameters at 300 K)	**Value**
a_0	0.32495 nm
c_0	0.52069 nm
a_0/c_0	1.602
u	0.345
Density	5.606 gcm^{-3}
Stable phase at 300 K	Wurtzite
Melting point	1975 °C
Thermal conductivity	0.6, 1–1.2
Linear expansion coefficient (/C)	a_0: 6.5×10^{-6}
	c_0: 3.0×10^{-6}
Static dielectric constant	8.656
Refractive index	2.008, 2.029
Energy gap	3.4 eV, direct
Intrinsic carrier concentration	$<10^6$ cm^{-3}
Exciton binding energy	60 meV
Electron effective mass	0.24
Electron Hall mobility at 300 K for low n-type conductivity	200 $cm^2V^{-1}s^{-1}$
Hole effective mass	0.59
Hole Hall mobility at 300 K for low p-type conductivity	5–50 $cm^2V^{-1}s^{-1}$

1.3 Crystal structure of ZnO

ZnO has a hexagonal wurtzite structure with lattice parameters a = 0.3296 and c = 0.52065 nm. Its structure consists of alternating planes composed of tetrahedrally coordinated Zn^{2+} and O^{2-} ions. These ions are stacked alternately along the c-axis, hence resulting in a symmetric, yet non-central structure.[17] This also explains why ZnO has piezoelectric and pyroelectric properties. It is known that ZnO has polar facets and the most common polar surface is the basal plane. Positively charged Zn-(0001) surfaces and negatively charged O-(0001) surfaces are produced by the oppositely charged ions. This in turn produces a normal dipole moment and spontaneous polarization along the c-axis as well as a divergence in surface energy.[18]

In order to maintain a stable structure, the polar surfaces generally have facets or exhibit massive surface reconstructions, but ZnO±(0001) faces are exceptions: they are atomically flat, stable and without reconstruction. The other two most commonly observed facets for ZnO are (11-20) and (10-10). These facets are non-polar surfaces and have lower energy than the (0001) facets.

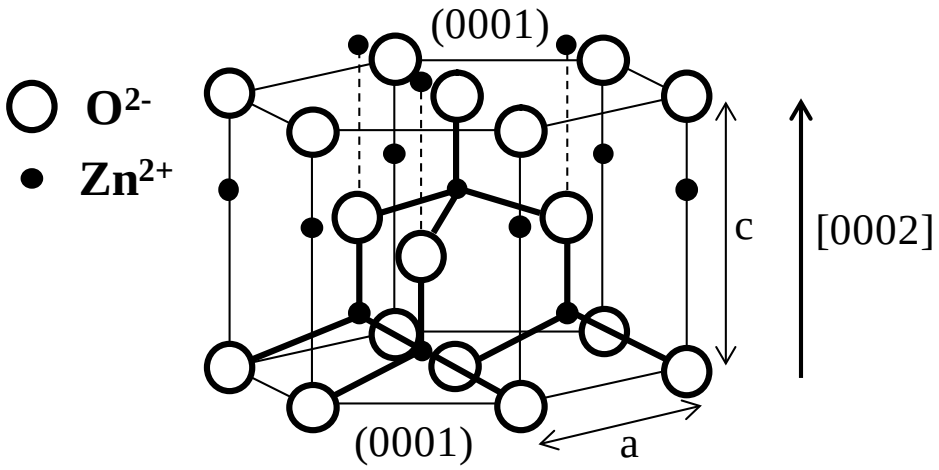

Figure 1.1. Wurtzite structure model of ZnO with tetrahedral coordination.

1.4 ZnO synthesis methods

ZnO nanostructures can be synthesized via a wide variety of methods, ranging from simple thermal evaporation to more complex state-of-the-art epitaxial growth techniques. Vapour phase transport methods such as thermal evaporation, MOCVD and MBE are commonly used. Electrochemical deposition and hydrothermal growth methods are also used. Some of these synthesis methods will be discussed in the following sections.

1.4.1 Molecular beam epitaxy (MBE)

Molecular beam epitaxy (MBE) is a complex evaporation process which takes place under ultra-high vacuum conditions (pressure $<10^{-10}$ Torr).[19] A schematic diagram of the MBE setup is shown in Figure 1.2. The Zn precursors are produced by heating the metallic Zn element until it evaporates while oxygen radicals are supplied

by a microwave plasma source. The vapours then condense onto the sapphire substrate to form ZnO.[20,21] The advantage of MBE is that it allows precise control over the thickness of ZnO produced. However, the process occurs at a very slow rate causing extremely low productivity. The equipments involved are also expensive which in turn increases the cost of the ZnO produced.

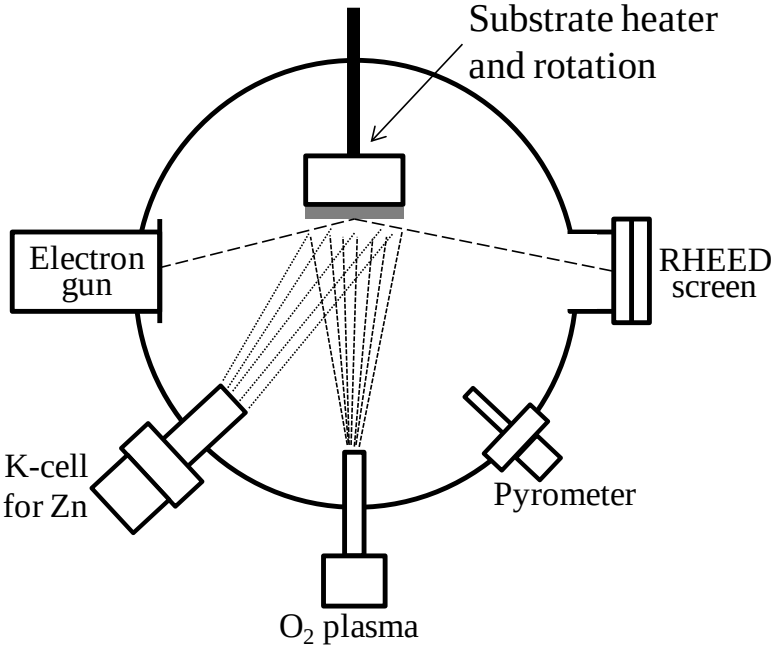

Figure 1.2. Schematic diagram of a MBE setup.

1.4.2 Metal-organic chemical vapour deposition (MOCVD)

Metal-organic chemical vapour deposition (MOCVD) takes place in a metal organic vapour-phase epitaxy (MOVPE) system using metal-organic precursors such as dimethlyzinc (DMZn) and diethyl zinc (DEZn) as the zinc source and nitrous oxide (N_2O) as the oxygen source.[22] The temperature required for the reaction to take place is around 200 to 500 °C. The carrier gas transports the reactants into the chamber where they decompose and react to form ZnO. The nitrous oxide decomposes to N_2 and an O atom, and then the O atoms react with DEZn to form diethoxyzinc (DEOZn), which decomposes to form dihydroxyzinc and ethylenes. Dihydroxyzinc then

dehydrates to form ZnO which deposits onto the substrate layer by layer. This method can be used to grow ZnO thin films and nanowires.[23]

$$N_2O \rightarrow N_2 + O \quad (1.1)$$

$$Zn(C_2H_5)_2 + 2O \rightarrow H_5C_2ZnOC_2H_5 + O \rightarrow Zn(OC_2H_5)_2 \quad (1.2)$$

$$Zn(OC_2H_5)_2 \rightarrow H_5C_2OZnOH + C_2H_4 \rightarrow Zn(OH)_2 + 2C_2H_4 \quad (1.3)$$

$$Zn(OH)_2 \rightarrow ZnO + H_2O \quad (1.4)$$

1.4.3 Thermal evaporation method

In the thermal evaporation method, powder source materials (e.g Zn[24] or ZnO and graphite[25]) are vaporized at elevated temperatures of 500 to 1000 ^oC[26,27] and the resultant vapours condense under certain conditions (temperature, pressure, atmosphere, substrate, etc) to form the desired ZnO nanostructures. The experimental parameters such as temperature, pressure, carrier gas (gas species and flow rate) and evaporation duration, can be manipulated to produce the desired nanostructures.[28] The synthesis is usually carried out in a tube furnace connected to a vacuum pump system and gas supply and control system as shown in Fig. 1.3.[29] In a typical synthesis process, the interior of the alumina tube is maintained at a certain pressure (e.g. 200 to 600 Torr) while vapours are produced from the heating of the ZnO powder placed at the center of the alumina tube. The carrier gas (Ar) which enters from the left end of the alumina tube then transports the vapours downstream towards the silicon (Si) substrate. The vapours condense and deposit ZnO on the Si substrate. The carrier gas is then pumped out at the right end of the tube. A wide variety of ZnO nanostructures can be grown using this method.[30]

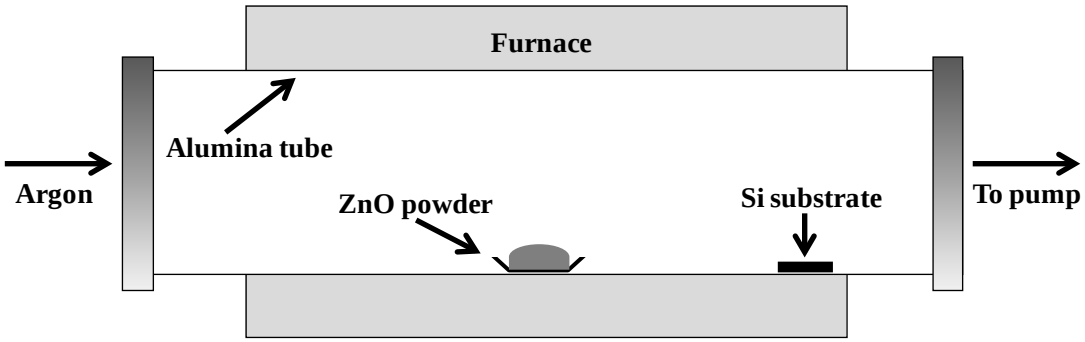

Figure 1.3. Schematic diagram of experimental apparatus for thermal evaporation process

1.4.4 Electrochemical deposition

A typical setup consists of 3 electrodes namely, a working electrode (cathode) which is the substrate (e.g. Au coated Si substrate), a counter electrode (e.g. 1 x 1 cm^2 platinum mesh) and a reference electrode which is a saturated calomel electrode (SCE). The three electrodes are placed into a beaker containing the electrolyte (e.g. zinc nitrate) and the beaker is immersed into a water bath with temperature being kept constant by a thermometer. The desired potential is applied on the working electrode and the reaction of interest occurs there. The counter electrode passes all the current needed to balance the current passing through the working electrode. The reference electrode is used only to measure potentials of working electrode. There is no current flow between the working and reference electrodes. The following reactions occur at the electrodes[31] and are illustrated in Fig. 1.4.

Dissociation: $Zn(NO_3)_2 \rightarrow Zn^{2+} + 2NO_3^-$ (1.5)

Hydrolysis: $NO_3^- + H_2O + 2e^- \rightarrow NO_2^- + 2OH^-$ (1.6)

Interaction of hydrated cation with OH- ions (reduction reactions at the cathode):

$Zn^{2+} + 2OH^- \leftrightarrow Zn(OH)_2$ (1.7)

Dehydration of the hydroxide: $Zn(OH)_2 \leftrightarrow ZnO + H_2O$ (1.8)

Reversible reactions (1.7) and (1.8) take place due to the higher solubility of ZnO. This intermediate step involving the formation of hydroxide ions due to the local

increase of pH, allows the growth of ZnO to occur under quasi-equilibrium conditions and produces high quality crystals. Thin film nanostructures are commonly grown via this process.[32-34]

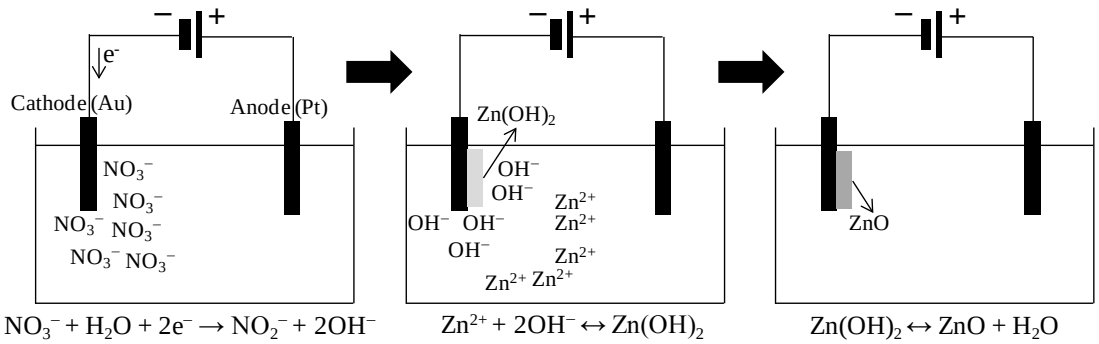

Figure 1.4. Schematic diagram of electrochemical deposition

1.4.5 Hydrothermal process

Hydrothermal processes are crystal growth from aqueous solutions under mild conditions at temperatures below 100 °C. The low process temperature makes it suitable for growth of ZnO nanostructures on plastic substrates such as polyethylene terephthalate (PET) which has a melting point of 250 °C. Generally, a base (e.g., KOH, NaOH, NH_4OH) is added to a zinc salt (e.g., $ZnCl_2$, $Zn(NO_3)_2$, $Zn(CH_3COO)_2$) to produce $Zn(OH)_2$ which dehydrates to ZnO at elevated temperatures in the hydrothermal vessel.[35-38] Hexamethylenetetramine (HMT) is also commonly used as a source of OH^- ions to form ZnO nanostructures with zinc nitrate.[39-47] The decomposition of HMT in solution produces OH^- ions with NH_4^+ as a buffer and gradually increases the pH of the growth solution.

Seeds are normally used as nucleation sites to define the orientation and direction of the crystal to be grown. ZnO colloids may be used as seeds in hydrothermal growth.[46] Alternatively, a buffer layer of ZnO can be deposited on the substrate by sputtering[48] or pulsed laser deposition (PLD).[49] The ionic compound of

Zn are dissolved in the solution to form Zn^{2+} ions. The Zn^{2+} ions would then react with the hydroxide ions from a base or HMT, and nucleate with the ZnO seed layer which acts as the growing site for the nanowires. Most of the compounds formed have low solubility which causes the formation of crystal structures due to super saturation. ZnO has the fastest growth rate along the [0002] direction, hence standing nanowires are usually obtained from the chemical reaction as shown in Figure 1.5. However, surfactants can be added to influence the growth habit of ZnO and modify the morphology of the products. Two surfactants will be used in this thesis, namely: trisodium citrate to promote coalescence of the ZnO film and polyethylenimine (PEI) to increase the aspect ratio of the nanowires. This method of synthesizing ZnO is highly cost effective as the equipments involved are simple, thus making it a cheap, non-toxic and low temperature synthesis method suitable for large-scale production.[45,50] The hydrothermal synthesis method will be used to synthesize the ZnO nanowires and film reported in this thesis and the growth mechanism will be described in detail in the next section.

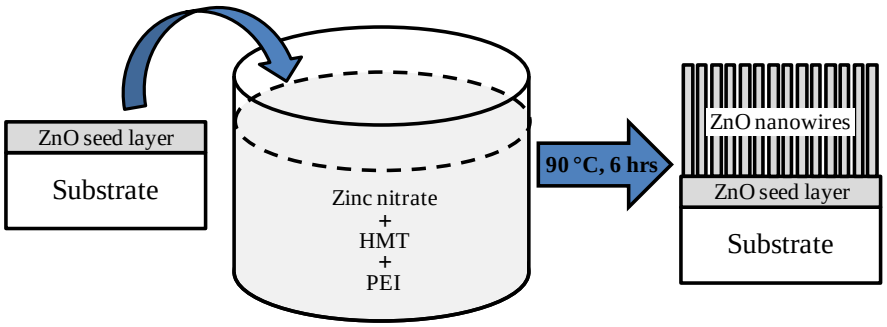

Figure 1.5. Schematic diagram of hydrothermal growth of nanowires.

1.5 Growth mechanism

Aqueous solution growth has been widely used to grow highly oriented ZnO nanowires and films. Andres-Verges *et al.*[51] reported the formation of ZnO rods in aqueous solutions containing zinc nitrate, zinc chloride and HMT for the first time in

1990. More than ten years later, Vayssieres *et al.*[52] used this method to grow nanorods on conducting glass and Si substrates using a seed layer. Several research groups have since then employed this method to synthesize various ZnO nanostructures and studied them in detail.[35-50,53,54] Fundamentally, solution systems containing Zn^{2+} ions as a zinc source are categorized into two main cases: an alkaline solution system with NH_3 or NaOH and a HMT solution system. The degree of the supersaturation, which is associated with the driving force of crystallization and growth of ZnO, is tuned by varying the pH of the chemical systems.

1.5.1 Hydrothermal ZnO films

ZnO films were synthesized from an aqueous solution of zinc nitrate, ammonium hydroxide and trisodium citrate. This procedure was first rigorously studied and documented by Lange *et al.*[55] as early as 2003. Zinc nitrate was dissolved in deionised (DI) water and dissociated to form Zn^{2+} ions:

$$Zn(NO_3)_2 \rightarrow Zn^{2+} + 2NO_3^- \quad (1.9)$$

The ammonium hydroxide solution containing NH_4^+ and OH^- ions is added to the zinc nitrate solution:

$$NH_4OH \leftrightarrow NH_4^+ + OH^- \quad (1.10)$$

The OH^- ions in the growth solution combines with the Zn^{2+} ions to form $Zn(OH)_2$ which then decomposes into zinc oxide.

$$Zn^{2+} + 2OH^- \leftrightarrow Zn(OH)_2 \quad (1.11)$$

$$Zn(OH)_2 \rightarrow ZnO + H_2O \quad (1.12)$$

The formation of ZnO crystals is determined by the supersaturation of the solution system which can be quantified by the supersaturation ratio:

$$S = C/C^* \quad (1.13)$$

where C is the concentration of Zn^{2+} ions present in the solution and C* is the solubility concentration of Zn. The system is supersaturated when S > 1, and no nucleation occurs when S≤ 1. When S is much greater than 1, the concentration of Zn^{2+} ions will be much higher than the solubility of Zn. In this case, most of the ZnO will precipitate out of the solution phase as ZnO powder in the growth solution and only some will be able to crystallize on the substrate. When S is slightly greater than 1, the concentration of Zn^{2+} ions will be slightly higher than the solubility of Zn. Most of the ZnO will be able to crystallize on the substrate and only some will form ZnO powder in the growth solution.

The solubility of the zinc complexes can be controlled by the pH value of the solution which is determined by the amount of ammonium hydroxide added to the solution. Calculations by Richardson *et al.*[56] has revealed that in the presence of NH_3 and OH^-, the solubility decreases with increasing temperature. This explains why supersaturation is only established when the solution is heated.[56] A large drop in solubility is also observed at higher concentrations of NH_3 when the pH of the solution is between 10 and 11. It is also noted that the presence of NH_3 in the solution is very important because without it, the solubility of zinc does not change considerably with temperature.

Trisodium citrate is added as a surfactant to encourage coalescence of the ZnO crystals to form smooth films. The negatively charged citrate ions adhere to the positively charged Zn-terminated (0001) plane, thus retarding the growth in the [0002] direction (c-direction), causing the lateral growth to be more pronounced.[50] For the formation of ZnO films, the substrate is sputtered with a ZnO seed layer which acts as a pre-oriented layer on the substrate for the nucleation and growth of the ZnO film with preferred c-direction alignment. As the nanowires start to grow, the increased

steric hindrance posed by the laterally expanding nanowires (due to the action of the citrate anions) served as a means by which nanowires with c-axis orientation parallel to the substrate normal were allowed to grow continuously, while misaligned nanowires collided with their neighbours, resulting in the termination of growth.[57,58] Over time, the nanowires grow large enough in size to coalesce with neighbouring nanowires and forms a single crystal film consisting of coalesced columnar single crystal nanowires.

1.5.2 Hydrothermal ZnO nanowires

For the synthesis of ZnO nanowires, the simple recipe involving zinc nitrate and HMT as precursors for the growth was used. Zinc nitrate provides the Zn^{2+} ions required for the synthesis of the ZnO nanowires, while HMT acts like a weak base and pH buffer.[54] Unlike the system involving zinc nitrate and ammonium hydroxide, the pH of the growth solution is not controlled directly. When the growth solution is heated, HMT hydrolyzes in water and gradually produced formaldehyde (HCHO) and ammonia (NH_3):

$$(CH_2)_6N_4 + 6\ H_2O \leftrightarrow 4\ NH_3 + 6\ HCHO \qquad (1.14)$$

The ammonia then decomposes in solution to form OH^- ions:

$$NH_3 + H_2O \rightarrow NH_3{\cdot}H_2O \qquad (1.15)$$

$$NH_3{\cdot}H_2O \leftrightarrow NH_4^+ + OH^- \qquad (1.16)$$

This is critical in the synthesis process because if HMT hydrolyzed very quickly and produced a large amount of OH^- ions in a short period of time, a high pH environment will be created in the growth solution. The Zn^{2+} ions in the solution would then react with the large amount of OH^- ions available and precipitate out quickly. This would result in a fast consumption of the precursors and affect the oriented growth of ZnO nanowires.[59] Real time measurements carried out by Ashfold *et al.*[59] revealed that the

pH of the growth solution lies betweeen 5.5 and 5.6 when heated. The Zn^{2+} ions from the dissociated zinc nitrate solution then reacts with the OH^- ions to form $Zn(OH)_2$ which undergo a condensation reaction to form a water molecule and solid ZnO:

$$Zn^{2+} + 2OH^- \leftrightarrow Zn(OH)_2 \quad (1.17)$$

$$Zn(OH)_2 \rightarrow ZnO + H_2O \quad (1.18)$$

During the hydrothermal growth process, $Zn(OH)_2$ dissolves with increasing temperature to form Zn^{2+} and OH^-. However, when the concentrations of Zn^{2+} and OH^- reach the critical supersaturation value, $Zn(OH)_2$ forms spontaneously in the aqueous complex solution and go on to dehydrate into ZnO.[60] In this supersaturated solution, ZnO begins to nucleate on the substrate sputtered with a ZnO seed layer which acts as a pre-oriented layer for the nucleation and growth of the ZnO nanowires with preferred c-direction alignment. The Zn- and O-terminated (0001) surfaces of wurtzite ZnO nanostructures grown along the c-axis direction are high energy polar surfaces.[61] Therefore, when a ZnO nucleus is newly formed, owing to the high energy of the polar surfaces, the incoming precursor molecules tend to adsorb favourably on the polar surfaces. This leads to a fast growth along the [0001] direction, forming ZnO nanowires.

PEI is added as a surfactant to improve the aspect ratio of the nanowires. The PEI molecules attach to the sides ({10-10} planes) of the ZnO nanowires, restricting the lateral growth. This causes the upward growth rate to be faster than the sideward growth rate, thus increasing the aspect ratio of ZnO crystals to form nanowires.

1.6 P-type doping of ZnO

ZnO nanostructures are intrinsically n-type and it is widely accepted that the intrinsic n-type is due to oxygen vacancies[62] and zinc interstials.[63] However, p-type ZnO is important for applications such as optoelectronics devices and homojunction

PN junctions for purposes such as light emitting diodes (LEDs), and they can be obtained via doping or growing in an oxygen rich environment.[64] It is proposed that the p-type behaviour is due to zinc vacancy,[65] oxygen interstitials[66] and oxygen antisite.[67] There has been work carried out to synthesize p-type ZnO nanowires[68] but reproducibility has been a problem. Non-reproducible and non-uniform doping often occurs due to limited access of dopants in the nanoscale structure. Other issues reported are unstable doping due to self-compensating doping, low dopant solubility and complex doping procedures. Recently, p-type conduction was observed in phosphorus-doped ZnO nanowire arrays,[68] however they switched to n-type after two months storage in an ambient environment.

There are two groups of possible candidates for p-type dopants: Group I elements which substitute Zn atoms and the group V elements which substitute the O atoms. The known acceptors in ZnO include group-I elements such as lithium (Li),[69-71] sodium (Na),[72] potassium (K),[73] copper (Cu),[74] silver (Ag),[75] and group-V elements such as nitrogen (N),[76] phosphorous (P),[68] and arsenic (As).[77] However, many of these form deep acceptors and do not contribute significantly to p-type conduction. It is believed that the most promising dopants for p-type ZnO are the group-V elements, although theory suggests some difficulty in achieving shallow acceptor level.[78] Among the acceptor impurities that substitute oxygen in ZnO, nitrogen is thought to be the most suitable p-type dopant due to both atomic-size and electronic-structure considerations. The nitrogen atom is the closest in atomic size to oxygen, therefore, it is expected to cause minimum strain in ZnO. The energy of the valence 2p states and the electronegativity of nitrogen are also the closest to those of the oxygen atom, particularly when compared with other group-V dopants.[79] Several groups have reported on the incorporation of nitrogen in ZnO, and many have claimed that

nitrogen substitutes for O;[80-89] however, the reports on p-type conductivity in nitrogen-doped ZnO still remain controversial.

Nitrogen is a shallow acceptor in other II–VI semiconductors[90] and has been considered as a suitable p-type dopant for ZnO for some time.[91] In recent years, considerable efforts have been made to create p-type ZnO using N as an acceptor dopant.[78,80,81,85,92-99] Minegishi *et al.*[80] reported p-type doping of ZnO films grown on sapphire (0001) by chemical vapour deposition at 650 to 800 °C, using NH_3 as the nitrogen source. They reported a carrier concentration of 1.5 x 10^{16} cm^{-3} with an estimated ionization energy of 100 meV, resistivity of 34 Ωcm and Hall mobility of 12 cm^2 $V^{-1}s^{-1}$. The authors also pointed out that hydrogen may play a role in the nitrogen incorporation, and that the appropriate growth/annealing conditions for obtaining p-type material are limited to such a narrow range that control turns out to be very difficult. Guo *et al.*[85] reported the growth of LED structures with nitrogen-doped ZnO films using plasma-enhanced laser deposition. The films were grown on n-type ZnO single crystal wafers at 390 °C, using N_2O as the nitrogen source in the N-doped ZnO layer. Four-probe van der Pauw measurements showed a relatively high resistivity of 100 to 200 Ωcm and a hole concentration of 4 x 10^{15} cm^{-3}, which led Guo *et al.* to suggest that N introduces a relatively deep level in ZnO. The observed bluish emission observed in the electroluminescence measurements by Guo *et al.* is consistent with sub-band-gap recombinations. Huang *et al.*[99] also tried to synthesize nitrogen-doped ZnO films by direct circuit reactive magnetron sputtering at 450 °C, using NH_3 gas as the dopant source. Oxygen and ammonia gases were introduced into the chamber in varying ratios of NH_3/O_2 from 0:1 to 3:2 to produce films with different levels of nitrogen-doping. The hole carrier concentrations increased from 1.14 x 10^{14} to 8.02 x 10^{18} cm^{-3} while the Hall mobility decreased from 4.1 to 0.802

cm^2/Vs and the resistivity decreased from 1.1 x 10^4 to 0.97 Ωcm. Nitrogen-doped p-type ZnO films were grown by Look *et al*.[81] using MBE at 525 °C. Pure (99.99995 %) Zn was supplied by means of a solid-source dual-zone effusion cell, and O and N were obtained from research-grade O_2 and N_2, respectively, flowing through a radio-frequency (RF) plasma source, operated at a power of 350 W. From the Hall effect measurements, the resistivity of the film was 40 Ωcm, hole mobility of 2 cm^2/Vs and hole concentration of 9 x 10^{16} cm^{-3}.

1.7 Hydrogen gas sensing

Metal oxide semiconductor (MOS) devices are commonly used in the fabrication of gas sensors. It was first discovered decades ago that the interaction of gas molecules with the semiconductor surfaces could influence the surface properties such as conductivity and surface potential. The first chemoresistive semiconductor gas sensors were reported by Seiyama in 1962.[100] From then on, metal oxide semiconductors have been widely studied for gas sensing applications due to the low cost and relative simplicity. Metal oxides also possess a wide range of physical, chemical and electrical properties that are sensitive to the changes in the chemical environment. Due to these properties, metal oxides have become one the most popular commercial sensors. Numerous materials have been reported to be suitable for metal oxide sensors including ZnO, SnO_2, WO_3, TiO_2 and Fe_2O_3.[101]

Oxygen vacancies on metal oxide surfaces such as ZnO are electrically and chemically active. These vacancies function as n-type donors, often significantly increasing the conductivity of the oxide. When the metal oxide is exposed to air, O_2 molecules adsorb at the vacancy sites and trap electrons from the surface of the metal oxide. Electrons are effectively depleted from the conduction band, leading to a

reduced conductivity of the n-type oxide. The process can be represented by the following equations:[102,103]

$$O_2(g) \rightarrow O_2(ad) \quad (1.19)$$

$$O_2(ad) + e^- \rightarrow O_2^-(ad) \quad (1.20)$$

$$O_2^-(ad) + e^- \rightarrow 2O^-(ad) \quad (1.21)$$

$$O^-(ad) + e^- \rightarrow O^{2-}(ad) \quad (1.22)$$

In these surface reactions, (g) and (ads) stands for free gas and species adsorbed on the surface respectively. It is noted that equations (1.19) to (1.22) occur at increasing temperatures, where O_2^- (ad) is the major oxygen species below 150 °C, O^-(ad) plays the major role in the range of 150 °C to 450 °C and O^{2-}(ad) becomes dominant when the temperature is above 450 °C.[102,104] Metal oxide gas sensors are commonly operated at elevated temperatures (250 to 500 °C) in order to enhance the chemical reactivity between the metal oxide and the analyte gases, primarily due to the formation of oxygen anions at these temperatures as discussed above.

When the metal oxide gas sensor is exposed to reducing gases such as CO and H_2, the incoming gas molecules would react with the surface adsorbed oxygen and consequently remove it, releasing the trapped electrons back into the conduction band. This leads to an increase in conductivity of the metal oxide. Most metal oxide gas sensors operate based on this principle.

$$2H_2(g) + O_2^-(ad) \rightarrow 2H_2O + e^- \quad (1.23)$$

The response of p-type ZnO is the opposite of n-type ZnO nanostructures because the major carriers are now holes instead of electrons. When p-type ZnO is exposed to hydrogen gas, the conductance decreases and exposing it to air causes the conductance to increase. The different variation in the conductance of n-type and p-type ZnO nanowires towards hydrogen gas and air can be attributed to the adsorption

of oxygen on the nanowire surfaces. The adsorbed oxygen molecules would attract electrons from ZnO nanowires, leading to reduced electron density in n-type ZnO nanowires but increased hole density in p-type nanowires.[105]

ZnO nanostructures have been widely used for sensing applications because of their high sensitivity to the chemical environment. Bulk and thin films of ZnO have been proposed for CO,[106] NH_3,[107] alcohol[108] and H_2[109] sensing. However, from the aspect of sensing performance, 1D ZnO nanostructures such as nanowires are expected to be superior to its thin film counterpart.[110] This is because 1D nanostructures have a large surface-to-volume ratio, which means a significant fraction of the atoms in such systems are surface atoms that can participate in surface reactions, resulting in high sensitivity to species adsorbed on the surfaces. Moreover, ZnO nanowires can be configured as two terminal sensing devices or FETs in which a transverse electric field can be utilized to tune the sensing property.[111] In addition, the diameters of the nanowires are small and comparable to the Debye length, hence chemisorption induced surface states can effectively affect the electronic structure of the entire channel, thus making 1D ZnO nanostructures more sensitive than thin film.

When the diameter of the ZnO nanowires is much larger than the Debye length λ_D (~ 30 nm for ZnO),[102,110,112,113] only the atoms in the space-charge region can participate in surface reactions, thus atoms in the core of ZnO crystals are not involved in the sensing of the analyte gas. However, when the diameter of the nanowires is similar or smaller than the Debye length of ZnO, the sensitivity of the ZnO should increase dramatically. With reducing diameter, the surface/volume ratio increases; and when the size of the wires is close to or even smaller than the Debye length, the whole wire can be treated as a surface.

Rao and co-workers[114] have synthesized ZnO nanostructures with different routes and studied the H_2 sensing property. ZnO nanorods with 30 - 40 nm diameters and 600 - 800 nm lengths were synthesized by a hydrothermal route, while ZnO nanowires with diameters of 20 - 30 nm and lengths of 1 - 2 μm were prepared by an electrodeposition method. At a working temperature of 150 ºC, the ZnO nanorods showed a sensitivity of 32 towards 1000 ppm of H_2 while the ZnO nanowires showed a sensitivity around 40. The sensitivity was calculated by:

$$\text{Sensitivity} = R_{air}/R_{gas} \quad (1.24)$$

where R_{air} is the resistance of the sensor in dry air and R_{gas} is the resistance in the test gas.

ZnO nanowires with a very high aspect ratio of more than 250 were synthesized by Kang *et al.*[115] via thermal chemical vapor deposition (CVD) on vertical nanowires grown by hydrothermal growth (HG). The synthesized ZnO nanowires displayed a sensitivity of 72 % and response time as fast as 30 s towards 10,000 ppm of H_2 at 200 °C. The sensitivity of the gas sensor in this case was calculated by:

$$\text{Sensitivity (\%)} = (R_{air} - R_{gas})/R_{air} \times 100\ \% \quad (1.25)$$

where R_{air} and R_{gas} indicates the resistivity under the air ambient and the resistivity when the target gas is injected. This is much higher than the sensitivity value of 50 % from the vertical HG-nanowire and the value of 35 % from the vertical CVD nanowires without the HG-nanowire. The results indicate that the method synthesizing the vertical ZnO nanowires by combining the HG process and thermal CVD is a very promising way to fabricate both the vertical nanowires and the highly sensitive gas sensors.

Catalytic metal clusters can be deposited on ZnO to improve the gas sensing performance. Wang *et al.*[116] deposited a variety of metal catalyst coatings (Pt, Pd, Au, Ag, Ti and Ni) on multiple ZnO nanorods and compared their effectiveness in enhancing sensitivity towards hydrogen at room temperature. Pt-coated nanorods showed a relative response of up to 8 % upon exposure to a hydrogen concentration of 500 ppm in N_2. This is a factor of two larger than that obtained with Pd and more than an order of magnitude larger than that achieved with the other metals. The sensitivity of the gas sensor was calculated by:

$$\text{Sensitivity (\%)} = |(R_{gas} - R_{air})/R_{air}| \times 100\ \% \qquad (1.26)$$

where R_{air} and R_{gas} indicates the resistivity under the air ambient and the resistivity when the target gas is injected. By comparison, the uncoated devices showed relative resistance changes of only ~0.25 % for 500 ppm H_2 in N_2. The Pt-coated ZnO nanorods could detect hydrogen down to 100 ppm, with a relative response of 4 % after exposure for 10 mins. The nanorods was able to recover fully when the ambient was switched back to air. The improvement in hydrogen sensing performance is due to the increased catalytic dissociation efficiency of molecular hydrogen to the more reactive atomic form by the catalytic metals.[117]

Gas sensors based on 1D oxide nanostructures are usually operated at high temperature (200 to 500 °C) to enhance the surface molecular adsorption/desorption kinetics and continuously clean the surface. However, the development of room temperature gas sensors will bring about very important advantages such as low power consumption, simple system configuration, reduced explosion hazards, and longer device lifetime.

1.8 Field emission of 1D ZnO nanostructures

Field emission is the process where electrons are emitted from a solid by tunneling through the surface potential barrier, when the potential barrier is lowered by the application of a strong electric field. Such a process is different from thermionic or photoelectric emission, in which the electrons overcome the surface potential barrier with energy obtained from heating or photoemission. The schematic of the potential-energy diagram for electrons at a metal surface under an applied field based on the basis of an ideal metal-vacuum interface is shown in Fig. 1.6. To achieve field emission, a potential difference is applied across the sample giving rise to an external field. This applied field distorts the potential of the sample enabling unexcited electrons to tunnel through.[118] The Fowler-Nordheim (F-N) theory assumes that the resultant potential is triangular and a relation between the current density, the applied electric field and the workfunction of the material can be determined.

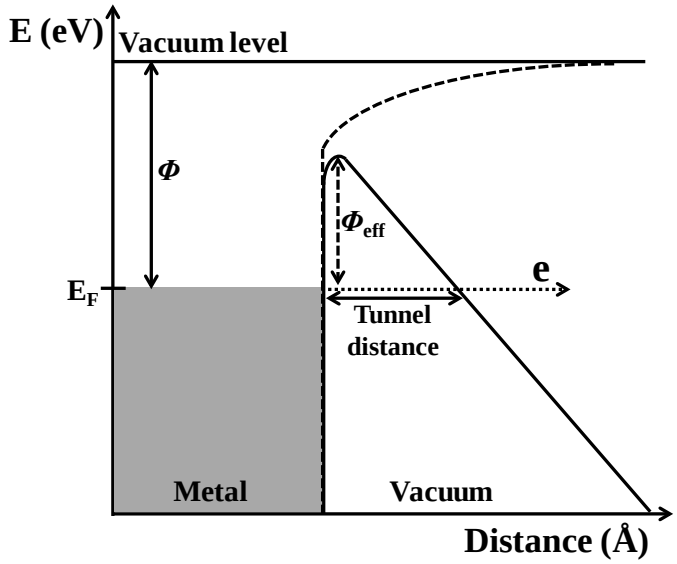

Figure 1.6. Schematic diagram showing the effective potential barrier between ideal metal and vacuum under a local electric field.

The F-N theory was developed by Fowler & Nordheim,[119] and other researchers such as Good & Mueller,[120] and Gadzuk & Plummer,[121] to describe the

relationship between the emission current density and the electric field applied on the metal surface. This theory was based on the idea of an ideal metal-vacuum interface, as schematically shown in Fig. 1.6. The simplified version of the F-N equation[122] is widely used to model field emission characteristics:

$$J = \frac{A\beta_{FN}{}^2 E^2}{\phi} \exp\left(-\frac{B\phi^{\frac{3}{2}}}{\beta_{FN} E}\right) \Rightarrow \ln\left(\frac{J}{E^2}\right) = -\frac{B\phi^{\frac{3}{2}}}{\beta_{FN}}\frac{1}{E} - \ln\frac{\phi}{A\beta_{FN}{}^2} \quad (1.27)$$

Where J is current density (A/cm^2),
E is electric field (V/ m),
φ is work function of the emitter,
β_{FN} is field enhancement factor,
A and B are constants of value 1.56 x 10^{-10} A V^{-2} eV and 6.83 x 10^3 V eV$^{-3/2}$ μm^{-1} respectively.

Eq. (1.27) means that if the emission process follows the F-N theory, the ln(J/E^2) versus 1/E curve (called a F-N plot) should be a straight line. From the slope of F-N plots, information on the work function or enhancement factor can be obtained and the intercept gives the effective emission area after the enhancement factor has been determined.

Since the discovery of field emission, many kinds of materials have been tested as cold cathodes for applications such as backlighting, flat panel displays, x-ray sources, and microwave amplifiers.[123] One of the milestones is the development of Spindt-type cathodes,[124] in which microfabricated Mo or Si tips arrays are used in a gated configuration for large scale addressable electron emitters for prototype field emission displays (FEDs). The study of the basic properties and potential applications led to the creation of vacuum microelectronics. Besides Spindt-type emitter arrays based on Mo and Si tips, diamond related materials have been utilized to fabricate field emitters due to their small or negative electron affinity.[125,126]

1D nanostructures have proven to be good field emitters because the local electric field near the tips can be greatly enhanced due to the high aspect ratio. As a

result, field emission studies based on a wide variety of 1D nanostructures have been actively pursued by researchers worldwide in the last decade. The nanostructures studied include nanotubes, nanowires/nanorods/nanoneedles, nanobelts and other complicated structures based on 1D blocks such as nanoflowers and networks. A good field emitter has qualities such as low turn on voltage, high emission current density, high field enhancement factor and stable emission. However, important factors such as geometry, crystallinity, presence of defects and good adhesion between nanowires and the substrate can also affect the field emission properties. Carbon nanotubes (CNTs) have attracted much attention as efficient field emitters due to their excellent field emission properties and high electrical conductivity.[127-129] The high aspect ratio of CNTs (a few micrometres in length and a diameter of several nanometres) makes it possible to achieve a high electric field at the tips for electron emission at moderate applied voltages. Several experiments have shown that the CNTs have the potential to be excellent field emitters.[130-135] However, the achievement of vertically well-aligned CNTs arrays for applicable field emission devices has not been facile and degradation of CNT field emitters at pressures higher than 10^{-9} mbar[136] by residual gases including oxygen is one of the problems to overcome for high performance field emission displays (FEDs).

After the discoveries of 1D ZnO nanostructures, many researchers suggested that these nanostructures have the potential to substitute CNTs as electron emitting sources because they have good thermal stability, good conductance, large aspect ratios such as CNTs and the degradation of field emission characteristics by residual gas may be reduced for an oxide surface of ZnO.[137] Some of the first experiments on field emission from ZnO nanowires were demonstrated by Lee *et al.*[138] Despite the array of ZnO nanowires being not vertically well aligned, the turn-on and the

threshold field were 6.0 V μm^{-1} at current density of 0.1 $\mu A\ cm^{-2}$ and 11.0 V μm^{-1} at 0.1 mA cm^{-2}, respectively. Although these field emission characteristics were lower than those of CNTs (turn-on field of 1 V μm^{-1} and field emission current of 1.5 mA at 3 V μm^{-1}; current density, J = 90 $\mu A\ cm^{-2}$)[135] they were good enough to be used as an electron emitter. Soon after the report of Lee *et al.*, several groups reported on electron emission from ZnO nanowires.[139-141] The reported results demonstrated that the field emission characteristics of 1D ZnO nanostructures are comparable to those of CNTs. Highly oriented vertical alignment has been considered as a factor in enhancing field emission properties since electrostatic models in metal cones were investigated by theoretical calculation.[142] ZnO nanowires that are vertically well-aligned were fabricated successfully by diverse methods and used to conduct field emission experiments. Li *et al.* showed that the vertical alignment of the ZnO nanowires plays an important role in determining the field emission characteristics.[143] Despite 1D ZnO nanostructures being considered by many researchers as good field emitters, additional experiments on various aspects including electrical conductivity, density control and device structures need to be done to yield excellent field emitters based on 1D ZnO nanostructures.

Density control of the 1D ZnO nanostructures is important because the field emission performance can be affected by screening effect due to electrostatic screening between adjacent emitters. This effect is also observed in CNT field emitters.[142,144] Theoretical and experimental studies have revealed that the electric field near the apex of emitters decreases with decreasing spacing between them. However, there will be insufficient emitters for a large emission current at very low emitter densities. Previous reports have suggested that the optimal spacing is twice the height,[142,145] or similar to the height of CNTs.[146,147] Teo *et al.*[148] experimentally

verified Nilsson's[142] simulation result with a CNT array which is 5 μm high and has spacing of 10 μm distance between each other. Li *et al.*'s[149] work on injector-like ZnO nanostructures had minimum screening effect when the distance between two neighbouring emitters was about 1.3 times the height of the needles.

Rigid substrates such as silicon, transparent conductive oxide-coated glass and metals which can withstand high temperatures are commonly used for field emission applications. However, with the increasing demand for flexible and transparent electronics, there is a need for mass fabrication of field emission sources on flexible substrates. The fabrication processes need to be low temperature due to the limitations of the flexible substrate. Therefore, the low cost, scalable, low temperature, substrate-independent hydrothermal synthesis method holds promise for realizing flexible field emission display devices on a commercial scale.

1.9 Objectives and significance of the study

The first broad scope of this thesis is to demonstrate the hydrothermal synthesis and control of the physical properties of ZnO films and nanowires. Under this scope, the first objective is to investigate the growth mechanisms and morphological control parameters such as precursor concentration, addition of surfactant and growth duration. This hydrothermal synthesis method will offer a low temperature, low cost and scalable route to synthesizing ZnO which is suitable for implementation on plastic substrates. Following this, the second objective will be to investigate the control of electrical properties of the ZnO films and nanowires by studying the changes in the electrical properties after surface modification by ammonia plasma treatment of varying durations. This will provide a facile, reliable and low temperature method of modifying the electrical conductivity of ZnO towards p-type.

The second broad scope of this thesis involves the exploitation of the nanowires for device applications and a study on the performance of the devices. In the first objective under this scope, flexible hydrogen gas sensors will be fabricated by synthesizing ZnO nanowires on plastic substrates and platinum (Pt) catalysts will be deposited on the nanowires to improve the hydrogen gas sensing performance at room temperature. The development of such a flexible gas sensor will be an answer to the demand for flexible electronic devices and the ability to operate at room temperature will mean lower power consumption and lower risk in combustible environments. The second objective is to study the feasibility and robustness of flexible field emission devices based on ZnO nanowires grown on plastic substrates. The influence of screening effect on field emission will be investigated by varying the spacing between the bundles of ZnO nanowires. This study will contribute to the development of high performance transparent and conformal electronic devices for portable display and other state-of-the-art electronics products. It will also add to the current literature reported on screening effect of ZnO field emitters.

1.10 Organization of thesis

This thesis consists of 6 chapters describing the works carried out on ZnO. Following the present chapter (**Chapter 1**) on the background of the project and the relevant literature review, the synthesis of ZnO films via the hydrothermal method will be discussed in **Chapter 2**. The effect of ammonia plasma treatment on ZnO films will also be studied in detail with a variation of the plasma treatment duration. The treatment duration with the optimum p-type properties will then be applied to the ZnO nanowires in **Chapter 3**. In this chapter, the synthesis of ZnO nanowires will be discussed and the electrical properties of the treated nanowires will be investigated. The nanowires will then be used in applications such as gas sensing and p-n junctions.

Chapter 4 will showcase the hydrogen gas sensing abilities of ZnO nanowires grown on flexible plastic substrates and the enhanced sensing performance with the addition of Pt catalyst. The patterned growth of ZnO nanowires on plastic substrate is demonstrated in **Chapter 5**. The field emission properties of the nanowires will be discussed with a study on the screening effect of a periodic array of nanowires with varying array spacing. Lastly, **Chapter 6** summarizes the findings in this project. A number of possible directions for future works will also be suggested.

References

1 Özgür Ü, Alivov Y I, Liu C, Teke A, Reshchikov M. A., Doğan S, Avrutin V., Cho S J, and Morkoç H. 2005 *Journal of Applied Physics.* **98**, 041301

2 Lukas S M and Judith L M D 2007 *Materials today.* **10** 40

3 Pearton S J, Norton D P, Ip K, Heo Y W and Steiner T 2005 *Materials Science.* **50** 293

4 Huang M H, Mao S, Feick H, Yan H, Wu Y, Kind H, Weber E, Russo R and Yang P D 2001 *Science* **292** 1897

5 Law M, Greene L E, Johnson J C, Saykally R and Yang P D 2005 *Nat. Mater.* **4** 455

6 Fan Z Y, Wang D W, Chang P C, Tseng W Y and Lu J G 2004 *Appl. Phys. Lett.* **85** 5923

7 Wang X D, Song J H, Liu J and Wang Z L 2007 *Science* **316** 102

8 Wang W W, Zhang G M, Yu L G, Bai S, Zhang Z X and Zhao X Y 2007 *Physica E* **36** 86

9 Park C H, Zhang S B and Wei S-H 2002 *Phys. Rev. B* **66** 073202

10 Tsukazaki A, Ohtomo A, Onuma T, Ohtani M, Makino T, Sumiya M, Ohani K, Chichibu S F, Fuke S, Segawa Y, Ohno H, Koinuma H and Kawasaki M 2005 *Nature Materials* **4** 42

11 Lin C C, Chen H P and Chen S Y 2005 *Chemical Physics Letters* **404** 30

12 Xiang B, Wang P W, Zhang X Z, Dayeh S A, Aplin D P R, Soci C, Yu D P and Wang D L 2007 *Nano Letters* **7** 323

13 Wei A, Sun X W and Wang J X 2006 *Appl. Phys. Lett.* **89** 123902

14 Suh H W, Kim G Y, Jung Y S and Choi W K 2005 *J. Appl. Phys.* **97** 044305

15 Bonard J M, Kind H, Stockli T and Nilsson L O 2001 *Solid-State Electron.* **45** 893

16 Lee C J, Lee T J, Lyu S C, Zhang Y, Ruh H and Lee H J 2002 *Appl. Phys. Lett.* **81** 3648

17 Wang Z L 2004 *J. Phys.: Condens. Matter* **16** R829

18 Kim D J 2009 *Growth and characterization of zinc oxide and PZT films for micromachined acoustic wave devices* (PhD thesis) Auburn University, USA

19 Brice J C 1986 "*Crystal growth processes*", Glasgow : Blackie ; New York: Halsted Press

20 Chen Y, Bagnall D and Yao T 2000 *Mater. Sci. Eng. B* **75** 190

21 Bakin A, El-Shaer A, Mofor A C, Kreye M., Waag A, Bertram F, Christen J, Heuken M and Stoimenos J 2006 *Journal of Crystal Growth* **287** 7

22 Maejima K, Kawabata H and Fujita S 2007 *Jpn. J. Appl. Phys.* **46** 7885

23 Du G T, Wang X S, Yang T P, Liang H W, Chang Y, Liu W F and Xu Y B 2005 *Journal of Crystal Growth* **285** 521

24 Pan N, Wang X, Zhang K, Hu H, Xu B, Li F and Hou J G 2005 *Nanotechnology* **16** 1069

25 Li M K, Wang D Z, Ding Y W, Guo X Y, Ding S and Jin H 2007 *Materials Science and Engineering A.* **452** 417

26 Fang F, Zhao D X, Zhang J Y, Shen D Z, Lu Y M, Fan X W, Li B H and Wang X H 2007 *Nanotechnology* **18** 235604

27 Jeong J S, Lee J Y, Cho J H, Lee C L, An S, Yi G and Gronsky R 2005 *Nanotechnology* **16** 2455

28 Dai Z R, Pan Z W and Wang Z L 2003 *Adv. Funct. Mater.* **13** 9

29 Wang Z L 2004 *J. Phys.: Condens. Matter* **16** R829

30 Li C, Fang G, Fu Q, Su F, Li G, Wu X, Zhao X 2006 *Journal of Crystal Growth.* **292** 19

31 Wang M 2009 *Zinc oxide nanostructures grown by low temperature methods* (PhD thesis) National University of Singapore, Singapore

32 Ichimua M and Fathy N 2006 *Journal of Crystal Growth* **294** 191

33 Fu M, Zhou J, Xiao Q F, Li B, Zong R L, Chen W and Zhang J 2006 *Adv. Mater.* **18** 1001

34 Cao B Q, Cai W P, Duan G T, Li Y, Zhao Q and Yu D P 2005 *Nanotechnology* **16** 2567

35 Li W J, Shi E W, Zhong W Z and Yin Z W 1999 *J. Crystal Growth* **203** 186

36 Chen D, Jiao X and Cheng G 2000 *Solid State Commun.* **113** 363

37 Wang B, Shi E, Zhong W and Yin Z 1997 *Chin. Sci. Bull.* **42** 1041

38 Lu C H and Yeh C H 2000 *Ceramics Intl.* **26** 351

39 Zhou Z and Deng Y 2009 *J. Phys. Chem. C* **113** 19853

40 Garcia S P and Semancik S 2007 *Chem. Mater.* **19** 4016

41 Peng Y, Xu A W, Deng B, Antonietti M and Cölfen H 2006 *J. Phys. Chem. B* **110** 2988

42 Vayssieres L 2003 *Adv. Mater.* **15** 464

43 Yang L L, Zhao Q X, Willander M and Yang J H 2009 *J. Cryst. Growth* **311** 1046

44 Tian Z R, Voigt J A, Liu J, Mckenzie B, Mcdermott M J, Rodrigues M A, Konishi H and Xu H 2003 *Nat. Mater.* **2** 821

45 Greene L E, Law M, Goldberger J, Kim F, Johnson J C, Zhang Y R, Saykally J and Yang P 2003 *Angew. Chem., Int. Ed.* **42** 3031

46 Greene L E, Law M, Tan D H, Montano M, Goldberger J, Somorjai G and Yang P 2005 *Nano Lett.* **5** 1231

47 Kenanakis G, Vernardou D, Koudoumas E and Katsarakis N 2009 *J. Cryst. Growth* **311** 4799

48 Liu S Y, Chen T, Wan J, Ru G P, Li B Z and Qu X P 2009 *Appl. Phys. A* **94** 775

49 Sun Y, Ndifor-Angwafor N G, Riley D J and Ashfold M N R 2006 *Chem. Phy. Lett.* **24** 352

50 Lange F F 1996 *Science* **273** 903

51 Verges M A, Mifsud A and Serna C J 1990 *J. Chem. Soc., Faraday Trans.* **86** 959

52 Vayssieres L 2001 *J. Phys. Chem. B* **105** 3350

53 Schmidt-Mende L and MacManus-Driscoll J L 2007 *Mater. Today* **10** 40

54 Govender K, Boyle D S, Kenway P B and O'Brien P 2004 *J. Mater. Chem.* **14** 2575

55 Andeen D, Loeffler L, Padture N and Lange F F 2003 *J. Cryst. Growth* **259** 103

56 Richardson J J and Lange F F 2009 *Crystal Growth & Design* **9** 2570

57 Drift A V D, 1967 *Philips Res. Rep.* **22** 267

58 Carter G 2000 *Vacuum* **56** 87

59 Ashfold M N R, Doherty R P, Angwafor N, Riley D J and SunY 2007 *Thin Solid Films* **515** 8679

60 Sillen L G, Martell A E, *Stability constants of metal–ion complexes,* The Chemical Society, Burlington House, London, 1964.

61Laudise R A and Ballman A A 1960 *J. Phys. Chem.* **64** 688

62 Vangeusden K, Seager C H, Warren W L, Tallant D R and Voigt J A 1996 *Appl Phys Lett* **68** 1377

63 Fang Z, Wang Y, Xu D, Tan Y and Liu X 2004 *Optical Materials* **26** 239

64 Zhao J L, Zhang W, Li X M, Feng J W and Shi X 2006 *J. Phys. Condens. Matter* **18** 1495

65 Look D C 2006 *J. Electron. Mater.* **35** 1299.

66 Janotti A and Van de Walle C G, 2006 *J. Crystal Growth* **287** 58

67 Lin B X, Fu Z X and Jia Y B 2001 *Appl Phys Letters* **79** 243

68 Xiang B, Wang P W, Zhang X Z, Dayeh S A, Aplin D P R, Soci C, Yu D P and Wang D L 2007 *Nano Lett.* **7** 323.

69 Schirmer O F and Zwingel D 1970 *Solid State Commun.* **8** 1559

70 Schirmer O F 1968 *J. Phys. Chem. Solids* **29** 1407

71 Valentini A, Quaranta F, Rossi M and Battaglin G 1991 *J. Vac. Sci. Technol. A* **9** 286

72 Liu W, Xiu F A, Sun K, Xie Y H, Wang K L, Wang Y, Zou J, Yang Z and Liu J L 2010 *J. Am. Chem. Soc.* **132** 2498

73 Tay C B, Chua S J and Loh K P 2010 *J. Phys. Chem. C* **114** 9981

74 Kanai Y 1991 *Jpn. J. Appl. Phys.* Part 1 **30**, 703

75 Kanai Y 1991 *Jpn. J. Appl. Phys.* Part 1 **30**, 2021

76 Li X, Yan Y, Gessert T A, DeHart C, Perkins C L, Young D and Coutts T J 2003 *Electrochemical and Solid-State Letters* **6** C56

77 Lee W, Jeong M C, Joo S W and Myoung J M 2005 *Nanotechnology* **16** 764

78 Park C H, Zhang S B and Wei S H 2002 *Phys. Rev. B* **66** 073202

79 Harrison W A 1999 *Elementary Electronic Structure* (Singapore: World Scientific)

80 Minegishi K, Koiwai Y, Kikuchi Y, Yano K, Kasuga M and Shimizu A 1997 *Japan. J. Appl. Phys. Part* II **36** L1453

81 Look D C, Reynolds D C, Litton C W, Jones R L, Eason D B and Cantwell G 2002 *Appl. Phys. Lett.* **81** 1830

82 Tsukazaki A *et al* 2005 *Nature Mater.* **4** 42

83 Carlos W E, Glaser E R and Look D C 2001 *Physica* B **308–310** 976

84 Thonke K, Gruber Th, Teofilov N, Sch¨ofelder R, Kerwien N, Waag A and Sauer R 2001 *Physica* B **308** 945

85 Guo X-L, Choi J-H, Tabata H and Kawai T 2001 *Japan. J. Appl. Phys.* **40** L177

86 Meyer B K, Alves H, Hofmann D M, Kriegseis W, Forster D, Bertram F, Christen J, Hoffmann A, Straßburg M, Dworzak M, Haboeck U and Rodina A V 2004 *Phys. Status Solidi* b **241** 231

87 Lautenschlaeger S, Eisermann S, Meyer B K, Callison G, Wagner M R and Hoffmann A 2009 *Phys. Status Solidi RRL* **3** 16

88 Fang Z-Q, Claflin B, Look D C, Lei Kerr L and Li X 2007 *J. Appl. Phys.* **102** 023714

89 Fons P, Tampo H, Kolobov A V, Ohkubo M, Niki S, Tominaga J, Carboni R, Boscherini F and Friedrich S 2006 *Phys. Rev. Lett.* **96** 045504

90 Van de Walle C G, Laks D B, Neumark G F and Pantelides S T 1993 *Phys. Rev.* B **47** 9425

91 Kobayashi A, Sankey O F and Dow J D 1983 *Phys. Rev.* B **28** 946

92 Lu J G, Ye Z Z, Wang L, Zhao B H and Huang J Y 2002 *Chin. Phys. Lett.* **19** 1494

93 Ye Z Z, Lu J G, Chen H H, Zhang Y Z, Wang L, Zhao B H and Huang J Y 2003 *J. Cryst. Growth* **253** 258

94 Lu J G, Ye Z Z, Zhuge F, Zeng Y J, Zhao B H and Zhu L P 2004 *Appl. Phys. Lett.* **85** 3134

95 Tsukazaki A, Kubota M, Ohtomo A, Onuma T, Ohtani K, Ohno H, Chichibu S F and Kawasaki M 2005 *Jpn. J. Appl. Phys.* **44** L643

96 Li X N, Keyes B, Asher S, Zhang S B, Wei S H, Coutts T J, Limpijumnong S and Van de Walle C G 2005 *Appl. Phys. Lett.* **86** 122107

97 Lu J G, Zhang Y Z, Ye Z Z, Zhu L P, Wang L, Zhao B H and Liang Q L 2006 *Appl. Phys. Lett.* **88** 222114

98 Georgobiani A N, Gruzintsev A N, Volkov V T and Vorob'ev M O 2002 *Semiconductors* **36** 265

99 Huang J Y, Ye Z Z, Chen H H, Zhao B H and Wang L 2003 *J. Mat. Sci. Lett.* **22** 249

100 Seiyama T, Kato A, Fujiishi K and Nagatani M 1962 *Anal. Chem.* **34** 1502

101 Hooker S A 2002 In *The Nanoparticles 2002 Conference* 1

102 Kolmakov A, Zhang Y, Cheng G and Moskovits M 2003 *Adv. Mater.* **15** 997

103 Williams D E 1999 *Sens. Actuators, B* **57** 1

104 Kohl D 1989 *Sens. Actuators* **18** 71

105 Yuan G D, Zhang W J, Jie J S, Fan X, Zapien J A, Leung Y H, Luo L B, Wang P F, Lee C S and Lee S T 2008 *Nano Letters* **8** 2591

106 Ryu H W, Park B S, Akbar S A, Lee W S, Hong K J, Seo Y J, Shin D C, Park J S and Choi G P 2003 *Sens. Actuator B* **96** 717

107 Sberveglieri G 1995 *Sens. Actuator B* **23** 103

108 Trivikrama Rao G S and Tarakarama Rao D 1999 *Sens. Actuator B* **55** 166

109 Cheng X L, Zhao H, Huo L H, Gao S and Zhao J G 2004 *Sens. Actuator B* **102** 248

110 Kolmakov A and Moskovits M 2004 *Annu. Rev. Mater. Res.* **34** 151

111 Wan Q, Li Q H, Chen Y J, Wang T H, He X L, Li J P and Lin C L 2004 *Appl. Phys. Lett.* **84** 3654

112 Goldberger J, Sirbuly D J, Law M and Yang P D 2005 *J. Phys. Chem. B* **109** 9

113 Harrison P G and Willett M J 1998 *Nature* **332** 227

114 Rout C S, Krishna S H, Vivekchand S R C, Govindaraj A and Rao C N R 2006 *Chem. Phys. Lett.* **418** 586

115 Kang D S, Han S K, Kim J H, Yang S M, Kim J G, Hong S K, Kim D J, Kim H J and Song J H 2009 *J. Vac. Sci. Technol. B* **27** 1667

116 Wang H T, Kang B S, Ren F, Tien L C, Sadik P W, Norton D P, Pearton S J and Lin J 2005 *Appl. Phys. A* **81** 1117

117 Tien L C, Sadik P W, Norton D P, Voss L F, Pearton S J, Wang H T, Kang B S, Ren F, Jun J and Lin J 2005 *Appl. Phys. Lett.* **87** 222106

118 Ng K T D 2008 *Synthesis and characterization of gallium nitride nanowires by pulsed laser ablation* (PhD thesis) National University of Singapore, Singapore

119 Fowler R H and Nordheim L W 1928 *Proc. R. Soc. Lond. A* **119** 173

120 Good R H and Mueller E W 1956 *Field emission*; Springer, **21**

121 Gadzuk J W and Plummer E W 1973 *Rev. Mod. Phys.* **45** 487

122 Tseng Y K, H C J, Cheng H M, Lin I N, Liu K S and Chen I C 2003 *Adv. Funct. Mater.* **13** 10

123 Li C, Y.Z., Mann M, Hiralal P, Unalan H E, Lei W, Wang B P, Chu D P, Pribat D, Amaratunga G A J and Milne W I 2010 *Applied Physics Letters* **96** 143114

124 Spindt C A 1968 *J. Appl. Phys.* **39** 3504

125 Xu N S and Huq S E 2005 *Mater. Sci. Eng. R* **48** 47

126 Geis M W, Efremow N N, Krohn K E, Twichell J C, Lyszczarz T M, Kalish R, Greer J A and Tabat M D 1998 *Nature* **393** 431

127 Chernozatonskii L A, Gulyaev Y V, Kosakovskaya Z Y, Sinitsyn N I, Torgashov G V, Zakharchenko Y F, Fedorov E A and Val'chuk V P 1995 *Chem. Phys. Lett.* **233** 63

128 Heer W A d, Chatelain A and Ugarte D 1995 *Science* **270** 1179

129 Rinzler A G, Hafner J H, Nikolaev P, Lou L, Kim S G, Tomanek D, Nordlander P, Colbert D T and Smalley R E 1995 *Science* **269** 1550

130 Temple D 1999 *Mater. Sci. Eng.* R **24** 185

131 Heer W A d, Chatelain A and Ugarte D 1995 *Science* **270** 1179

132 Gulyaev Yu V, Chernozatonskii L A, Kosakovskaja J Z, Sinitsyn N I, Torgashov G V and Zakharchenko Yu F 1995 *J. Vac. Sci. Technol.* B **13** 435

133 Wang Q H, Setlur A A, Lauerhaas J M, Dai J Y, Seelig E W and Chang R P H 1998 *Appl. Phys. Lett.* **72** 2912

134 Nalwa H S and Rohwer L S 2003 *Handbook of Luminescence, Display Materials, and Devices* (Stevenson Ranch, CA: American Scientific Publishers)

135 Choi W B, Chung D S, Kang J H, Kim H Y, Jin Y W, Han I T, Lee Y H, Jung J E, Lee N S, Park G S and Kim J M 1999 *Appl. Phys. Lett.* **75** 3129

136 Jonge N d, Allioux M, Doytcheva M, Oostveen J T, Teo K B K and Milneet W I 2005 *Appl. Phys. Lett.* **87** 133118

137 Wei A, C.X., Sun X W, Huang W, and Lo G Q 2008 *Journal Of Display Technology* **4** 9

138 Lee C J, Lee T J, Lyu S C, Zhang Y, Ruh H and Lee H J 2002 *Appl. Phys. Lett.* **81** 3648

139 Dong L F, Jiao J, Tuggle D W, Petty J M, Elliff S A and Coulter M 2003 *Appl. Phys. Lett.* **82** 1096

140 Jo S H, Lao J Y, Ren Z F, Farrer R A, Baldacchini T and Fourkas J T 2003 *Appl. Phys. Lett.* **83** 4821

141 Xu C X, Sun X W and Chen B J P 2004 *Appl. Phys. Lett.* **84** 1540

142 Nilsson L, Groening O, Emmenegger C, Kuettel Q, Schaller E, Schlapbach L, Kind H, Bonard J M and Kern K 2000 *Appl. Phys. Lett.* **76** 2071

143 Li S Y, Lin P, Lee C Y and Tseng T Y 2004 *J. Appl. Phys.* **95** 3711

144 Jo S H, Tu Y, Huang Z P, Carnahan D L, Wang D Z and Ren Z F 2003 *Appl. Phys. Lett.* **82** 3520

145 Bonard J M, Weiss N, Kind H, Stockli T, Forro L, Kern K and Chatelain A 2001 *Adv. Mater.* **13** 184

146 Yoon S M, Chae J and Suh J S 2004 *Appl. Phys. Lett.* **84** 825

147 Suh J S, Jeong K S, Lee J S and Han I 2002 *Appl. Phys. Lett.* **80** 2392

148 Teo K B K, Chhowalla M, Amaratunga G A J, Milne W I, Pirio G, Legagneux P and Hasko D G 2002 *Appl. Phys. Lett.* **79** 1534

149 Li C, Yang Y, Sun X W, Lei W, Zhang X B, Wang B P, Wang J X, Tay B K, Ye J D, Lo G Q and Kwong D L 2007 Nanotechnology **18** 135604

Chapter 2 Synthesis of ZnO Films and Post-Growth Ammonia Plasma Treatment for Tuning of Electrical Characteristics

In this chapter, the growth of ZnO films on c-sapphire substrates via the hydrothermal method is investigated. Experimental parameters are varied to understand the optimal parameters needed to produce a fully coalesced film with the shortest growth duration. The films are then treated with ammonia plasma in an effort to modify the electrical properties of the film towards p-type conductivity. The duration of the plasma treatment is varied to study the effect of treatment duration on the characteristics of the film.

2.1 Introduction

As recently reviewed,[1] ZnO is considered a candidate for a wide variety of applications including room temperature UV lasers,[2] transparent conducting electrodes,[3] surface-acoustic wave devices[4] because of its large piezoelectric constant,[5] and gas sensors.[6,7] The wide bandgap of 3.37 eV and large exciton binding energy of 60 meV, which is almost 3 times that of GaN (21 meV) makes ZnO a potential material for use in opto-electronic devices such as light emitting diodes (LEDs) and laser diodes.[8,9] High quality epitaxial films are needed in some applications such as transparent conducting electrodes and LEDs. Epitaxial ZnO films are commonly deposited using high cost vacuum deposition techniques such as metal-organic chemical vapour deposition (MOCVD),[10,11] metal-organic vapour-phase epitaxy (MOVPE),[12-16] pulsed laser deposition (PLD),[17-19] and molecular beam epitaxy (MBE).[20-23] However, there has been an increasing interest in cheap and scalable production of ZnO films using a low temperature and environmentally friendly method in recent years. The aqueous route to synthesize ZnO films fulfil

these requirements because the investment of thermal energy required for such low temperature growth is minimal and expensive vacuum pumps and chambers associated with vapour deposition are not required. This process offers scalability where films can be grown on large-sized substrates and numerous films can be grown simultaneously, offering high production throughput. The synthesis is also based on green chemistry and does not give rise to any significant process hazard or environmental concern.

However, the lack of a stable p-type doping for ZnO is hindering the application of ZnO in opto-electronics. ZnO is n-type by nature due to native defects such as oxygen vacancies and zinc interstitials.[24-26] There are several issues that limit the efficiency of p-type doping in ZnO, namely: low dopant solubility, deep acceptor level, and "self-compensation" of shallow acceptors resulting from native donor defects.[27] To overcome these problems, many growth techniques and post-treatment methods[28-31] using Group I elements (Li, Na) and group V elements (N, P, As, Sb) were employed to realize the p-type conductivity in ZnO. For many reasons, nitrogen seems to be the ideal choice for p-doping in ZnO[32]: nitrogen and oxygen have similar ionic radii,[33] N has the lowest ionisation energy of all possible Group V elements, and it does not form the N-on-Zn antisite (N_{Zn}).

In this chapter, ZnO films were synthesized by the low temperature and environmentally friendly hydrothermal growth method.[34] The growth parameters were varied to understand and obtain the optimal parameters needed to produce a fully coalesced ZnO film in the shortest time. P-type characteristics in the film was obtained by surface modification using ammonia (NH_3) plasma treatment without delibrate heating of the substrate. The duration of the plasma treatment was varied to tune the electrical characteristics of the film towards optimal p-type conductivity. The

set of parameters which produced the best p-type electrical properties in the ZnO films will be applied to ZnO nanowires in the next chapter.

2.2 Experimental procedures

ZnO films were grown on c-sapphire substrates using the hydrothermal method. The substrates were cleaned by sonicating in isopropyl alcohol (IPA) (5 min) followed by ethanol (5 min). The substrates were blown dry with a stream of nitrogen gas. A 100 nm thick ZnO seed layer was sputtered on the c-sapphire substrates via RF magnetron sputtering (Denton Vacuum Discovery 18 system) at room temperature. The buffer layer acts as a seed layer to encourage growth of the ZnO film and it also serves to reduce the lattice mismatch between ZnO and c-sapphire. The seeded substrates were then placed into a 25 ml growth solution containing zinc nitrate hexahydrate ($Zn(NO_3)_2 \cdot 6H_2O$), ammonium hydroxide (NH_4OH, 33 %) to adjust the pH of the growth solution to 10.9 and trisodium citrate ($Na_3C_6H_5O_7$) as surfactant to promote coalescence of nanowires to form a continuous film. The growth process was carried out at 90 °C for 1 to 3 hours. The synthesis steps are illustrated in the schematic diagram in Fig. 2.1. To obtain a better understanding of the growth mechanism and the effect of growth parameters on the physical attributes of the film such as coalescence and height of the film, several growth parameters were varied, namely: (i) growth solution concentration (25 to 100 mM of zinc nitrate), (ii) amount of trisodium citrate added (0 to 1.94 mM), and (iii) growth duration (1 to 3 hours).

Based on the results from these studies, ZnO films with the ideal morphology were synthesized using the optimal growth conditions of 50 mM zinc nitrate, 0.97 mM trisodium citrate and growth duration of 1.5 hours. The films were then treated with NH_3 plasma without any additional heating. The RF power was 250 W and the treatment was carried out at a pressure of 0.4 mbar. The treatment duration was varied

from 30 to 180 s to investigate how the plasma treatment duration affects the characteristics of the film.

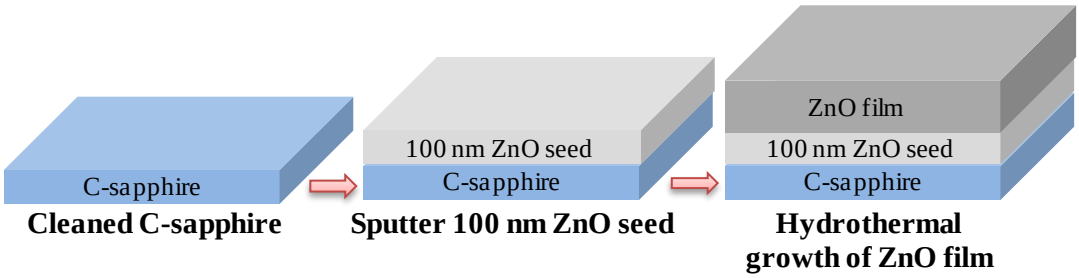

Figure 2.1. Schematic diagram of hydrothermal growth of ZnO films on c-sapphire substrates.

Various characterization techniques were carried out on the samples. Scanning electron microscopy (SEM, JEOL FEG JSM 7001F) and transmission electron microscopy (TEM, Phillips FEG CM300) characterized the morphology of the synthesized products while the crystalline structure of the ZnO film was analyzed using X-ray diffraction (XRD, Philips X-ray diffractometer equipped with graphite-monochromated Cu Kα radiation at λ = 1.541 Å). XRD was also used to study the shift in the ZnO (002) peak from the lattice expansion due to the presence of the N or N-H atom pairs in the crystal lattice of the ZnO film. Room temperature optical properties were measured with the micro-photoluminescence (PL) with He-Cd laser at 325 nm. The change in the intensity of the defect peak with the variation of plasma treatment duration was investigated. Hall measurements were carried out on 1 x 1 cm^2 samples using the Van der Pauw sample configuration with nickel (Ni) contacts at room temperature by a Bio-Rad Hall system. X-ray photoelectron spectroscopy (XPS) was employed to study the elemental composition of the intrinsic and NH_3 plasma treated ZnO films.

2.3 Results and discussion

2.3.1 Effect of precursor concentration

The concentration of the growth solution was varied to determine the minimum amount of zinc nitrate needed for film formation. Zinc nitrate of concentrations 25, 50, 75 and 100 mM were studied without the addition of trisodium citrate to the growth solution. Ammonium hydroxide was added as required to bring the pH of the solution to 10.9 and the growth was carried out at 90 °C for 3 hours.

The ZnO nanowires synthesized had average diameters ranging from 54.9 to 650.2 nm and average heights ranging from 2.53 to 11.55 μm for increasing concentrations of growth solution as shown in the SEM images in Fig. 2.2. The morphology changed from nanowires at 25 mM of zinc nitrate to almost film-like at 100 mM. The observed increase in the height and diameter of the nanowires with the concentration of the precursor is due to the greater amounts of precursor available, which induced higher growth rate in both lateral and upward directions.

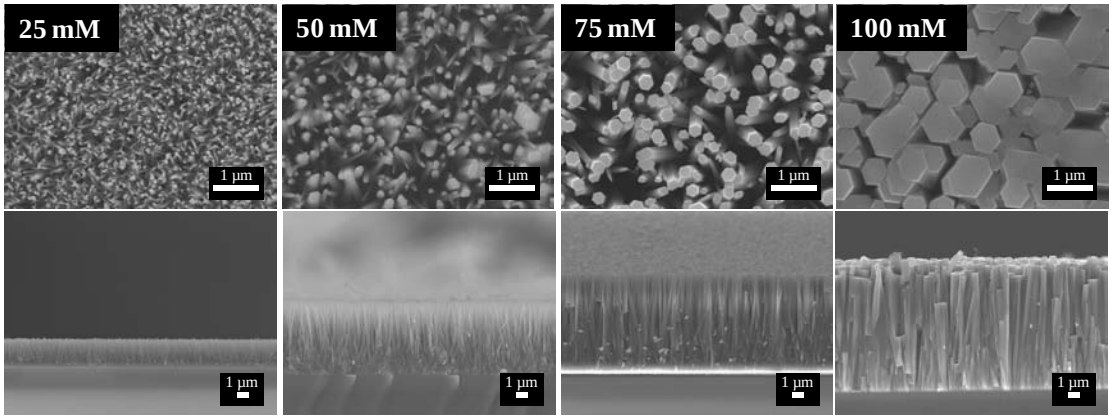

Figure 2.2. SEM images (top and cross-sectional views) of ZnO films of various growth solution concentrations without trisodium citrate.

When 0.97 mM of trisodium citrate was added to the 4 growth solutions with various concentrations of zinc nitrate (25, 50, 75 and 100 mM), ZnO films were observed instead of nanowires (Fig. 2.3). The film obtained at 25 mM of zinc nitrate

had not fully coalesced and some discontinuities could be observed in the film. As the concentration increased, the film seems to coalesce better but the surface seems to become rougher at higher concentrations (100 mM). This could be due to competition between lateral growth of neighbouring crystals pushing against each other, which resulted in buckling of the film surface. The height of the film was also observed to increase with precursor concentration from 1.94 μm for 25 mM to 7.89 μm for 100 mM. However, the height is noted to be generally shorter than the samples grown without trisodium citrate for all concentrations of zinc nitrate. This is because the presence of trisodium citrate in the growth solution caused the precursors to be directed towards lateral growth of the nanowires rather than upward growth, hence forming a coalesced but shorter film.

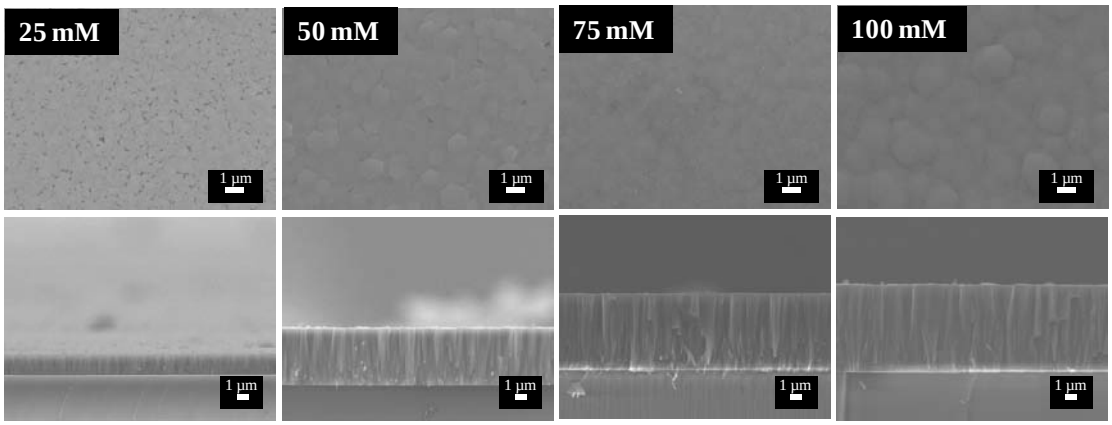

Figure 2.3. SEM images (top and cross-sectional views) of ZnO films of various growth solution concentrations with 0.97 mM of trisodium citrate.

The results from this set of experiments are summarized in Table 2.1 and Fig. 2.4. It is observed that the presence of trisodium citrate in the growth solution aids the formation of films and a zinc nitrate concentration of 50 mM is sufficient for film formation when 0.97 mM of trisodium citrate is added.

Table 2.1. Summary of average diameter and height of ZnO nanowires and films of various growth solution concentrations.

Zinc nitrate (mM)	Trisodium citrate (mM)	Average diameter (nm)	Average height (μm)
25	0.00	54.9	2.53
50	0.00	126.5	6.91
75	0.00	270.8	8.72
100	0.00	650.2	11.55
25	0.97	-	1.94
50	0.97	-	5.01
75	0.97	-	7.46
100	0.97	-	7.89

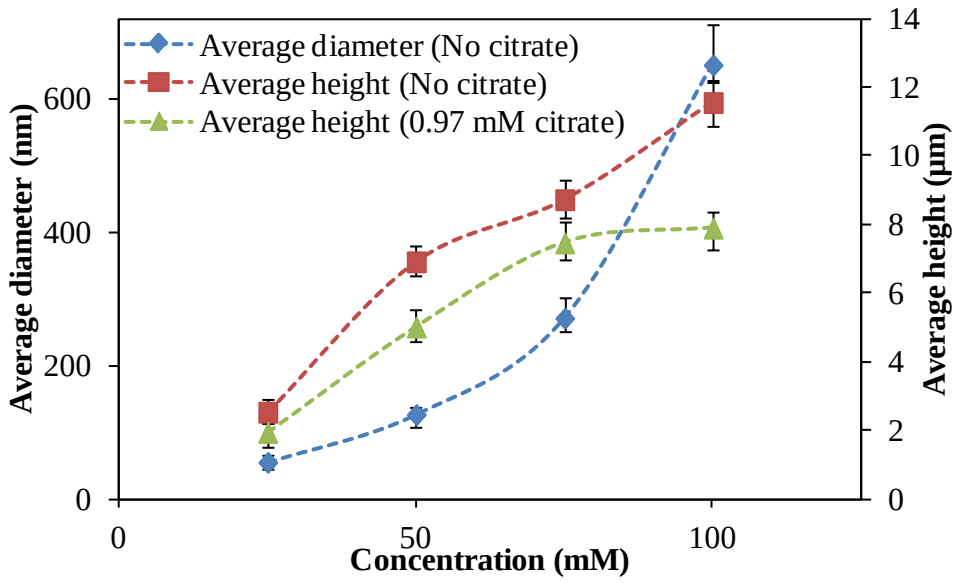

Figure 2.4. Plot of average diameter and height of ZnO nanowires and films of various growth solution concentrations.

2.3.2 Effect of trisodium citrate concentration

The amount of trisodium citrate added to a growth solution with 50 mM of zinc nitrate was then varied to study its effect on the coalescence of the nanowires and the height of the film. The samples were grown at 90 ^{o}C for 3 hours. The amounts of trisodium citrate added were 0.49, 0.97, 1.46 and 1.94 mM. Trisodium citrate is a surfactant which promotes lateral growth of the nanowires, causing them to coalesce into a continuous film. The negatively charged citrate ions adhere to the positively charged Zn-terminated (0001) plane and retard growth in the [0002] direction (c-

direction), while growth rate in the lateral [10-10] direction remains unchanged (Fig. 2.5).[34]

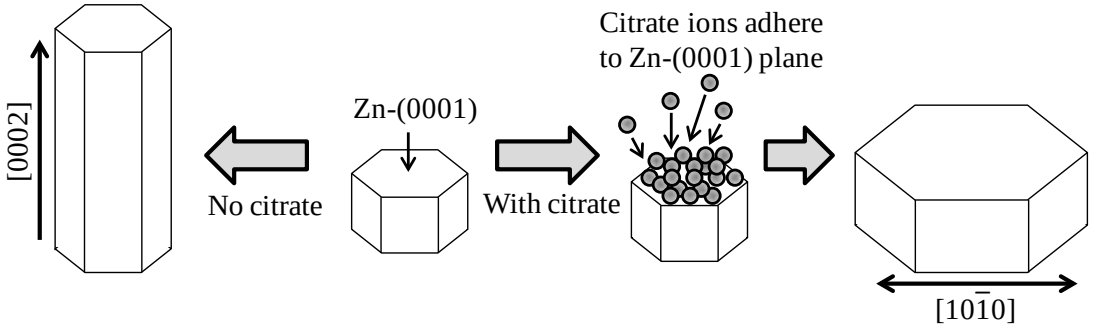

Figure 2.5. Schematic illustration of citrate anions adhering to ZnO nanowires.

This causes the diameter of the nanowires to increase with citrate anion concentration. It can be seen from the SEM images in Fig. 2.6 that the film started to coalesce when 0.49 mM of trisodium citrate was added, but some discontinuities were still visible in the film. A fully coalesced film was obtained when 0.97 mM or more trisodium citrate was added to the growth solution. The grain size was observed to increase as the amount of trisodium citrate increased. The amount of trisodium citrate also affected the height of the film as seen in the cross-sectional SEM images in Fig. 2.6. The average height of the film decreased from 6.93 to 3.97 μm as the amount of trisodium citrate increased (Fig. 2.7 and Table 2.2). This is because the citrate anions restrict the vertical growth of the film, causing the growth in the upward direction to be slower, resulting in shorter films.

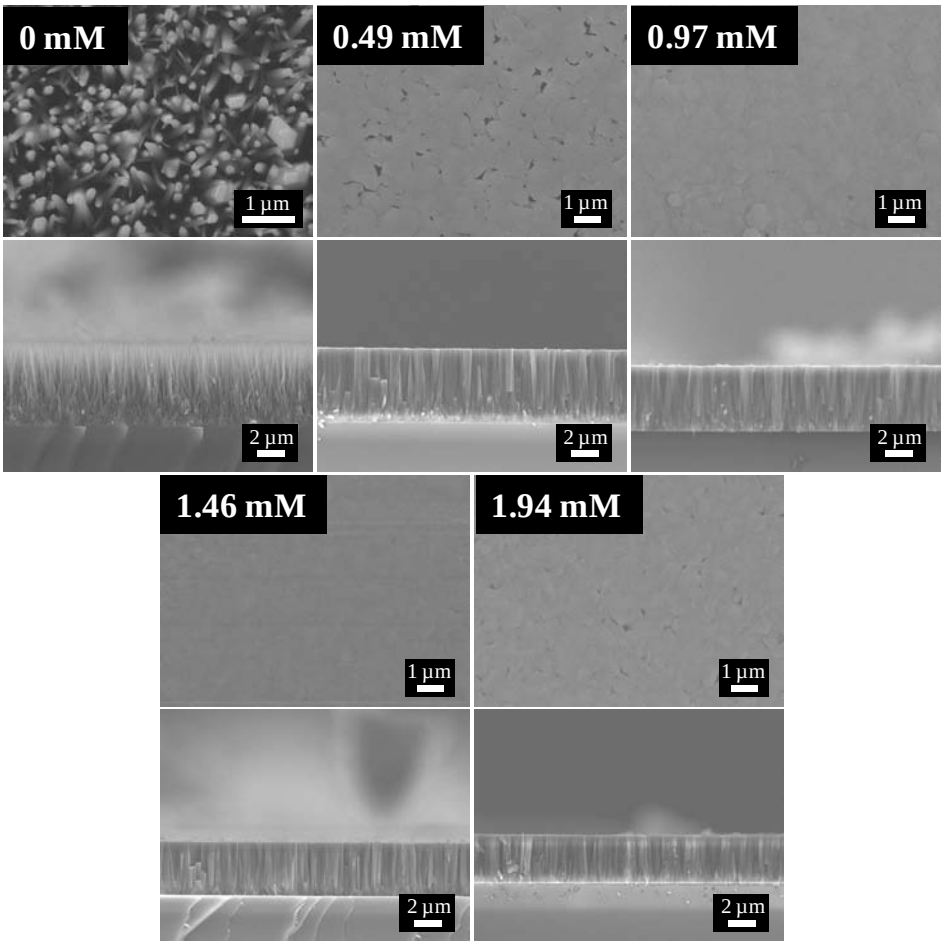

Figure 2.6. SEM images (top and cross-sectional views) of ZnO films of various amounts of trisodium citrate.

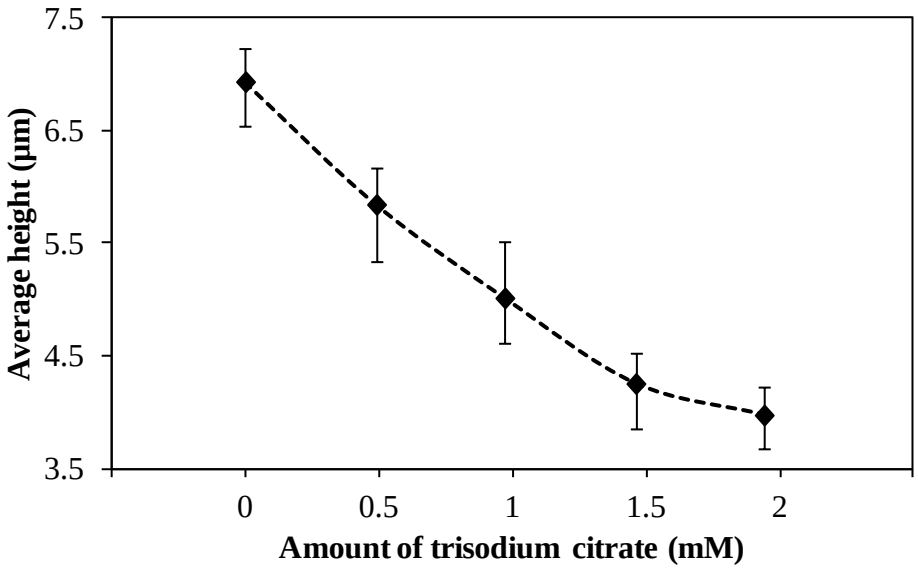

Figure 2.7. Plot of average height of ZnO films for various amounts of trisodium citrate.

Table 2.2. Summary of average height of ZnO films for various amounts of trisodium citrate.

Trisodium citrate (mM)	Average height (μm)
0.00	6.93
0.49	5.84
0.97	5.01
1.46	4.25
1.94	3.97

2.3.3 Effect of growth duration

The growth of the ZnO film in a growth solution containing 50 mM of zinc nitrate and 0.97 mM of trisodium citrate for various time durations was carried out to study the growth over time. The results obtained will provide a better understanding of the growth mechanism for the film and how the height of the film changes with time. The amount of time needed for the film to fully coalesce could also be obtained. The growth was carried out for 1 to 3 hours and the SEM images are shown in Fig. 2.8.

Individual nanowires were still observable in the sample grown for 1 hour but a fully coalesced film was observed after 1.5 hours of growth. The samples that were grown for longer than 1.5 hours maintained the coalesced film morphology. This indicates that it takes about 1.5 hours for the nanowires in a 50 mM growth solution with 0.97 mM of trisodium citrate to grow large enough to come into contact with the neighbouring nanowires and coalesce to form films. The average height of the film also increased from 0.5 to 5.01 μm as the growth time increased as shown in Table 2.3 and Fig. 2.9. However, since a thick film is not required for this work, the growth time chosen is the minimum time necessary to form a fully coalesced film which is 1.5 hours. A film with an average height of 2.75 μm was obtained with this growth duration.

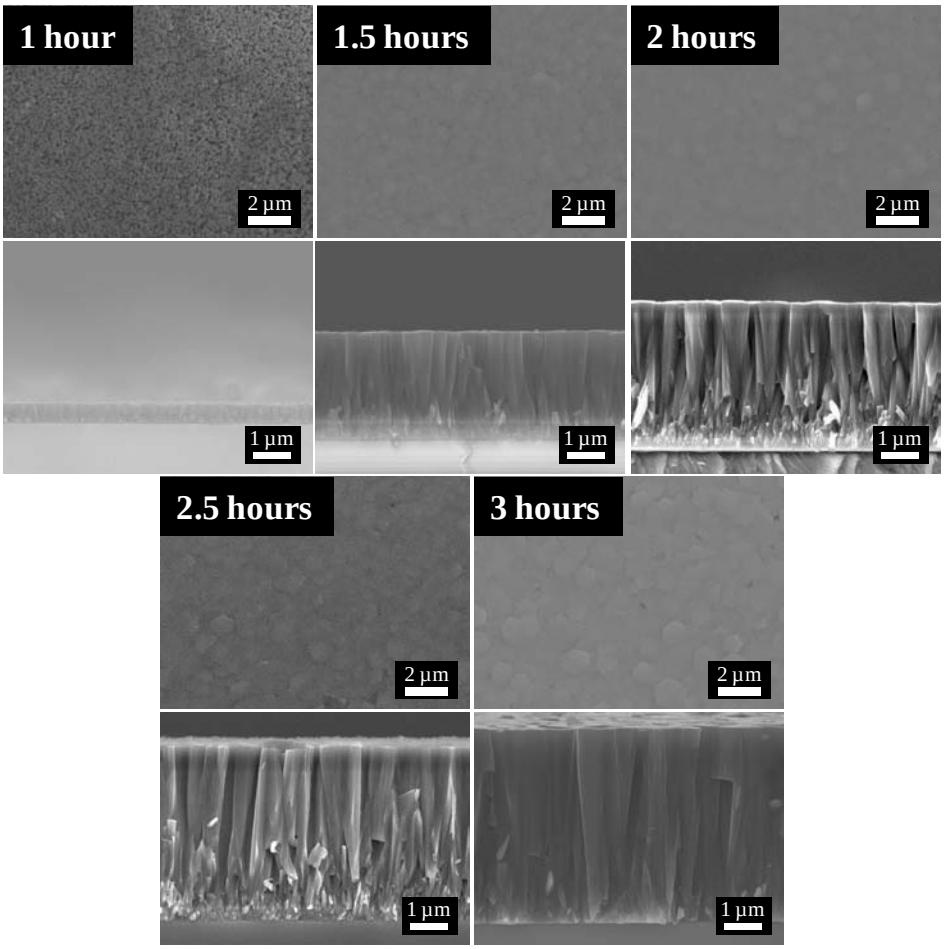

Figure 2.8. SEM images (top and cross-sectional views) of ZnO films of various growth duration for 50 mM growth solution and 0.97 mM of trisodium citrate.

Table 2.3. Summary of average height of ZnO films of various growth duration for 50 mM growth solution and 0.97 mM of trisodium citrate.

Duration (hours)	Average height (µm)
1	0.50
1.5	2.75
2	3.82
2.5	4.53
3	5.01

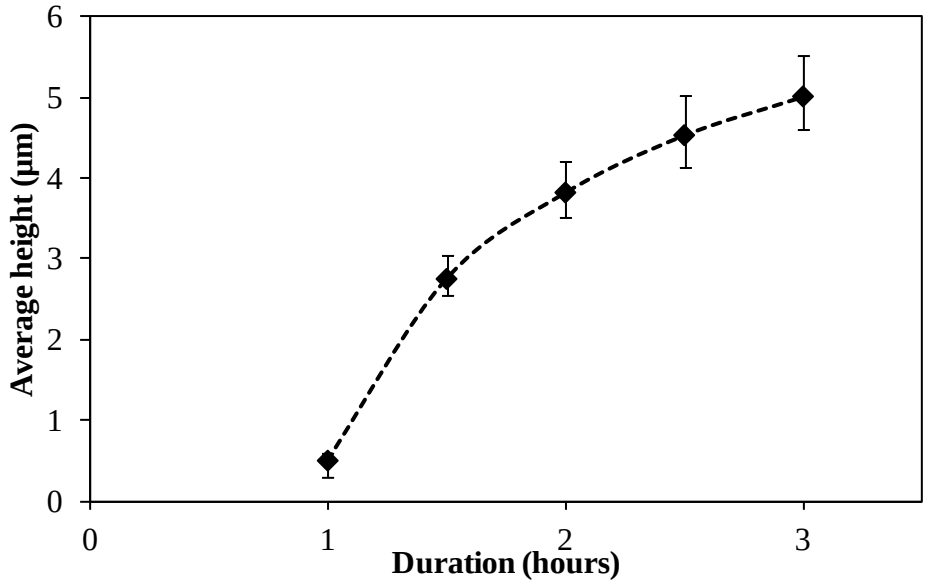

Figure 2.9. Plot of average height of ZnO films of various growth duration for 50 mM growth solution and 0.97 mM of trisodium citrate.

2.3.4 Materials characterization

The top view and cross-sectional SEM images of the ZnO films grown at the optimal parameters (50 mM zinc nitrate, 0.97 mM trisodium citrate, growth duration of 1.5 hours) are shown in Fig. 2.10. The films are well-coalesced and hexagonal shaped grains which are characteristic of the ZnO c-plane were observed on the surface of the film. From the cross-sectional SEM image, it can be seen that the nanowires are vertically aligned before coalescing together and a film thickness of about 2.75 µm was obtained. The cross-sectional TEM image of the film is shown in Fig. 2.10d. The film was observed to comprise of large single-crystal grains which emanated from the surface of the c-sapphire substrate. Fig. 2.10e shows the high resolution TEM (HRTEM) image of a single-crystal grain with the corresponding fast Fourier transform (FFT) image in Fig. 2.10f. The grains were of single crystalline structure and highly c-oriented in the out-of-plane direction.

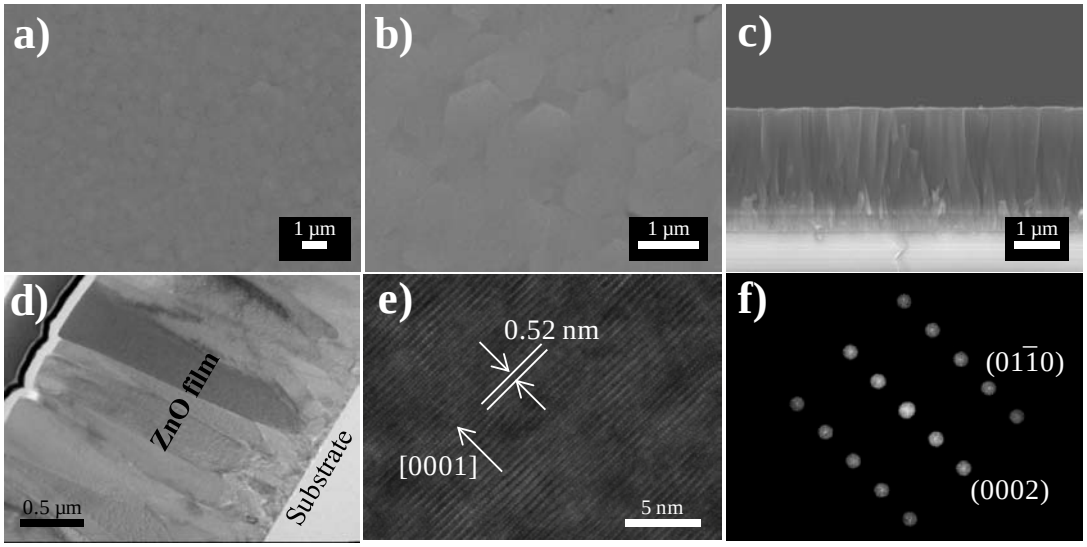

Figure 2.10. SEM images of as-synthesized ZnO film. Top view at (a) 8000x and (b) 20000x. (c) Cross-section view at 15000x. (d) Cross section TEM image of ZnO film. (e) HRTEM image of a single crystal grain within the film. (f) Fast Fourier transform (FFT) image of HTRTEM result.

XRD was carried out to characterize the crystallinity of the as-synthesized and NH_3 plasma treated ZnO films. The diffraction patterns of the pristine and plasma treated (120 s) films are shown in Fig. 2.11. The ZnO (002) and Al_2O_3 (006) peaks were present in the as-synthesized and plasma treated films, and similar diffraction pattern was also observed in the other plasma treated films of various treatment durations (JCPDS Card No. 79-0205). This implies that the crystallinity of the films is not degraded after plasma treatment. The presence of the ZnO (002) peak indicates that the films are crystallized in the wurzite phase and present a preferential orientation along the c-axis. However, a closer observation of the ZnO (002) peak (Fig. 2.11b) revealed a shift in the peak position towards a smaller diffraction angle for all the plasma treatment durations. From the Bragg diffraction law,

$$2d\sin\theta = \lambda \qquad (2.1)$$

The diffraction angle will become smaller when the lattice spacing increases. Therefore, the shift in the (002) peak indicates an increase in the lattice spacing after plasma treatment. This is most probably due to the incorporation of nitrogen-related

species from the NH_3 plasma into the lattice structure of the ZnO film. The species that was or were incorporated into the surface of the film during the NH_3 plasma treatment is expected to have an ionic radius larger than that of oxygen, in order to create an asymmetrical expansion of the crystal lattice.

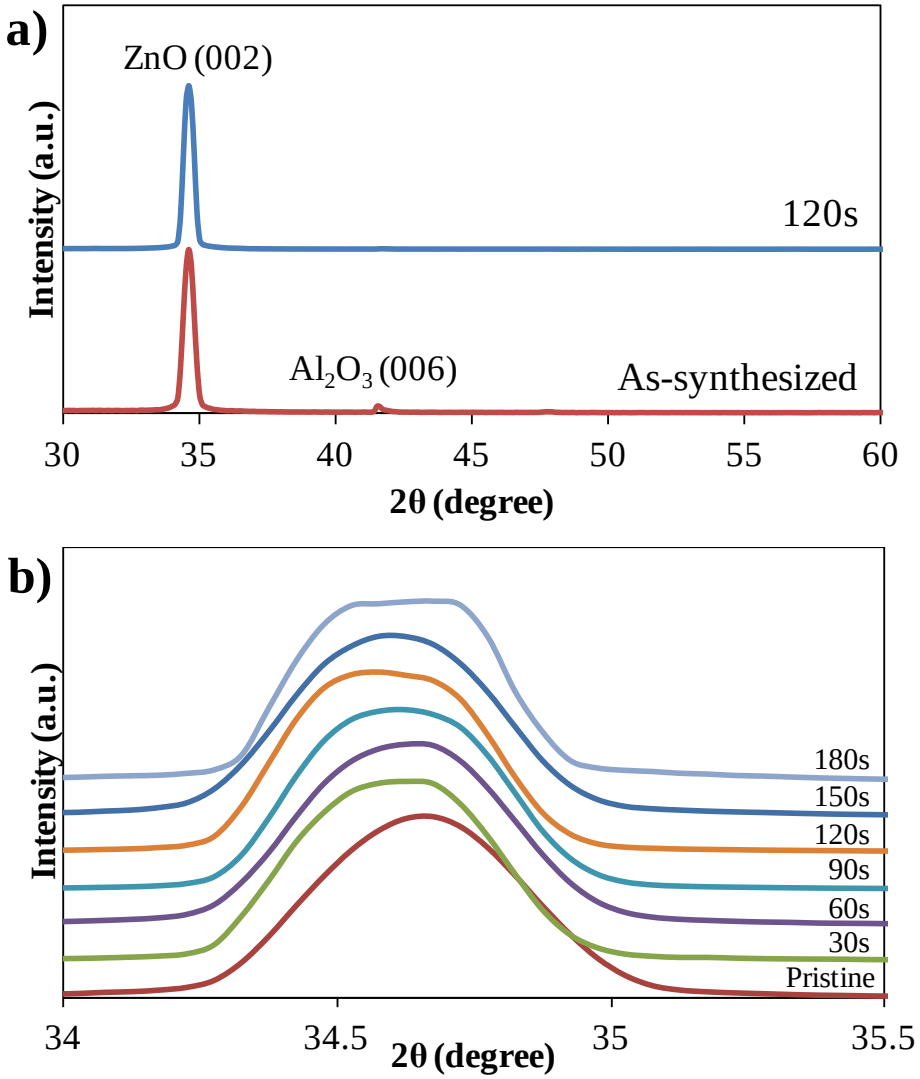

Figure 2.11. XRD pattern of (a) as-synthesized ZnO film and NH_3 plasma treated ZnO film (120 seconds), and (b) shift of (002) peak for various NH_3 plasma treatment durations.

Room temperature PL measurement was carried out on the ZnO films which were treated with NH_3 plasma for various durations and shown in Fig. 2.12. The PL spectrum of the pristine ZnO films consists of a visible emission band which peaks at 590 nm and a UV peak located at 381 nm. The UV peak is also known as near-band-

edge (NBE) emission which originates from free-excitons recombination through an exciton-exciton collision process.[35] The visible emission corresponds to deep level emission due to native defects including oxygen vacancies (V_O).[36] The intensity of the defect peak is higher than the UV peak, indicating the presence of a large amount of defects in the ZnO film. When the film was treated with NH_3 plasma, a reduction in the intensity of the visible emission was observed, suggesting a decrease in the amount of defects. The decrease in visible emission is probably due to the substitution of the defect sites by the nitrogen-related radicals from the NH_3 plasma. The amount of reduction in the intensity of the defect peak was noted to increase with the treatment duration. This suggests that the amount of nitrogen-related radicals incorporated into the ZnO film corresponds to the time duration of plasma treatment: the longer the treatment time, the greater the amount of radicals incorporated into the film, and the fewer the amount of defect sites remaining in the film. The native defects found in the film are n-type defects. Therefore, the reduction in the number of defects by the NH_3 plasma treatment reduces the n-type characteristics of the films.

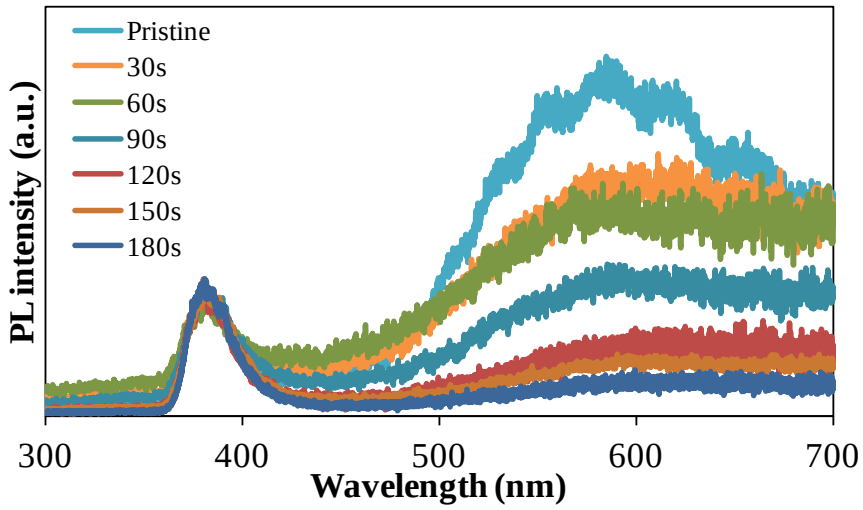

Figure 2.12. PL spectra of ZnO film treated for various durations.

Hall measurements were carried out to study the change in resistivity, Hall mobility, carrier concentration and conductivity type of the NH_3 plasma treated ZnO samples with respect to the plasma treatment duration. Good ohmic contacts between the electrodes and the film were confirmed before carrying out the measurements. The Hall measurement results are summarized in Table 2.4 and a plot to illustrate the relationship between the electrical properties and treatment duration is shown in Fig. 2.13. All of the NH_3 plasma treated ZnO films showed p-type conductivity regardless of the treatment duration, with average resistivity ranging from 0.57 to 95.52 Ω cm, average carrier concentration ranging from 1.13 X 10^{17} to 1.95 X 10^{18} cm^{-3} and average mobility from 0.3 to 5.67 cm^2/Vs. This conversion from n-type to p-type conductivity can be attributed to the incorporation of nitrogen-related radicals from the NH_3 plasma into the surface of the ZnO films.

Table 2.4. Average resistivities, mobilities and carrier concentrations of intrinsic and NH_3 plasma treated ZnO films.

Duration (s)	Average resistivity (Ω cm)	Average mobility (cm^2/Vs)	Average carrier concentration (x $10^{17}cm^{-3}$)	Carrier type (n/p)
0	95.52	0.35	1.90	n
30	73.35	0.30	2.83	p
60	7.01	1.61	5.53	p
90	0.57	5.67	19.48	p
120	7.15	1.61	2.54	p
150	42.7	0.91	1.61	p
180	63.33	0.87	1.13	p

The sample treated for 90 s showed the best electrical characteristics with the lowest average resistivity and highest average mobility and carrier concentration (Fig. 2.13). The samples treated for durations shorter or longer than 90 s exhibited poorer electrical properties with higher resistivity and lower mobility and carrier concentrations. When the treatment duration was 30 s, the amount of nitrogen-related

radicals incorporated into the surface of the ZnO films was sufficient for the sample to exhibit p-type electrical properties. As the treatment duration increased to 90 s, the amount of radicals from the NH_3 plasma being incorporated also increased, causing the resistivity to decrease while the mobility and carrier concentration increases, making the film more p-type. However, when the treatment duration increased beyond 90 s, the electrical properties of the treated ZnO films started to deteriorate. The resistivity was increased while the mobility and carrier concentration decreased. The large influx of nitrogen-related radicals into the ZnO film surface at treatment durations of more than 90 s degrades the ZnO film quality,[37] and induces compensation of the acceptor states to occur, thus reducing the p-type characteristics of the film.

The Hall results obtained are comparable to that of nitrogen-doped p-type ZnO reported in literature as shown in Table 2.5. Carrier concentrations ranging from 1.14 x 10^{14} cm^{-3} to 7.3 X 10^{17} cm^{-3} with corresponding mobility and resistivity in the range of 0.82 to 12 cm^2/Vs and 5.7 to 11000 Ω cm respectively were reported.[38-44] The resistivity (0.57 Ω cm) and carrier concentration (1.948 X 10^{18} cm^{-3}) of the ZnO film plasma treated for 90 s are better than these reported values. Although the mobility (5.67 cm^2/Vs) of the treated film is lower than the 12 cm^2/Vs reported by Minegishi,[40] it still outperforms the rest of the results in Table 2.5. From the Hall results, it is evident that NH_3 plasma can be an effective method to tune the electrical conductivity of ZnO films, and this method can possibly be extended to other ZnO nanostructures such as ZnO nanowires. Moreover, the plasma treatment was carried out without heating, thus making it possible to fabricate devices on substrates of low melting point such as plastics.

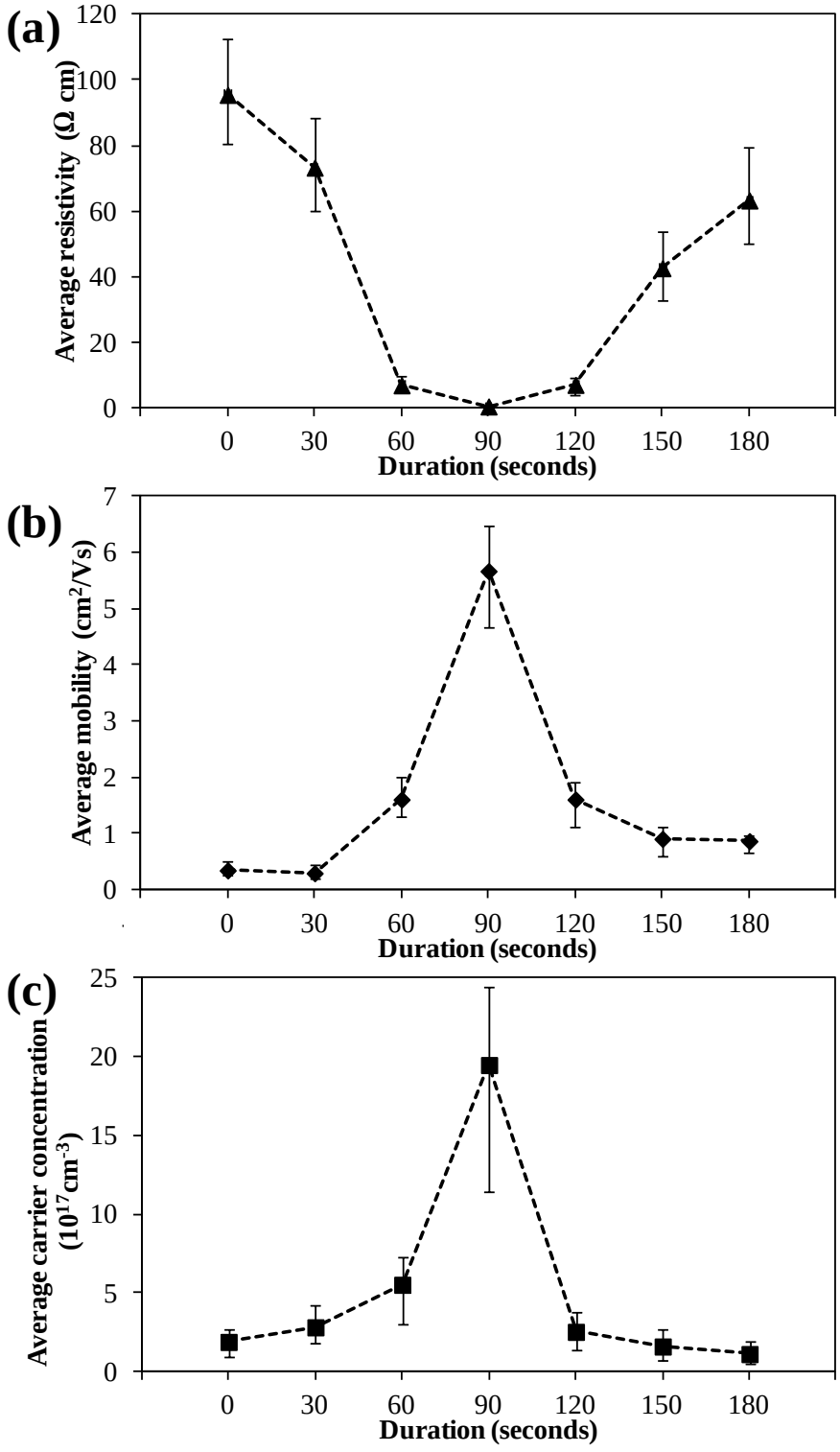

Figure 2.13. Plot of (a) average resistivity, (b) average mobility and (c) average carrier concentration of intrinsic and NH_3 plasma treated ZnO films against duration of plasma treatment.

Table 2.5. Nitrogen-doped p-type ZnO films reported in the literature.

Ref number	Technique	Dopant source	Resistivity (Ω cm)	Mobility (cm^2/Vs)	Carrier concentration (cm^{-3})
38	Plasma	NH_3	3.3×10^2	0.82	3.3×10^{16}
39	DC reactive magnetron sputtering	NH_3	1.1×10^4	4.1	1.14×10^{14}
40	CVD	NH_3	34	12	1.5×10^{16}
41	DC reactive magnetron sputtering	NH_3	31	1.3	7.3×10^{17}
42	MOCVD	NH_3	5.7	4.6	3.0×10^{17}
43	MBE	NO	78	0.18	4.45×10^{17}
44	MBE	N_2	40	2	9×10^{16}

XPS characterisation was carried out on the pristine ZnO film and the NH_3 plasma treated ZnO film with the best electrical properties (90 s) to identify the elements present in the film and the corresponding chemical states. Most importantly, it is to determine the presence of nitrogen and its chemical state. The XPS spectra in Fig. 2.14a show the Zn $2p_{3/2}$ peak obtained from the intrinsic ZnO film before and after surface modification with NH_3 plasma (treatment duration of 90 s). The peak for the intrinsic sample is located at 1021.7 eV which corresponds to Zn bonded to O in ZnO. However, after plasma treatment, the peak shifted to a higher binding energy of 1022.94 eV. This shift occurs because the symmetry of the crystal lattice has been degraded, causing the electrical cloud surrounding the Zn atom to be asymmetric.

Since the position of the Zn $2p_{3/2}$ core level is related to the charge and chemical environments around the Zn atom, the shift in peak position would imply the infusion of NH_3 complexes into the ZnO film during the plasma treatment,

creating an asymmetry in the lattice structure.[45] Besides the Zn $2p_{3/2}$ peak, the N1s peak was also detected in the plasma treated film. No nitrogen peak was detected in the pristine ZnO film, thus the N1s peak is contributed by the NH_3 plasma treatment. The presence of N1s peak in the XPS spectra of the treated ZnO film (Fig. 2.14b) shows that nitrogen-based radicals have been successfully incorporated into the film by NH_3 plasma. The N1s peak is centered at 399 eV and deconvolution of the N1s peak revealed two peaks centered at 398.6 eV and 399.8 eV, which can be attributed to the N-Zn and N-H bonds respectively.[38] The higher binding energy peak 399.8 eV related to N ion corresponds to amines, N-H,[38] and it can be derived from the hydrogen-passivated N acceptor or N-H radicals. The peak related to the N-Zn bond has a slightly lower intensity than the N-H peak. This indicates a lower concentration of N-Zn bonds relative to N-H pairs in the treated ZnO film and suggests low solubility of N acceptor. No substitutional N_2 molecules at oxygen sites (404.2 eV)[46] and also no N-O bonds (407 eV)[47] were found in the ZnO films after NH_3 plasma treatment.

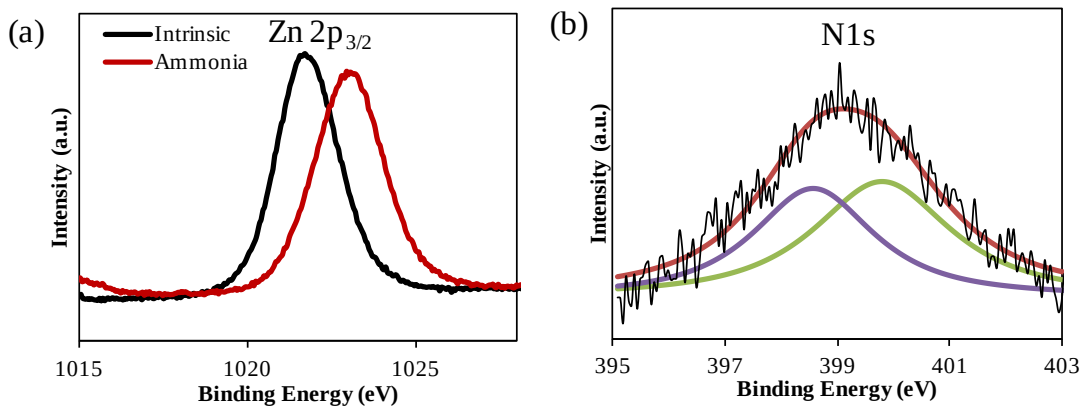

Figure 2.14. XPS spectra of (a) Zn 2p3/2 peak obtained from the ZnO films before and after NH_3 plasma treatment, and (b) N1s peak from ZnO films after NH_3 plasma treatment.

The results from the XPS can explain the trends observed in the XRD and PL spectra. The shift in the XRD peak Zn (002) is due to the incorporation of N-H pairs

into the surface of the ZnO film. The ionic radius of N-H is bigger than that of oxygen, thus their incorporation into the ZnO films causes asymmetry expansion of the crystal lattice, and a shift of the (002) to a smaller angle. The reduction in the visible emission band of the PL spectra is also due to the occupation of N-H atom pair on the defect sites.[39] N-H will most likely be incorporated into oxygen substitute site (V_O) since the valence charge and activation energy of the N-H is similar to that of oxygen.[39] Therefore, when the plasma treatment duration was increased, the amount of N-H pairs incorporated into the defect sites also increased, causing the amount of defects in the film and the corresponding intensity of the emission peak in the PL spectra to decrease.

This surface modification technique which introduces a variety of atomic and molecular radicals (N, H, NH, and NH_2)[48] into ZnO lattices through NH_3 plasma was successful in tuning the electrical conductivity from n to p-type. The NH_3 plasma treatment actually involves a competitive process of simultaneous introduction and compensation of acceptors resulting from the NH_3 plasma. Essentially, N radicals from the NH_3 plasma can be incorporated into the ZnO lattice in at least two chemical states, either as a N_2 molecule or a N atom occupying an O site. However, it is evident from the XPS results that N_2 does not exist in the ZnO film since the peak at binding energy of 404 eV is absent. The peak at 398.6 eV indicates that N radicals from NH_3 are incorporated substitutionally at O sites. As for atomic radical H from the NH_3 plasma, an isolated interstitial H is exclusively a donor in ZnO. Moreover, passivation of the acceptors by hydrogen impurities leads to a reduction in hole concentration.[49] First-principles calculations have shown that nitrogen acceptors may be compensated via the formation of defects such as oxygen vacancies,[50] zinc antisites, and complexes with zinc interstitials or N_2 molecules.[51-53] However, the presence of neutral N–H

complexes can prove to be useful in achieving high p-type conductivity. In contrast to N acceptors, neutral N-H complexes do not result in the formation of compensating n-type defects. The N–H complexes has no effect on reducing the electron concentration since it is electrically inactive. Thus, optimization of annealing temperature (not in this present work) to dissociate N-H complexes after NH_3 plasma treatment can be used to activate a large concentration of N acceptors to achieve high p-type conductivity.[49] The occupation of N-H complexes at the oxygen vacancy sites may also aid in reducing the oxygen vacancy related n-type defects, hence making the ZnO films less n-type.

2.4 Conclusions

ZnO films were grown on c-sapphire substrates via the hydrothermal method and the growth parameters were varied to understand the optimal parameters needed to produce a fully coalesced film with the shortest growth duration. It was observed that as the precursor concentration increased, both the diameter and height of the nanowires also increased, and begin to approach a film-like morphology at a precursor concentration of 100 mM. The minimum amount of trisodium citrate needed to form a smooth film was 0.97 mM. However, the height of the film decreased with increasing amounts of trisodium citrate. This is because the citrate anions ions adhere to the positively charged Zn-terminated (0001) plane, hence reducing the growth rate in the upward direction, resulting in shorter films. When the growth duration was increased, the height of the film also increased, and a time of 1.5 hrs was sufficient for the film to fully coalesce. Effective tuning of the electrical conductivity of hydrothermally synthesized ZnO films by surface modification using NH_3 plasma without heat treatment was demonstrated. The XRD results show that the plasma treatment does not degrade the crystallinity of the films. The incorporation of

the N-H complexes also aids in reducing the number of defects present in the film as observed in the PL spectra. Hall measurements of the modified ZnO films revealed p-type conductivity with resistivity ranging from 0.57 to 95.52 Ω cm, carrier concentration ranging from 1.13 X 10^{17} to 1.95 X 10^{18} cm^{-3} and mobility from 0.3 to 5.67 cm^2/Vs. The presence of a N1s peak in the XPS spectrum of the surface modified ZnO film indicates the successful incorporation of NH_3 complexes into the film. The results obtained shows that NH_3 plasma treatment is a feasible way to tune the electrical conductivity of ZnO films.

References

1 Pearton S J, Norton D P, Ip K, Heo Y W and Steiner T 2005 *Prog. Mater. Sci.* **50** 293

2 Sun X W, Yu S F, Xu C X, Yuen C, Chen B J and Li S 2003 *Jpn. J. Appl. Phys. Part 2* **42** 1229

3 Minami T 2005 *Semicond. Sci. Technol.* **20** S35

4 Chen J J, Zeng F, Li D M, Niu J B and Pan F 2005 *Thin Solid Films* **485** 257

5 Yamazaki O, Mitsuyu T and Wasa K 1980 *IEEE Trans. Sonics Ultrason.* **27** 369

6 Gao T and Wang T H 2005 *Appl. Phys. A* **80** 1451

7 Ding G Q, Zheng M J, Xu W L and Shen W Z 2005 *Nanotechnology* **16** 1285

8 Tang Z K, Wong G K L and Yu P 1998 *Appl. Phys. Lett.* **72** 3270

9 Service R F 1997 *Science* **276** 895

10 Dai J N, Liu H C, Fang W Q, Wang L, Pu Y, Chen Y F and Jiang F Y 2005 *J. Cryst. Growth* **283** 93

11 Zhao B J, Yang H J, Du G T, Miao G Q, Zhang Y T, Gao Z M, Yang T P, Wang J Z, Li W C, Ma Y, Yang X T, Liu B Y, Liu D L and Fang X J 2003 *J. Cryst. Growth* **258** 130

12 Pierce J M, Adekore B T, Davis R F and Stevie F A 2005 *J. Cryst. Growth* **277** 345

13 Dadgar A, Oleynik N, Forster D, Deiter S, Witek H, Blasing J, Bertram F, Krtschil A, Diez A, Christen J and Krost A 2004 *J. Cryst. Growth* **267** 140

14 Smith T P, McLean H A, Smith D J, Miraglia P Q, Roskowski A M and Davis R F 2004 *J. Electron. Mater.* **33** 826

15 Oleynik N, Dadgar A, Blasing J, Adam M, Krtschil A, Forster D, Bertram F, Diez A, Seip M, Greiling A, Christen J and Krost A 2003 *Jpn. J. Appl. Phys. Part 1* **42** 7474

16 Smith T P, Mecouch W J, Miraglia P Q, Roskowski A M, Hartlieb P J and Davis R F 2003 *J. Cryst. Growth* **257** 255

17 Kumar M, Mehra R M, Wakahara A, Ishida M and Yoshida A 2005 *Thin Solid Films* **484** 174

18 Wang R P, Muto H, Yamada Y and Kusumori T 2002 *Thin Solid Films* **411** 69

19 Vispute R D, Talyansky V, Choopun S, Sharma R P, Venkatesan T, He M, Tang X, Halpern J B, Spencer M G, Li Y X, Salamanca- Riba L G, Iliadis A A and Jones K A 1998 *Appl. Phys. Lett.* **73** 348

20 Oh D C, Suzuki T, Kim J J, Makino H, Hanada T, Cho M W, Yao T, Song J S and Ko H J 2005 *J. Vac. Sci. Technol. B* **23** 1281

21 Jang K W, Minegishi T, Suzuki T, Hong S K, Oh D C, Hanada T, Cho M W and Yao T 2005 *J. Ceram. Process. Res.* **6** 167

22 Oh D C, Setiawan A, Kim J J, Ko H, Makino H, Hanada T, Cho M W and Yao T 2004 *Curr. Appl. Phys.* **4** 625

23 Hong S K, Chen Y, Ko H J, Wenisch H, Hanada T and Yao T 2001 *J. Electron. Mater.* **30** 647

24 Walukiewicz W 1994 *Phys. Rev. B* **50** 5221

25 Look D C, Hemsky J W and Rizelove J R 1999 *Phys. Rev. Lett.* **82** 2552

26 Zhang S B, Wei S H and Zunger A 2001 *Phys. Rev. B* **63** 075205

27 Park C H, Zhang S B and Wei S H 2002 *Phys. Rev. B* **66** 073202

28 Jiao S J, Zhang Z Z, Lu Y M, Shen D Z, Yao B, Zhang J Y, Li B H, Zhao D X, Fan X W and Tang Z K 2006 *Appl. Phys. Lett.* **88** 031911

29 Allenic A, Guo W, Chen Y B, Katz Y B, Zhao G Y, Che Y, Hu Z D, Liu B, Zhang S B and Pan X Q 2007 *Adv. Mater. (Weinheim, Ger.)* **19** 3333

30 Ye J D, Gu S L, Zhu S M, Liu W, Liu S M, Zhang R, Shi Y and Zheng Y D 2006 *Appl. Phys. Lett.* **88** 182112

31 Wang P, Chen N F and Yin Z G 2006 *Appl. Phys. Lett.* **88** 152102

32 Özgür Ü, Alivov Ya I, Liu C, Teke A, Reshchikov M A, Doğan S, Avrutin V, Cho S -J and Morkoç H 2005 *J. Appl. Phys.* **98** 041301

33 Look D C, Claflin B, Alivov Ya I and Park S J 2004 *Phys. Status Solidi A* **201** 2203

34 Lange F F 1996 *Science* **273** 903

35 Umar A, Karunagaran B, Suh E K and Hahn Y B 2006 *Nanotechnology* **17** 4072

36 Mensah S L, Kayastha V K, Ivanov I N, Geohegan D B and Yap Y K 2007 *Appl. Phys. Lett.* **90** 113108

37 Wang H, Ho H P, Lo K C and Cheah K W 2007 *J. Phys. D: Appl. Phys.* **40** 4682

38 Cao P, Zhao D X, Zhang J Y, Shen D Z, Lu Y M, Yao B, Li B H, Bai Y and Fan X W 2008 *Appl. Surf. Sci.* **254** 2900

39 Huang J Y, Ye Z Z, Chen H H, Zhao B H and Wang L 2003 *J. Mat. Sci. Lett.* **22** 249

40 Minegishi K, Koiwai Y, Kikuchi Y, Yano K, Kasuga M and Shimizu A 1997 *Jpn. J. Appl. Phys.* **36** L1453

41 Lu J G, Zhang Y Z, Ye Z Z, Wang L, Zhao B H and Huang J Y 2003 *Mater. Lett.* **57** 3311

42 Pan M, Nause J, Rengarajan V, Rondon R, Park E H and Ferguson I T 2007 *J. Electron. Mater.* **36** 457

43 Sun J W, Lu Y M, Liu Y C, Shen D Z, Zhang Z Z, Li B H, Zhang J Y, Yao B, Zhao D X and Fan X W 2006 *Solid State Commun.* **140** 345

44 Look D C, Reynolds D C, Litton C W, Jones R L, Eason D B and Cantwell G 2002 *Appl. Phys. Lett.* **81** 1830

45 Xiao Z Y, Liu Y C, Zhang J Y, Zhao D X, Lu Y M, Shen D Z and Fan X W 2005 *Semicond. Sci. Technol.* **20** 796

46 Ahn K S, Yan Y F, Lee S H, Deutsch T, Turner J, Tracy C E, Perkins C L and Jassim M A 2007 *J. Electrochem. Soc.* **154** B956

47 Bian J M, Li X M, Gao X D, Yu W D and Chen L D 2004 *Appl. Phys. Lett.* **84** 541

48 Kang S J and Donnelly V M 2007 *Plasma Sources Sci. Technol.* **16** 265

49 Jokela S J and McCluskey M D 2007 *Phys. Rev. B* **76** 193201

50 Janotti A and Van de Walle C G 2005 *Appl. Phys. Lett.* **87** 122102

51 Lee E- C, Kim Y -S, Jin Y -G and Chang K J 2001 *Phys. Rev. B* **64** 085120

52 Park C H, Zhang S B and Wei S -H 2002 *Phys. Rev. B* **66** 073202

53 Limpijumnong S, Li X, Wei S -H and Zhang S B 2005 *Appl. Phys. Lett.* **86** 211910

Chapter 3 Synthesis of ZnO Nanowires and Ammonia Plasma Modification Towards P-type Conductivity

In this chapter, ZnO nanowires are synthesized by the hydrothermal method. Variation in the growth parameters is carried out to obtain a better understanding of the growth mechanism and also to study the effect of growth parameters on the physical attributes of the nanowires such as diameter and height. Transfer of the nanowires from Si substrate to the flexible polyethylene terephthalate substrate is also demonstrated. The as-synthesized nanowires are treated with ammonia plasma for a duration of 90 seconds without deliberate heating and the changes in electrical properties are studied. A P-N junction was fabricated and room temperature hydrogen gas sensing measurements are carried out using the treated nanowires.

3.1 Introduction

ZnO has been used as liquid-crystal displays, energy-efficient white lighting, room temperature gas sensors,[1] transparent conductor in solar cells and transistors. The combination of a large direct band-gap of 3.37 eV and 60 meV excitonic binding energy[2] has promoted ZnO as the next generation of electronic and optoelectronic materials.[3] ZnO nanowires are of interest because nanoscale devices with arrays of ZnO nanowires are expected to deliver enhanced performance and unique functions with diverse applications as compared to thin film counterparts. The traditional approaches to synthesize ZnO nanowires are the vapour-phase transport process with the assistance of metal catalysts, thermal evaporation and template-assisted growth.[4-6] However, the introduction of catalysts or templates involves a much more complicated process and may introduce impurities into the final product. The vapour-phase synthesis methods also involve high temperature and high cost vacuum setups.[7] Therefore, the simple, fast, less expensive, low growth temperature, high yield and

scalable hydrothermal growth method will be a better choice to synthesize ZnO nanowires.[8]

Similar to ZnO thin film devices, the success of ZnO nanowires devices depends on the ability to control and tune transport and electrical properties effectively and economically. However, doping remains a challenge for nanostructured materials. Non-reproducible and non-uniform doping often occurs due to limited access of dopants in the nanoscale structure. Other issues reported are unstable doping due to self-compensating doping, low dopant solubility and complex doping procedures. Recently, p-type conduction was observed in phosphorus-doped ZnO nanowire arrays,[9] however they switched to n-type after two months of storage in an ambient environment. Despite the considerable efforts that have been carried out to tune ZnO nanostructures' electrical properties, low temperature and facile tuning of carrier density in one dimensional ZnO nanowires is not available.

In this chapter, the hydrothermal method is used to synthesize ZnO nanowires and the growth parameters are varied to study the effect on the physical attributes of the nanowires such as diameter and height. Through this study on the growth parameters, a better understanding of the growth mechanism is obtained. Three methods of transferring the as-synthesized nanowires from Si substrate to the flexible polyethylene terephthalate (PET) substrate are also demonstrated and discussed. An easy surface modification of the ZnO nanowires using ammonia (NH_3) plasma which results in an effective tuning of ZnO nanowires' conductivity is then carried out. The variation of electron concentration at the surface of the ZnO nanowires dictates the sensing and electrical properties. To the best of our knowledge, there are no reports on p-type conductivity ZnO nanowires by surface modification using NH_3 plasma with no heat treatment. With the synthesis and plasma treatment both conducted at low

temperature, this technique not only provides a low-cost and easy implementation of electrical properties modification, but also a processing flow compatible with silicon technologies. In addition, it provides a feasible methodology to fabricate devices on flexible substrates with surface modified ZnO nanowires. Most importantly, the resulting functional groups on ZnO nanowires are stable in air for more than a year.

3.2 Experimental procedures

ZnO nanowires were synthesized via the simple and low temperature hydrothermal method,[10,11] consisting of a seeding step followed by the growth step. The 100 nm thick seed layer was coated onto the Si substrates by radio-frequency (RF) magnetron sputtering (Denton Vacuum Discovery 18 system) at 450 ^{o}C. The elevated temperature during the sputtering process ensures good crystallinity of the sputtered ZnO layer. The presence of the ZnO seed layer encourages growth of the ZnO nanowires and it also serves to reduce the lattice mismatch between ZnO and the substrate. The seeded substrates were then placed into the precursor solution containing hexamethylenetetramine (HMT), zinc nitrate hexahydrate and poly(ethyleneimine) solution (PEI) in 25 ml of de-ionized (DI) water, and heated at 90 °C for several hours. Zinc nitrate and HMT were always added to the growth solution in 1:1 molar ratio regardless of the concentration. Variation in the growth parameters was carried out to obtain a better understanding of the growth mechanism and also to study the effect of growth parameters on physical attributes of the nanowires such as diameter and height. The growth parameters varied were: (i) growth solution concentration (5 to 100 mM), (ii) amount of PEI (0 to 0.5 g), and (iii) growth duration (0.5 to 6 hours). Based on the results from these studies, the optimal set of experimental parameters consisting of 25 mM zinc nitrate, 25 mM HMT, 0.05 g

PEI and growth duration of 6 hours were derived and used to synthesize ZnO nanowires for further studies.

The as-synthesized nanowires were then transferred to a flexible polyethylene terephthalate (PET) substrate via 3 methods, namely: slide transfer, roll transfer and heat transfer. In the slide transfer method, the silicon substrate with the ZnO nanowires (donor) was placed face down onto the PET substrate (receiver) and slid against the receiver by applying gentle pressure as shown in Fig. 3.1a. For the roll transfer method, the receiver substrate was first placed firmly on a flat substrate and the donor substrate was then placed face down on top of the receiver. A cylindrical rod was then positioned onto the donor substrate and rolled from one end to the other to transfer the ZnO nanowires onto the receiver substrate (Fig. 3.1b). To transfer nanowires using the heat transfer method, the receiver substrate (PET) was first placed on a hotplate at 180 °C, just slightly higher than the glass transition temperature (T_g) of PET. A piece of donor substrate of a size slightly smaller than the receiver substrate was then placed on top of the PET and left there for 30 minutes. After 30 minutes, the substrates were left to cool down to room temperature and the donor substrate was gently removed from the receiver substrate. A schematic illustration of the steps is shown in Fig. 3.1c. The nanowires grown on substrate were treated with NH_3 plasma and the carrier characteristics of the treated ZnO nanowires were investigated. The samples were plasma treated for 90 seconds at a pressure of 0.4 mbar with a RF power of 250 W.

Several characterizations and device fabrication were carried out on the intrinsic and treated ZnO nanowires. Scanning electron microscopy (SEM, JEOL FEG JSM 6700 F) and transmission electron microscopy (TEM, Phillips FEG CM300) characterized the morphology of the synthesized products. X-ray photoelectron spectroscopy (XPS)

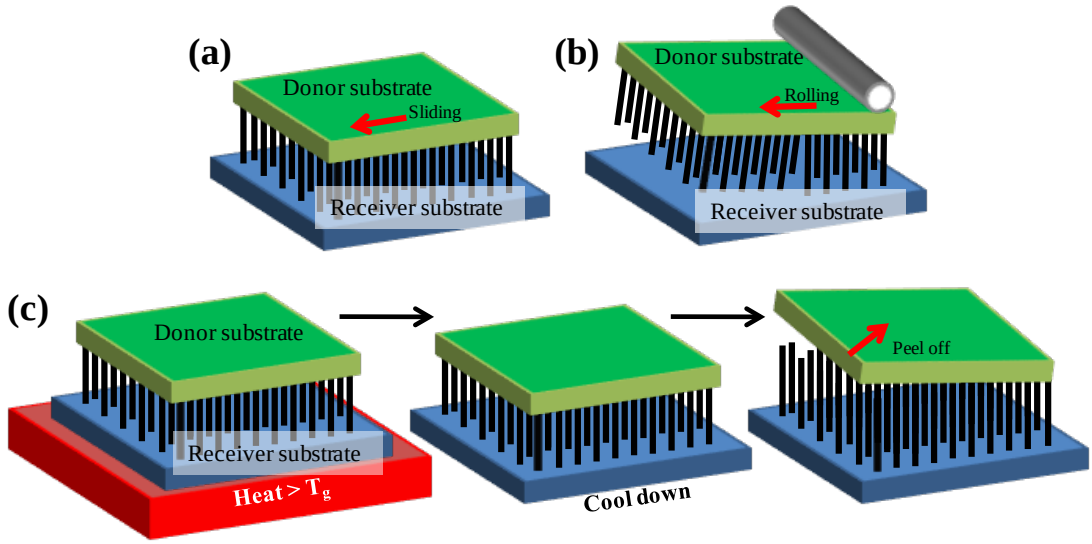

Figure 3.1. Schematic diagrams of (a) Slide transfer method, (b) Roll transfer method, and (c) Heat transfer method.

was employed to study the elemental composition of the intrinsic and NH_3 plasma treated ZnO nanowires. X-ray diffraction (XRD, Philips X-ray diffractometer equipped with graphite-monochromated Cu Kα radiation at λ = 1.541 Å) characterized the crystal structures of the ZnO nanowires.

The room temperature photoluminescence (PL) of the nanowires was measured by micro-PL with a He-Cd laser at 325 nm. Low-temperature PL measurement was performed at 5 K in a helium closed cycle cryostat using the 325 nm line of a He-Cd laser. The Hall measurements were carried out on 1 x 1 cm^2 samples using the Van der Pauw sample configuration at room temperature with a Bio-Rad Hall system. The hydrogen gas sensors were fabricated by sputtering Pt electrodes onto the nanowires sample, with a 10 μm gap and attaching copper wires to the electrodes with silver paste. Flexible sensors on plastic substrates can be fabricated by transferring the synthesized nanowires onto the PET substrate via the three transfer methods described previously. The hydrogen gas sensors were tested in hydrogen ambient of various concentrations at room temperature. A p-n homojunction was formed between NH_3 plasma treated ZnO nanowires on n-type ZnO seed layer.

Metal contacts were fabricated by evaporating aluminum (Al) on the seed layer and platinum (Pt) onto the treated nanowires. A Metal-Oxide-Semiconductor (MOS) capacitor was also fabricated by spin coating PMMA onto the ZnO nanowires to fill the gaps. A layer of SiO_2 (20 nm) was then sputtered on the nanowires followed by Cr/Au (10/100 nm) as the metal contact to form the capacitor. For the formation of ohmic contacts on the seed layer, Cr/Au was deposited on the intrinsic ZnO seed layer while Pt was deposited on the NH_3 plasma treated seed layer. The current-voltage (I-V) and capacitance-voltage (C-V) measurements were carried out using a Keithley 4200-SCS semiconductor characterization system.

3.3 Results and discussion

3.3.1 Effect of precursor concentration

The precursor concentration was varied from 5 to 100 mM without the addition of any surfactant to study the effect of precursor concentration on diameter and height of the nanowires. Since the concentrations of zinc nitrate and HMT in the precursor solution were always fixed at a ratio of 1:1, a solution with precursor concentration of 5 mM will contain 5 mM of zinc nitrate and 5 mM of HMT. From the SEM images shown in Fig. 3.2, it was observed that as the concentration of the precursor solution increased from 5 to 100 mM, the average diameter and height of the nanowires also increased from 40.2 to 395.7 nm and 0.82 to 2.05 μm respectively.

A summary of the average diameter and height of the nanowires grown at various precursor concentrations is presented in Table 3.1. Since the height of the nanowires increases with precursor concentration, it could be possible to obtain long nanowires by growing in highly concentrated precursor solutions. However, this is not a feasible approach for growing long nanowires, especially nanowires with high aspect ratio, because when the precursor concentration increases, both the height and

diameter increases with the precursor concentration. Moreover, at a concentration of 100 mM, the large diameter nanowires were observed to coalesce and form a film-like morphology. This could instead be a possible approach to synthesize ZnO films. One way to obtain tall nanowires with high aspect ratio will be to retard the increase in the diameter of the nanowires by adding surfactants (e.g. PEI) into the growth solution. The PEI molecules in the solution will restrict the growth in the lateral direction.

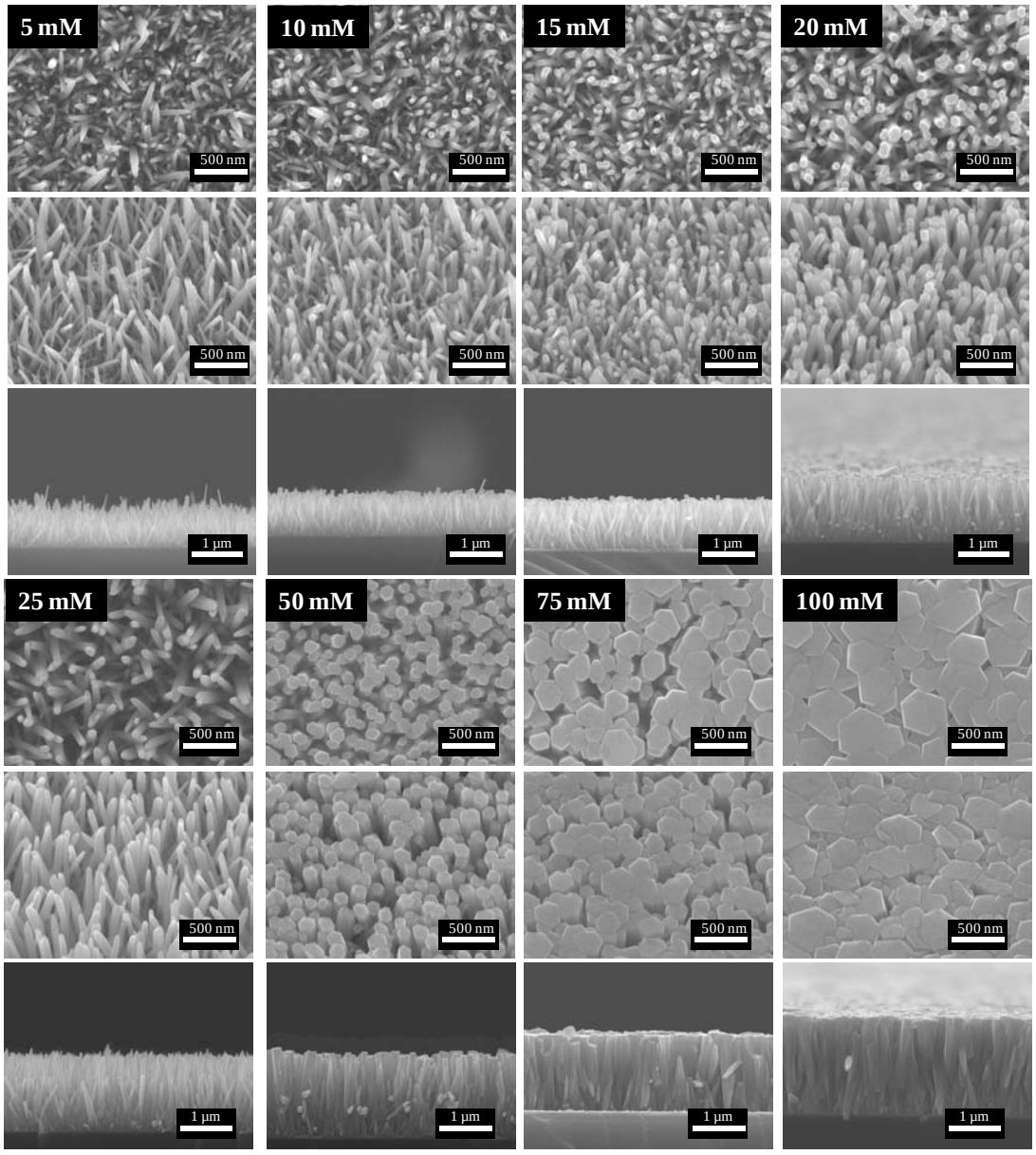

Figure 3.2. SEM images (top, 30° titled and cross-sectional views) of ZnO nanowires with varying precursor concentrations.

Table 3.1. Average diameter and height of nanowires for varying precursor concentrations.

Concentration (mM)	Average diameter (nm)	Average height (µm)
5	40.2	0.82
10	45.4	0.86
15	49.1	1.12
20	70.5	1.38
25	73.2	1.40
50	120.3	1.53
75	252.2	1.65
100	395.7	2.05

The plot of the average diameter and height of the nanowires against the precursor concentration is shown in Fig. 3.3. From these results, it was observed that nanowires with diameters less than 100 nm were obtained from precursor concentrations of 25 mM or less. Among these nanowires, the tallest nanowires with an average height of 1.4 µm were obtained at a precursor concentration of 25 mM. Therefore, the optimum precursor concentration is 25 mM.

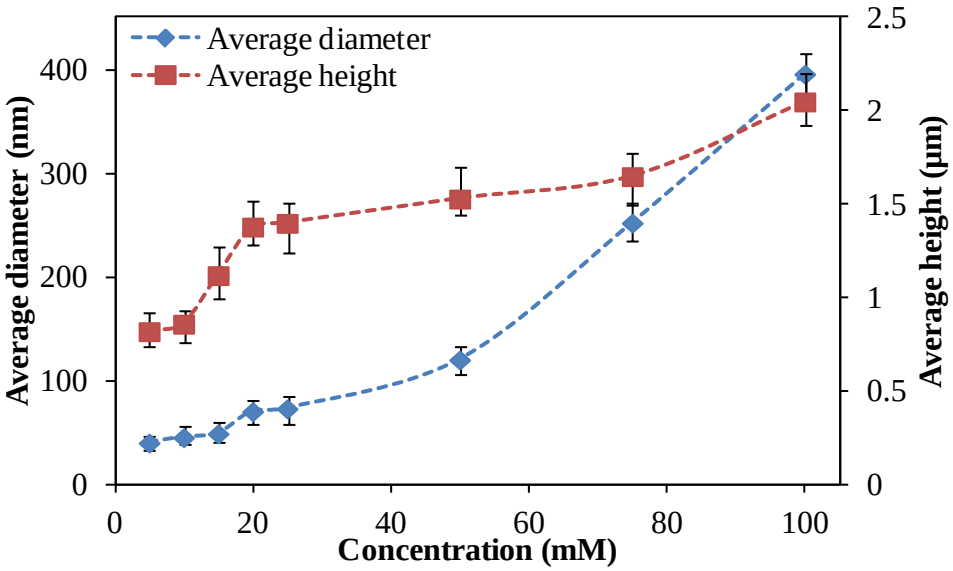

Figure 3.3. Plot of average diameter and height of nanowires for varying precursor concentrations.

3.3.2 Effect of PEI amount

It was previously mentioned that surfactants can be added into the growth solution to retard the increase in the diameter of the nanowires by restricting the growth in the lateral direction. One very popular surfactant used for ZnO nanowires is PEI, a non-polar polymer with a large quantity of side amino-groups ($–NH_2$), which can be protonated and positively charged over a wide range of pH values (3–11).[12] The pH value of the growth solution falls within this range, thus producing protonized PEI molecules in the solution. ZnO has a polar hexagonal wurtzite structure, which consists of the positive top Zn^{2+} plane (001), the negative basal O^{2-} plane (00-1) and the non-polar (-100), (-110) and (0-10) facets. The positive (001) facet has the highest surface energy, resulting in the fastest growth rate along the c-axis. During growth, the sides facets of the ZnO nanowires should be negatively charged because the potential of zero charge point (ZCP) of ZnO is 7.2.[13] Therefore, the positively charged PEI molecules will be adsorbed on the negative facets, acting as capping agents to hinder the lateral growth of ZnO nanowires (Fig. 3.4). In contrast, growth solutions without PEI displayed a higher lateral growth rate under the same growth conditions.

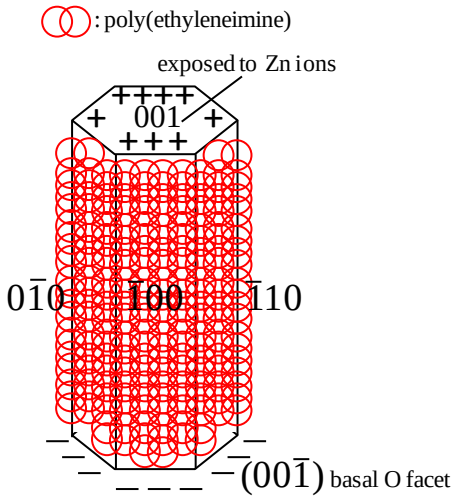

Figure 3.4. Polar facets of ZnO nanowire and effect of PEI.

Four different amounts of PEI were added to a 25 mM growth solution: 0.05, 0.1, 0.25 and 0.5 g. The SEM images of the nanowires grown are shown in Fig. 3.5. It can be seen that the diameter of the nanowires decreased after adding PEI while the height increased. The results are summarized in Table 3.2.

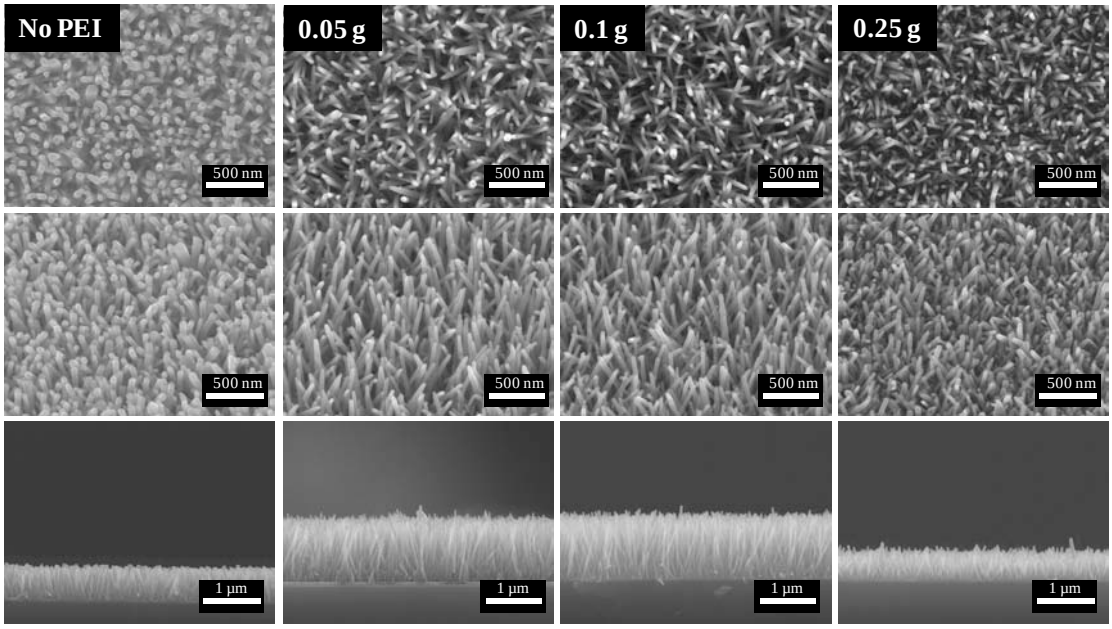

Figure 3.5. SEM images (top, 30° titled and cross-sectional views) of ZnO nanowires with various amounts of PEI solution added.

Table 3.2. Average diameter and height of nanowires for various amounts of PEI added

Amount of PEI (g)	Average diameter (nm)	Average height (µm)
0.00	51.0	0.75
0.05	32.3	1.15
0.10	30.0	1.15
0.25	31.9	0.58
0.50	No growth	No growth

When the amount of PEI in the growth solution increases from 0 to 0.1 g, the amount of positively charged PEI molecules attached to the side planes of the nanowires also increases. This slows down the lateral growth of the nanowires and causes more reactants to be available for the upward growth, thus producing thinner and taller nanowires. However, when 0.25 g of PEI was added to the growth solution,

the nanowires did not grow thinner and taller. Instead, the height of the nanowires decreased by about 50 % compared to those grown with 0.10 g of PEI. This decrease in height of the nanowires with an increased amount of PEI could be due to the PEI molecules attaching to some of the ZnO nuclei in solution, restricting the growth and reducing the amount of precursors available, hence resulting in shorter nanowires. When the amount of PEI added was further increased to 0.5 g, large amounts of protonized PEI molecules present in the solution will attach to the ZnO nuclei and ZnO nanowires at a very early stage of growth, hence terminating the growth of the nanowires prematurely. From the results, it can be seen that an amount of PEI between 0.05 g and 0.1 g will be ideal for the growth of thin and long nanowires. However, 0.05 g of PEI will be used for subsequent synthesis of nanowires so as to achieve a recipe which requires only minimal amounts of precursors. A plot of the average diameter and height of the nanowires is shown in Fig. 3.6.

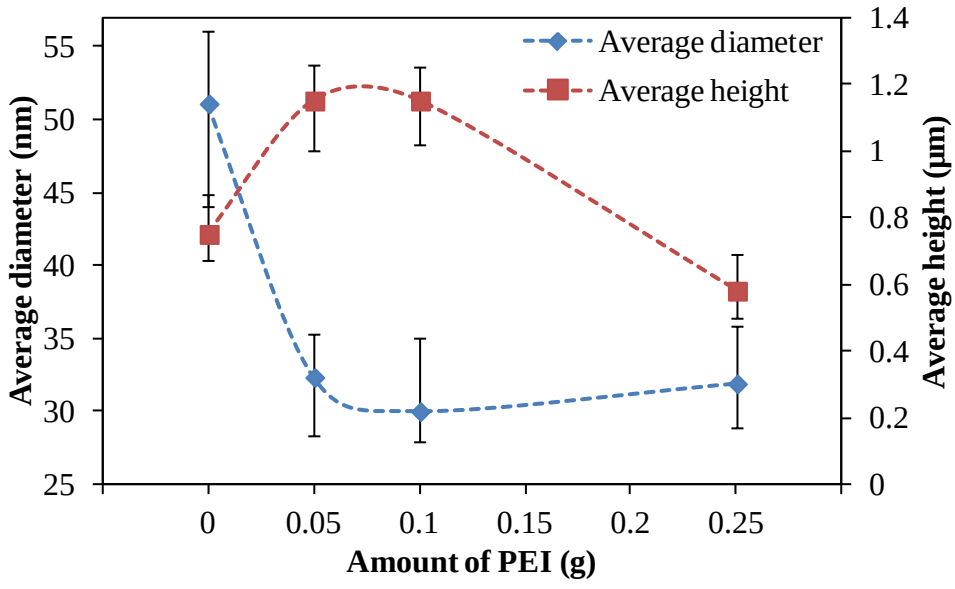

Figure 3.6. Plot of average diameter and height of nanowires for various amounts of PEI added

The effect of adding PEI can also be observed in a 100 mM growth solution (Fig. 3.7). When 0.05 g of PEI was added, a film-like morphology was obtained.

However, when the amount of PEI was increased to 0.2 g, ZnO nanowires could be observed and there was an increase in height from 1.7 µm to 2 µm due to the channelling of the precursors towards the upward growth rather than lateral growth of the nanowires.

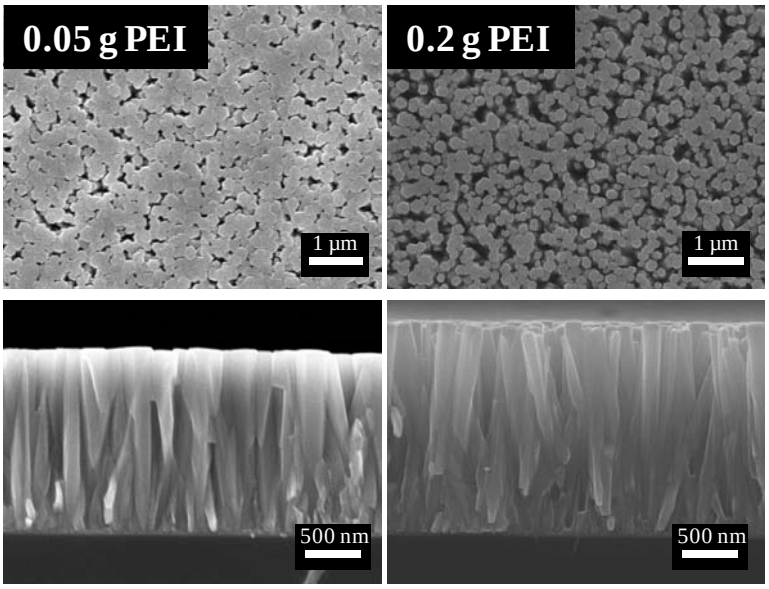

Figure 3.7. SEM images (top and cross-sectional views) of nanowires from a 100 mM growth solution with 0.05 g and 0.2 g of PEI solution

3.3.3 Effect of growth duration

The growth of ZnO nanowires in a 25 mM growth solution with 0.05 g of PEI for various time durations was also carried out to study the growth over time. This would provide a better understanding of the growth mechanism for ZnO nanowires and also how the diameter and height of the nanowires increase with time. The growth was carried out for 0.5 to 6 hours and the SEM images are shown in Fig. 3.8. The results are summarized in Table 3.3.

After 30 minutes of growth, short ZnO nanowires could be observed, suggesting that the nucleation of the $Zn(OH)_2$ complexes on the ZnO seeds takes place within a relatively short time. At 1 hour, the nanowires doubled in height and the growth of nanowires across the entire substrate seems to be denser. After 3 hours,

a dense array of ZnO nanowires could be seen and the height was about 1.15 μm. As the growth time was increased from 3 to 6 hours, the overall morphology of the ZnO nanowires appeared to be the same, but the height increased from 1.15 μm to 1.62 μm.

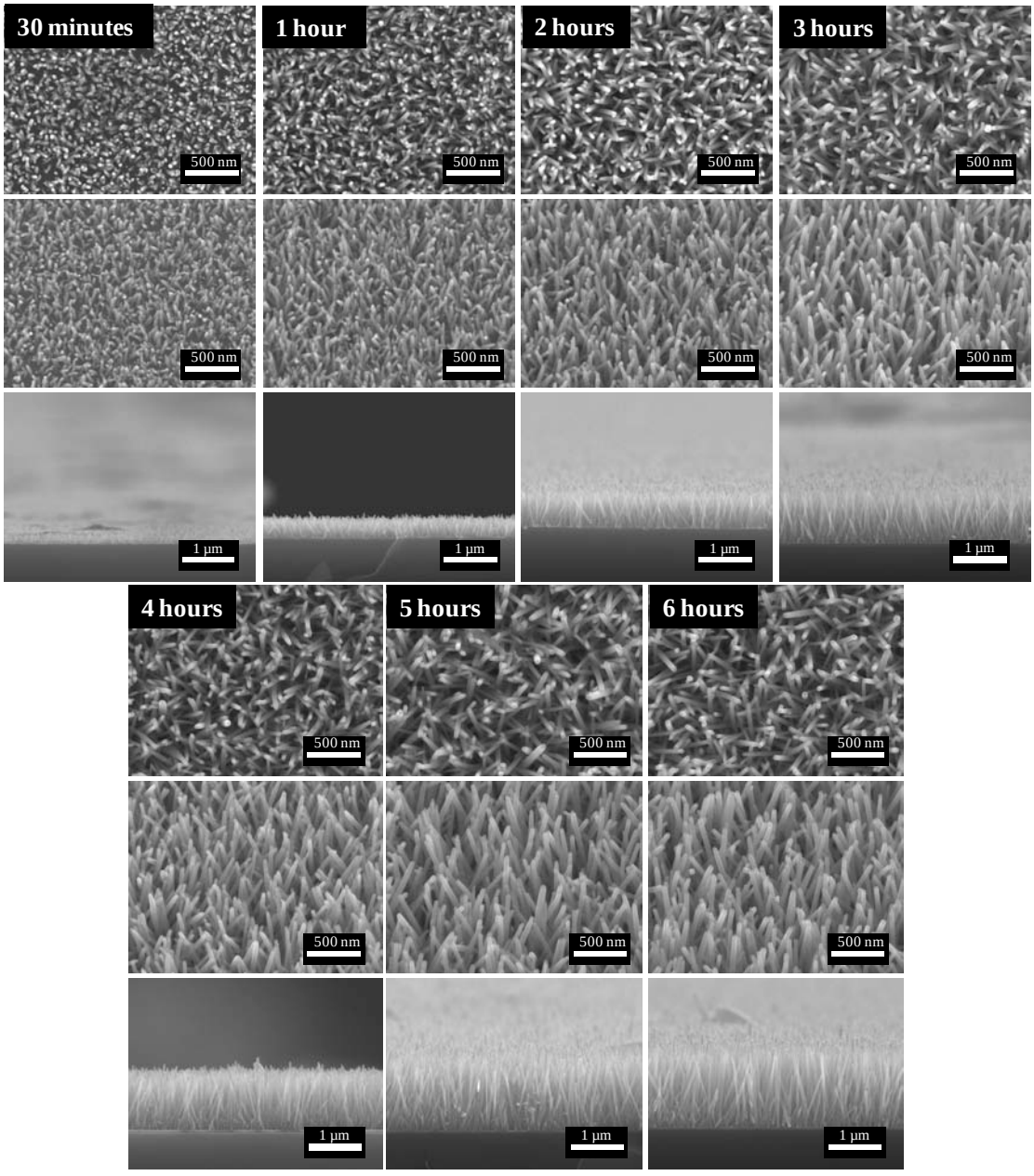

Figure 3.8. SEM images (top, 30° titled and cross-sectional views) of ZnO nanowires synthesized for various growth durations.

Table 3.3. Average diameter and height of nanowires synthesized for various growth durations.

Duration (hours)	Average diameter (nm)	Average height (µm)
0.5	35.5	0.24
1	30.1	0.41
2	33.3	0.76
3	32.3	1.15
4	30.7	1.22
5	38.4	1.39
6	36.5	1.62

Based on the plot in Fig. 3.9, it seems that the height of the nanowires may continue to increase if the growth time was increased to more than 6 hours. This suggests that the amount of reactants in the growth solution might be able to support growth of nanowires beyond 6 hours. It was also observed that the diameter did not increase much with growth duration and it maintained within the range of 30.1 to 38.4 nm. This suggests that long growth duration with the addition of PEI is a possible approach to obtaining long ZnO nanowires without significantly increasing the diameter. A growth duration of 6 hours will be adopted for subsequent synthesis of nanowires in this thesis because among the nanowires grown for 0.5 to 6 hours, the nanowires grown for 6 hours has the highest aspect ratio.

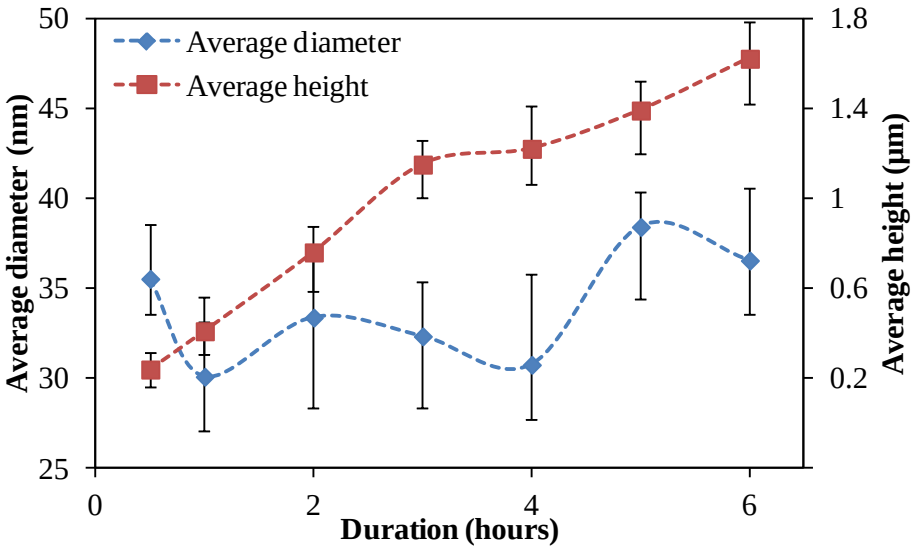

Figure 3.9. Plot of average diameter and height of nanowires synthesized for various growth durations.

3.3.4 Materials characterization

The growth of ZnO nanowires on Si substrate at the optimal parameters of 25 mM zinc nitrate, 25 mM HMT, 0.05 g PEI and growth duration of 6 hours is quite dense and has an average length of 1.62 µm with an average diameter of about 36.5 nm (Fig. 3.10a). The cross-sectional view in Fig. 3.10b shows that the nanowires are vertically aligned on the substrate. Structural characterization of the hydrothermally grown nanowires was carried out via TEM. Fig. 3.10c shows that the nanowires have a uniform diameter with a smooth surface. The lattice fringes in the HRTEM image (Fig. 3.10d) have an interplanar spacing of about 0.52 nm, confirming that the pristine ZnO nanowires are single crystalline and have a preferential growth in the [0001] direction.[10] No morphological changes of the nanowires were observed after plasma treatment and the surfaces of the nanowires remained smooth.

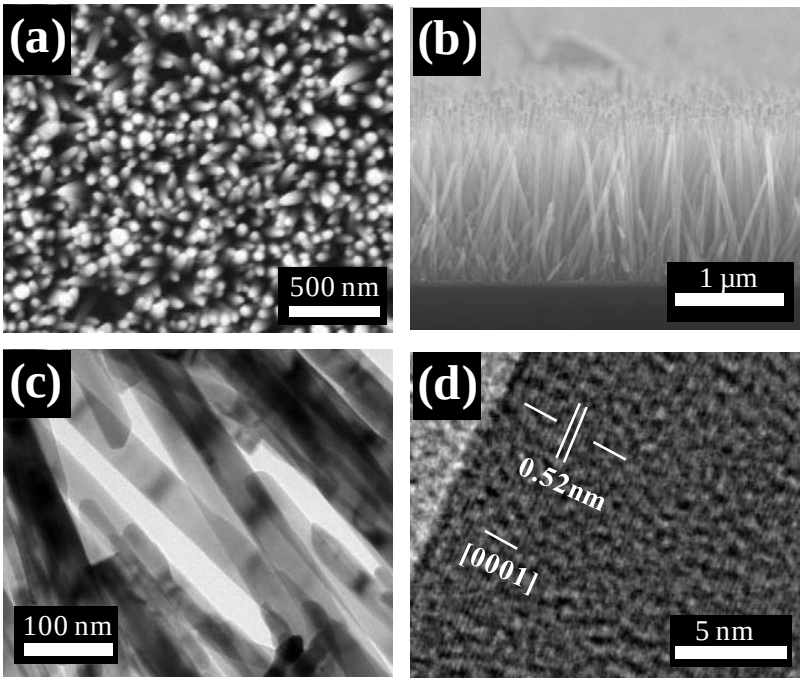

Figure 3.10. (a) Top view and (b) cross-sectional SEM images of hydrothermally synthesized ZnO nanowires, (c) TEM image of synthesized ZnO nanowires, and (d) HRTEM image showing the [0001] growth direction and lattice spacing.

To fabricate flexible ZnO-based devices, the nanowires can be transferred onto PET substrates. Fig. 3.11a shows an SEM image of the ZnO nanowires slide transferred onto a PET substrate. When the donor is rubbed against the receiver, the shear force of the rubbing and sliding motion causes the nanowires on the donor substrate to break and align along the sliding axis on the receiver substrate. This transfer method is also applicable for other receiver substrates such as silicon (Fig. 3.11b and 3.11c). Platinum electrodes can easily be sputtered onto the PET sample for device fabrication. Fig. 3.11d and 3.11e shows an optical micrograph and SEM image respectively of the PET sample with sputtered Pt electrodes and an electrode spacing of 10 μm. In the roll transfer process, the shear forces experienced by the nanowires caused them to break and get transferred onto the receiving substrate. However, the lack of a directional force caused the nanowires on the receiver to be less aligned than that obtained from the slide transfer method (Fig. 3.11f). An optical micrograph of the PET substrate after the heat transfer process is shown in Fig. 3.11g and some patches can be seen in the image. The patches represent the transferred ZnO nanowires (inset of Fig. 3.11g). It can be observed that not all the ZnO nanowires were successfully transferred onto the PET. During the peeling of PET from the donor substrate, some of the ZnO nanowires remained on the donor substrate. It was also observed that some of the transferred patches of ZnO nanowires did not adhere strongly to the PET substrate. From the study of these three transfer methods, it can be seen that the slide transfer method gave the best alignment with a high density of transferred nanowires.

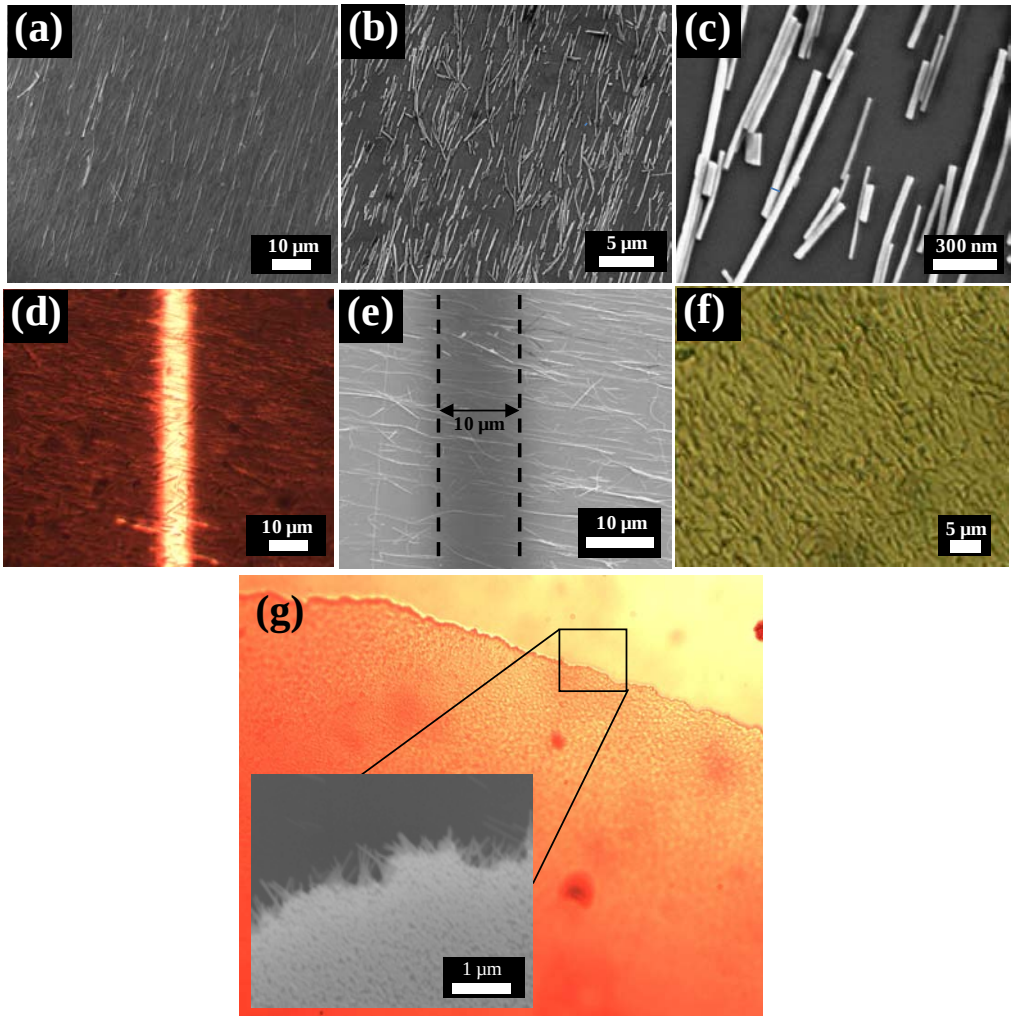

Figure 3.11. (a) SEM images of slide transferred ZnO nanowires on (a) PET substrate, (b) Si substrate at magnification of 3000x, (c) magnification of 200,000x, (d) optical micrograph of slide transferred nanowires with Pt electrodes, (e) SEM image of nanowires with spacing of about 10 µm between Pt electrodes, (f) optical micrograph of nanowires after roll transfer, and (g) optical micrograph of PET substrate with heat transferred ZnO nanowires (inset shows the edge of a patch of nanowires).

The XPS spectra in Fig. 3.12a show the Zn $2p_{3/2}$ peak obtained from the intrinsic ZnO nanowires before and after surface modification with NH_3 plasma. The intrinsic sample has a peak located at 1021.7 eV which corresponds to Zn bonded to O in ZnO. The peak was observed to shift by 1.19 eV towards higher binding energy after plasma treatment. This shift is due to an asymmetry in the electrical cloud surrounding the Zn atom which is caused by the degradation in the symmetry of the crystal lattice. The position of the Zn $2p_{3/2}$ core level is representative of the charge and chemical environments around the Zn atom, therefore, a shift in the peak position

implies that ammonia complexes have diffused into the ZnO nanowires, causing an asymmetry in the lattice structure.[14] The presence of the N1s peak in the XPS spectra of the treated ZnO nanowires (Fig. 3.12b) shows that nitrogen has been successfully incorporated into the nanowires. The peak is centered at 399.3 eV with a full width at half maximum (FWHM) of approximately 3 eV, suggesting the presence of more than one chemical state of N. Two peaks centered at 398.5 eV and 399.6 eV were obtained from the deconvolution of the N1s peak and can be attributed to the N-Zn and N-H bonds respectively[15]. The presence of the N-H bonds (399.6 eV) could possibly be due to hydrogen-passivated N acceptor or N-H radicals from the NH_3 plasma. It was also observed that there is a lower concentration of N-Zn bonds relative to N-H pairs in the treated ZnO nanowires, indicating low solubility of N acceptor. No other N-related peaks such as substitutional N_2 molecules at oxygen sites (404.2 eV)[16] or N-O bonds (407 eV)[17] were observed in the treated nanowires.

This simple surface modification technique was successful in tuning the electrical conductivity from n to p-type. During the NH_3 plasma treatment, various atomic and molecular radicals such as N, H, NH, and NH_2[18] may be introduced into the ZnO lattice. The modification in the conductivity type of ZnO can be attributed to a competitive process involving introduction and compensation of acceptors from the NH_3 plasma. The N radical from the plasma can be incorporated into the ZnO lattice either as a N_2 molecule or a N atom occupying an O site. The chemical state of N_2 was not observed in these ZnO nanowires because no peak was observed at 404 eV in the XPS spectrum. On the other hand, the presence of the peak at 398.5 eV indicates that N radicals from NH_3 occupy the O sites substitutionally. As for atomic radical H from the NH_3 plasma, it has been reported that an isolated interstitial H is exclusively a donor in ZnO.[19] However, H and N tend to interact strongly to form a neutral N_O–H

complex, which in turn leads to an overall reduction in hole concentration due to passivation of the acceptors by H. As for N–H complexes, it has no effect on reducing the electron concentration since it is neutral/electrically inactive. The neutral N-H complexes also do not result in the formation of compensating n-type defects. Therefore, the introduction of neutral N–H complexes can be a step towards achieving high p-type conductivity. Optimization of annealing temperature to dissociate N-H complexes after NH_3 plasma treatment can be used to activate a large concentration of N acceptors to achieve high p-type conductivity.[20] The amount of oxygen vacancies in the nanowires may also be reduced by the occupation of N-H complexes at these n-type related defect sites, thus reducing the n-type characteristics of the ZnO nanowires.

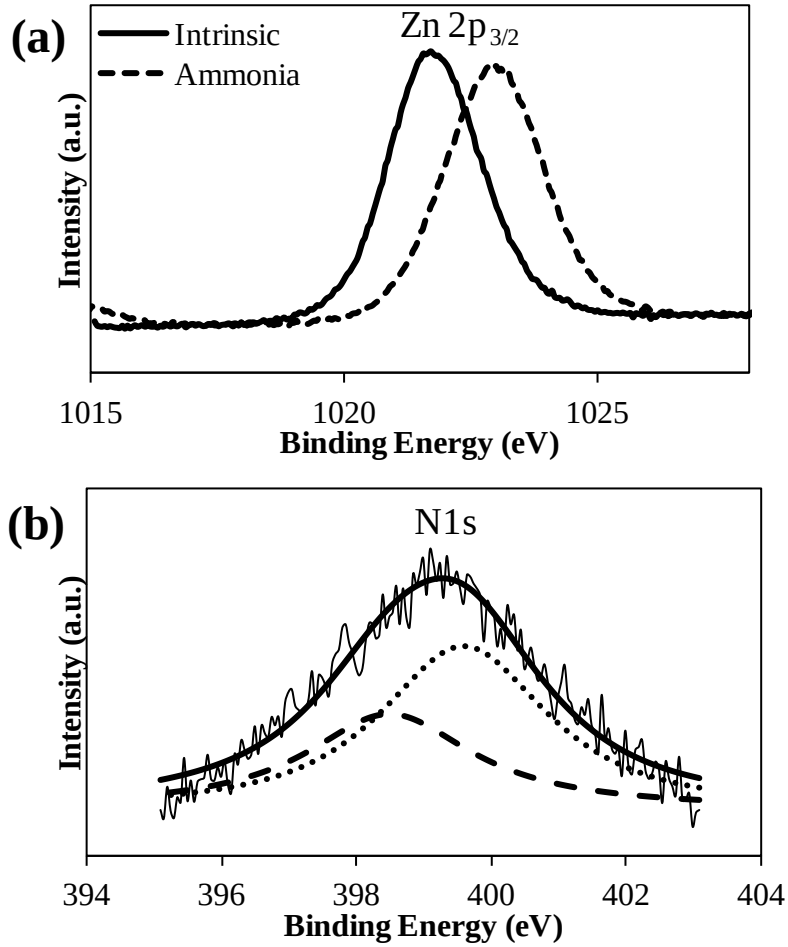

Figure 3.12. High resolution XPS spectra of (a) Zn 2p3/2 peak obtained from the ZnO nanowires before and after NH_3 plasma treatment, and (b) N1s peak from ZnO nanowires after NH_3 plasma treatment.

Fig. 3.13a shows the XRD patterns of pristine and NH_3 modified ZnO nanowires which exhibit a dominant peak at 34–35 °, corresponding to the ZnO (002) diffraction (JCPDS Card No. 79-0205). This indicates that the nanowires are crystallized in the wurzite phase and present a preferential orientation along the c-axis. The (002) peak position of ZnO nanowires was noted to have shifted after NH_3 plasma treatment. This shift in the peak is an indication of the incorporation of N-H into the crystal lattice. Since the ionic radius of N-H is bigger than that of oxygen, their incorporation into the surface of the ZnO nanowires brings about asymmetry expansion of crystal lattice. The peak position of (002) of the NH_3 modified ZnO nanowires will in turn shift to a smaller angle, according to the Bragg diffraction law:

$$2d\sin\theta = \lambda \qquad (3.1)$$

Room temperature PL measurement was carried out on the as-synthesized and NH_3 plasma treated ZnO nanowires as shown in Fig. 3.13b. The as-synthesized nanowires has a UV peak at 379 nm, corresponding to the near-band-edge (NBE) emission of ZnO. A broad visible emission band centered at 600 nm was also observed, signifying the presence of intraband defect levels including oxygen vacancies, V_O.[21] After NH_3 plasma modification, the ZnO nanowires displayed a significant visible emission quenching which may be attributed to the reduction of the defect concentration due to the occupation of N-H atom pairs on the defect sites.[22] N-H will most likely be incorporated into oxygen substitute site (V_O) since the valency charge and activation energy of the N-H is similar to that of oxygen.[22] The NH_3 plasma treated sample was characterized by room temperature PL again after 14 months. The PL spectrum still displayed similar optical characteristic of a strong UV emission with insignificant defect peak.

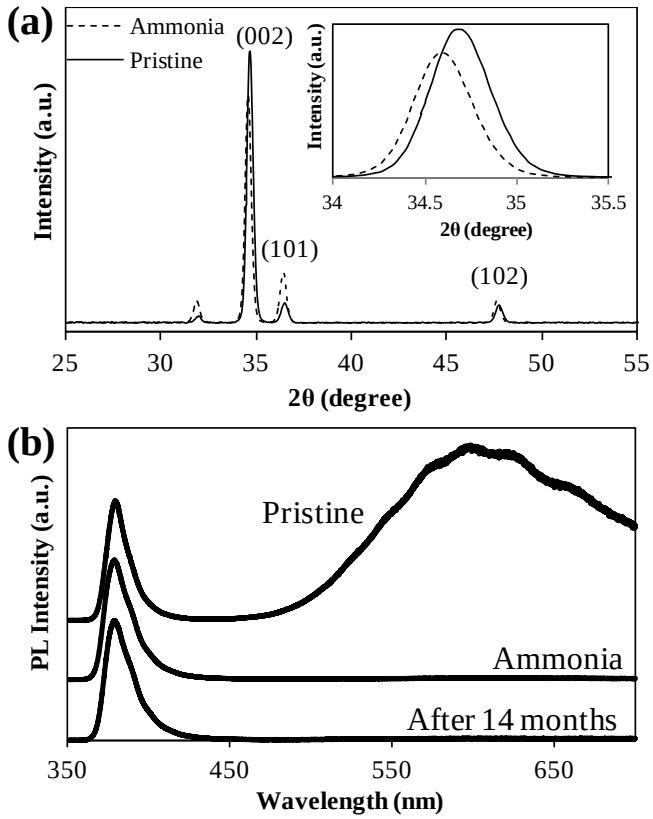

Figure 3.13. (a) XRD pattern and (b) PL spectra of as-synthesized and NH_3 plasma treated ZnO nanowires; inset of (a) shows the corresponding shift of the (002) peak

The optical properties of the NH_3 plasma treated ZnO nanowires were further investigated using low temperature PL measurement at 5 K. Two peaks could be observed in the PL spectrum in Fig. 3.14a, namely at 369 nm and 372.5 nm. The peak at 372.5 nm can be attributed to the excitons bound to the acceptor (A^0X) and the existence of this strong peak signifies the presence of acceptors in the nanowires after NH_3 plasma treatment. The emission at 369 nm is attributed to the near-band-edge emission of excitons bound to donors (D^0X).[23] Low temperature PL measurement at 5 K was also carried out for as-synthesized ZnO nanowires as shown in Fig. 3.14b and only the donor bound exciton peak at 370 nm was observed.[24] The absence of the acceptor bound exciton peak provides additional evidence that the acceptors were derived from the NH_3 plasma treatment.

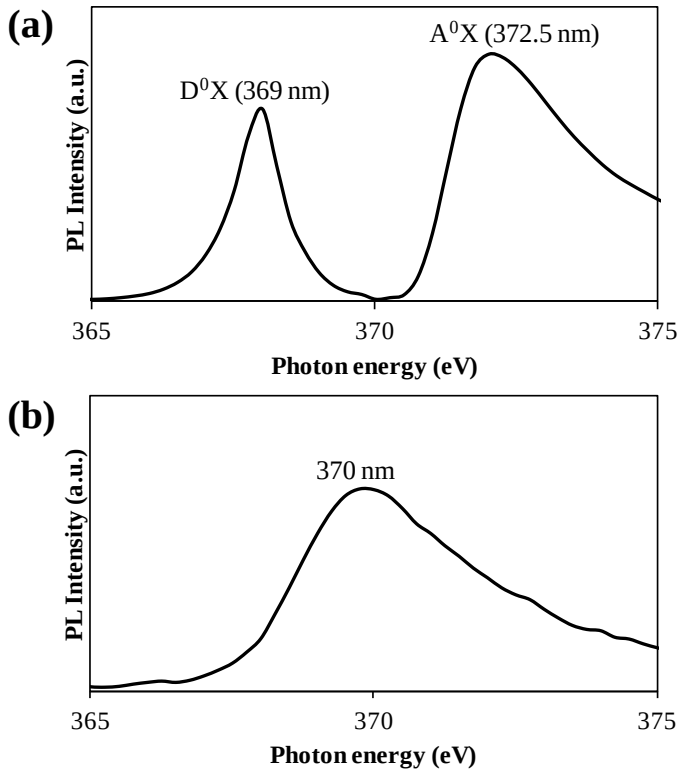

Figure 3.14. (a) Low temperature PL spectrum at 5 K for NH_3 plasma treated nanowires, and (b) pristine nanowires.

Hall measurements were also carried out to determine the conductivity type, resistivity, carrier concentration and Hall mobility of the NH_3 plasma treated ZnO nanowires and the intrinsic samples. Good ohmic contacts between the electrodes and the nanowires were confirmed before carrying out the measurements. Table 3.4 is a summary of the Hall measurement results and the plot is shown in Fig. 3.15. The NH_3 plasma treated ZnO nanowires show p-type conductivity with an average resistivity of 6.04 Ω cm with an average carrier concentration of 1.42 X 10^{17} cm^{-3} and average mobility of 7.34 cm^2/Vs. The electrical properties obtained are comparable to p-type ZnO nanowires of various dopants reported in literature (Table 3.5).

Table 3.4. Average resistivities, mobilities and carrier concentrations of intrinsic and NH_3 plasma treated ZnO nanowires.

Sample	Average resistivity (Ω cm)	Average mobility (cm^2/Vs)	Average carrier concentration (x $10^{17} cm^{-3}$)	Carrier type (n/p)
NH_3 plasma treated	6.04	7.34	1.42	p
Intrinsic	6.18	3.7	2.73	n

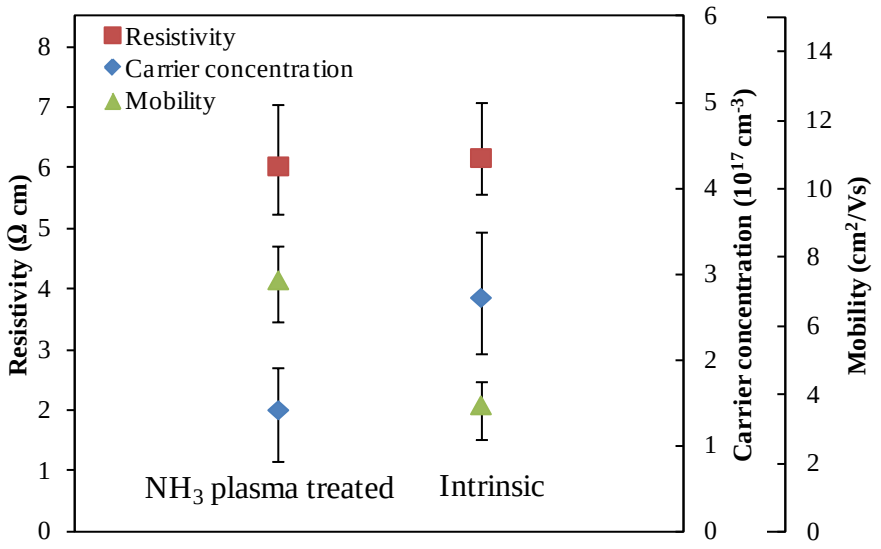

Figure 3.15. Plot of Hall results from intrinsic and NH_3 plasma treated ZnO nanowires.

The p-type ZnO nanowires listed in Table 3.5 were doped with Na, P, Ag, Sb and N via both aqueous and CVD methods. The nanowires have carrier concentrations ranging from 1.3 X 10^{16} cm^{-3} to 1.19 X 10^{18} cm^{-3} with corresponding carrier mobilities in the range of 0.18 – 40.4 cm^2/Vs.[25-29] The carrier mobility of the NH_3 plasma treated ZnO nanowires is comparable to these p-type nanowires reported in literature. The carrier concentration of the plasma treated ZnO nanowires has the same order of magnitude as that of the Ag and Sb-doped nanowires and is one order of magnitude higher than that of Na and P-doped nanowires. However, the treated nanowires have a carrier concentration one order of magnitude lower than that of the N-doped nanowires reported by Yuan *et al.*[29] which exhibited a carrier concentration of 1.19 X 10^{18} cm^{-3}. The higher carrier concentration and mobility of Yuan *et al.*'s

nanowires could be due to the doping process being carried out at a high temperature of 750 °C, resulting in higher doping efficiency and also more effective activation of the N dopants.

Table 3.5. P-type ZnO nanowires reported in the literature.

1st author	Technique	Dopant	Mobility (cm^2/Vs)	Carrier concentration (cm^{-3})
Liu[25]	CVD	Na	2.1	1.3×10^{16}
Li[26]	CVD	P	40.4	5×10^{16}
Wang[27]	CVD	Ag	0.18	4.9×10^{17}
Wang[28]	aqueous solution	Sb	1.2	6×10^{17}
Yuan[29]	CVD	N	10.5	1.19×10^{18}

It should be noted that in the derivation of the mobility and carrier concentration values for the NH_3 modified nanowires, the length of the nanowires was used as the film thickness. Due to uncertainty in estimating the nanowires film's thickness/porosity, the Hall measurement results should be taken as an indication of relative change in the conductivity type and electrical properties of the nanowires after plasma modification, and not an absolute result. These results should be considered complementary alongside other characterization results reported in this work. However, the Hall measurements were carried out on 10 pristine and plasma treated samples, and the results obtained were consistent and reproducible.

The intrinsic ZnO sample showed n-type conductivity and had an average resistivity of 6.18 Ω cm with average carrier concentration of 2.73×10^{17} cm^{-3} and average mobility of 3.7 cm^2/Vs. This carrier concentration is about twice that of the plasma treated nanowires, but it results in more scattering, hence leading to lower mobility in the intrinsic nanowires. The reasons for the lower carrier concentration in the plasma treated ZnO nanowires could be due to the substitution of oxygen by a small fraction of N to become an acceptor and/or a large part of the acceptors being

compensated or passivated in the form of N-H complexes. Nevertheless from the Hall results, it is evident that NH_3 plasma treatment can be an effective method to tune the electrical conductivity of ZnO nanowires. Moreover, the plasma treatment was carried out without heating which makes it possible to fabricate devices on flexible substrates with NH_3 modified ZnO nanowires. This is an efficient method (90 s) to modify the conductivity of ZnO nanowires as compared to other synthesis and doping methods.[15,25-29] The functionality of these surface modified nanowires will be proven through testing of devices built upon these nanowires.

3.3.5 Electrical devices demonstration

The follow-up electrical device demonstrations of both intrinsic and surface modified ZnO nanowires are based on the p-n junction diode, capacitor and chemical sensor. The sensing and electrical properties are dictated by the variation of electron concentration at the surface of the ZnO nanowires. Hydrogen gas sensors were fabricated from the intrinsic and NH_3 plasma treated ZnO nanowires and were tested at various concentrations of hydrogen, without any operating temperature (room temperature) (Fig. 3.16a). The gas sensing setup was home-made using vacuum parts and the hydrogen gas (0.5 %, He balanced) and clean dry air (CDA) were supplied to the setup via mass flow controllers as shown in Fig. 3.16b. The hydrogen gas sensor was placed in the sensing chamber and electrical leads from the sample were connected to a source-meter (Keithley 4200-SCS) via an electrical feed-through. A chemical sensor fabricated on plastic substrate is shown in the sensing chamber of Fig. 3.16b.

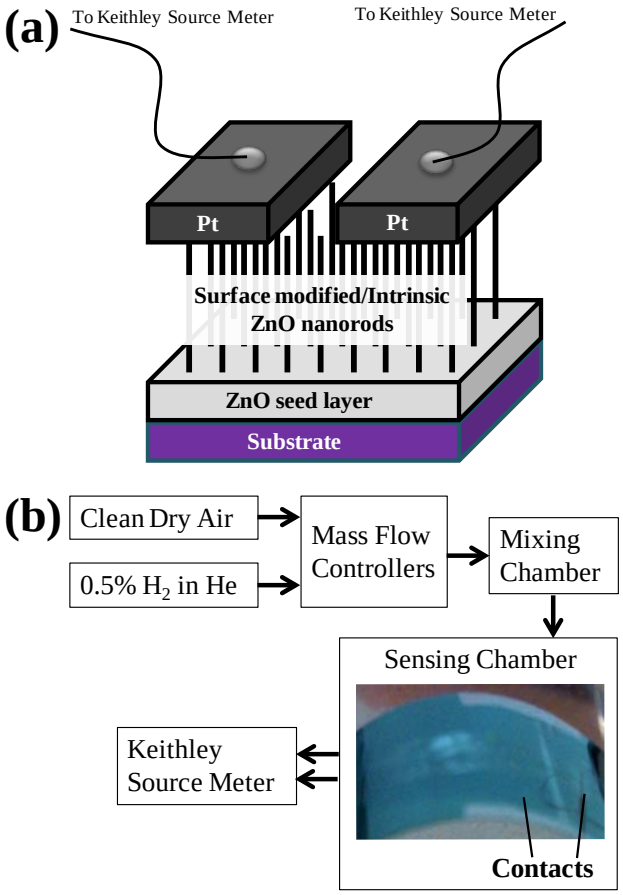

Figure 3.16. Schematic diagram of (a) hydrogen gas sensor and (b) gas sensing setup (a plastic chemical sensor is shown in the sensing chamber).

Hydrogen ambient of various concentrations was created by varying the flowrates of the hydrogen gas and CDA. From Fig. 3.17a, the resistance of the intrinsic nanowires was observed to decrease in hydrogen ambient and increase in air ambient, indicating n-type behaviour. Fig. 3.17b shows the sensitivity of the device in response to various concentrations of hydrogen gas. The sensitivity of the device to hydrogen gas was calculated by

$$\text{Sensitivity} = \frac{R_H - R_{CDA}}{R_{CDA}} \times 100\%, \qquad (3.2)$$

where R_H and R_{CDA} are resistances of the device in hydrogen gas and CDA respectively. At 1000 ppm, the hydrogen gas sensor showed a sensitivity of 5.0 % and

the sensitivity increased with the concentration of hydrogen gas, attaining a sensitivity of 26.4 % at a hydrogen concentration of 5000 ppm.

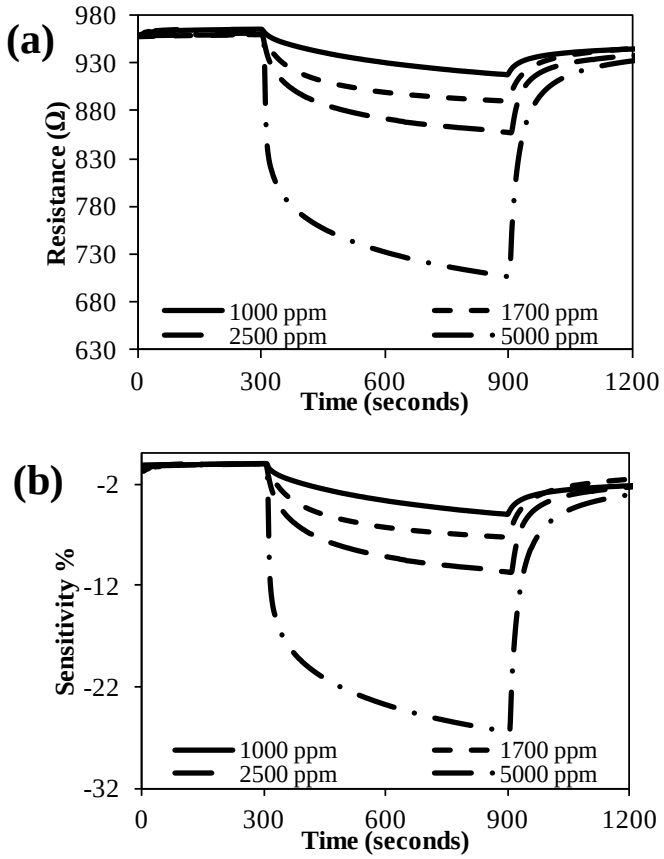

Figure 3.17. Time dependent (a) resistance and (b) sensitivity change of intrinsic ZnO nanowires in 1000-5000 ppm of hydrogen at room temperature.

When ZnO is exposed to gases such as O_2, the charge accepting molecules adsorbs at the vacancy sites, and electrons are effectively depleted from the conduction band, leading to a reduced conductivity of the n-type ZnO. On the other hand, when the metal oxide is exposed to gases such as hydrogen, the molecules would react with the surface adsorbed oxygen and consequently remove it, leading to an increase in conductivity.[30] The response of the surface modified ZnO nanowires is the opposite of intrinsic ZnO nanostructures. When the modified ZnO is exposed to O_2 gas, the depletion of electrons actually results in increased hole density, leading to increased conductivity. Exposing the NH_3 modified nanowires to H_2 gas will cause

the hole density to decrease hence leading to lower conductance.[29] From the plot in Fig. 3.18a, the resistance of the NH_3 plasma treated nanowires was observed to increase when exposed to hydrogen and decrease in air ambient, indicating p-type behaviour in the treated nanowires. The sensitivity of this device to hydrogen ambient of various concentrations is shown in Fig. 3.18b. The NH_3 modified ZnO nanowires has a sensitivity of 15 % at 500 ppm hydrogen ambient and it increased to 27 % at a hydrogen concentration of 2500 ppm.

This shows that the device is capable of showing different levels of sensitivity at different concentrations of hydrogen, hence the device could possibly be used to determine the amount of hydrogen gas present in the ambient. The NH_3 modified nanowires were tested again after 14 months and the hydrogen sensing result is shown in the inset of Fig. 3.18b. There is no apparent degradation in the gas sensing performance and the device exhibited the same p-type behaviour as before. It is also noted that an advantage of operating a ZnO gas sensor at room temperature is that it will not result in subsequent adverse structural instability which in turn causes electrical drift due to grain coalescence, porosity modification or grain-boundary occurrence.

The schematic drawing of the p-n junction diode using Pt and Al as contacts is shown in Fig. 3.19a and the ohmic I-V characteristics of the plasma treated ZnO nanowires is shown in the inset of Fig. 3.19b. The I-V curve of Fig. 3.19b exhibits an apparent rectifying behaviour of the p-n junction and the turn-on voltage appears at ~ 3.3 V under forward bias. The leakage current under reverse bias could be due to incomplete contact between the Pt electrode and some nanowires. A schematic diagram of the MOS capacitor is shown in Fig. 3.19c and C-V measurements were carried out on the MOS capacitor by sweeping the voltage from -3 to 3 V at 100 kHz

(Fig. 3.19d). The C-V curve shows that NH_3 treated ZnO nanowires exhibits p-type conductivity as opposed to the C-V curve of a MOS capacitor fabricated using intrinsic (n-type) ZnO nanowires (inset of Fig. 3.19d). The interface traps are not able to respond to the a.c. signal and causes the C–V curve to stretch out along the voltage axis. This suggests the presence of interface traps between the oxide and the ZnO nanowires.

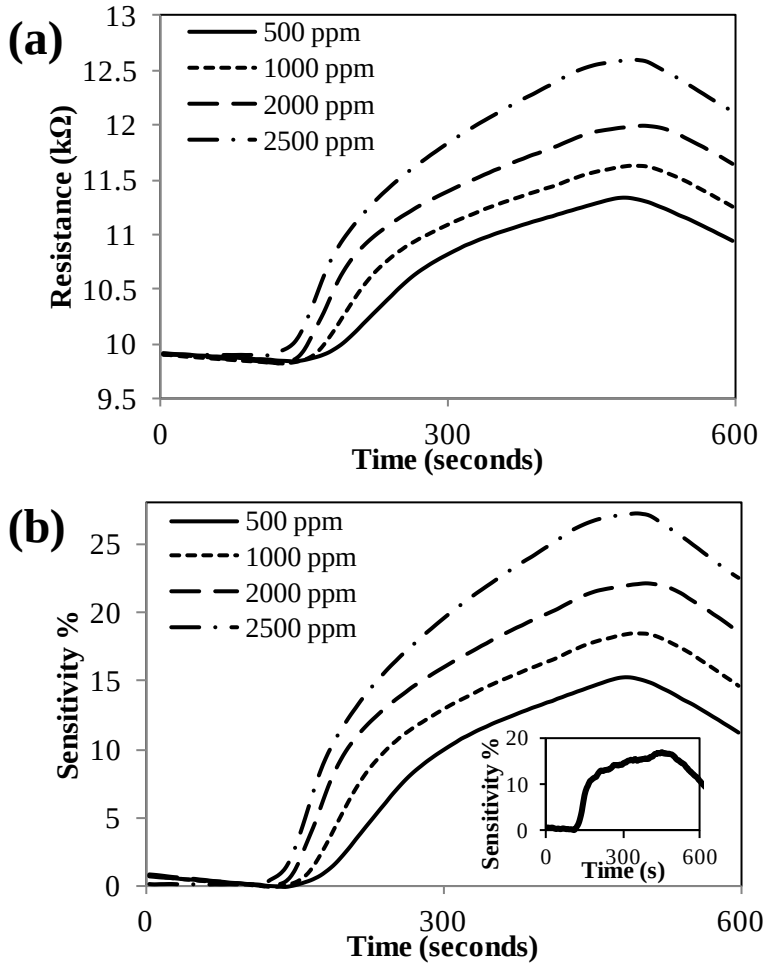

Figure 3.18. Time dependence (a) resistance and (b) sensitivity change of surface modified ZnO nanowires as the gas ambient is switched from air to various concentrations (500-2500 ppm) of hydrogen at room temperature. Inset of (b) shows the sensitivity of the device to 500 ppm of hydrogen after 14 months.

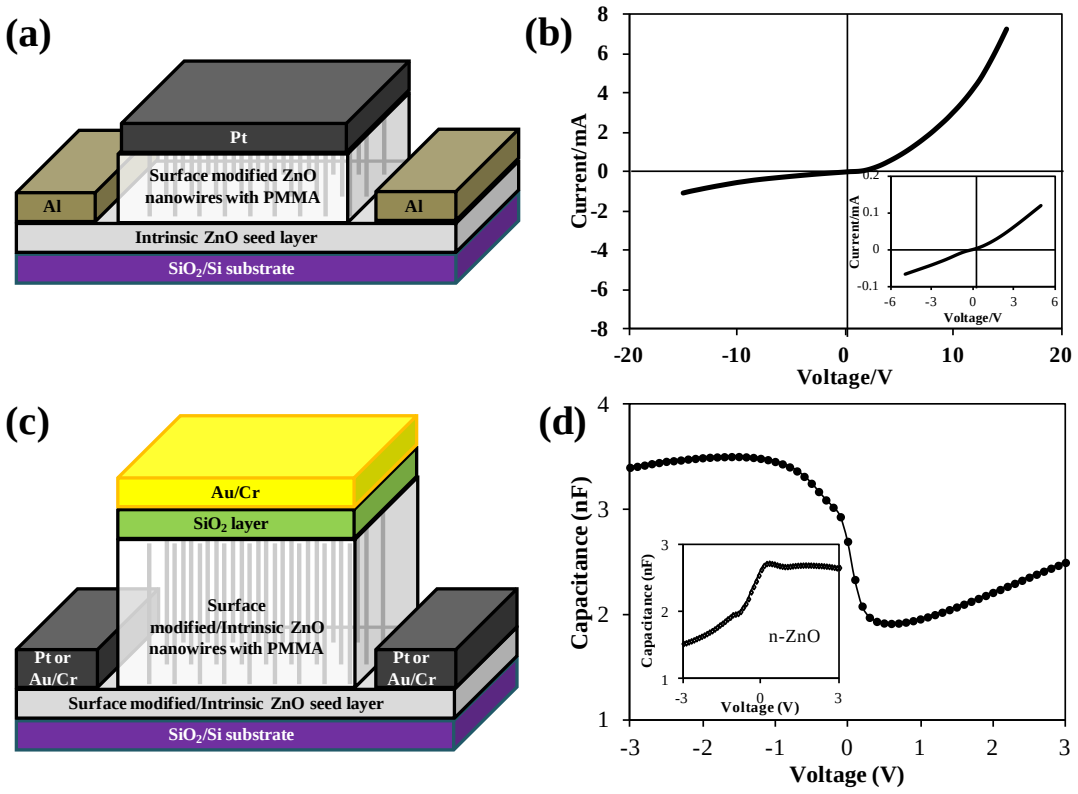

Figure 3.19. (a) Schematic diagram of p-n junction, (b) I-V characteristic of p-n junction; the inset shows the ohmic I-V characteristics of surface modified ZnO nanowires, (c) schematic diagram of MOS capacitor, and (d) C-V measurement of NH_3 treated ZnO nanowires; the inset shows the C-V characteristic of intrinsic ZnO.

3.4 Conclusions

We have demonstrated that the physical dimensions of the ZnO nanowires can be controlled by varying the growth parameters. When the precursor concentration was increased, the diameter and length of the nanowires also increased. However, at a concentration of 100 mM, the large diameter nanowires were observed to coalesce and form a film-like morphology. Adding PEI to the solution helped to reduce the diameter by reducing lateral growth of the nanowires but when more than 0.5 g of PEI was added, no growth of nanowires were observed. When the growth duration was increased, the height of the nanowires also increased but the diameter did not show much change. It was also shown that the electrical conductivity of hydrothermally synthesized ZnO nanowires can be effectively tuned by surface modification using

NH_3 plasma without heat treatment. Hall measurements of the modified ZnO nanowires revealed p-type conductivity with an average resistivity of 6.04 Ω cm with an average carrier concentration of 1.42 X 10^{17} cm^{-3} and average mobility of 7.34 cm^2/Vs. Significant quenching of the visible emission in the room temperature PL spectrum was also observed after NH_3 plasma modification, indicating a reduction in the amount of defects in the nanowires due to the occupation of N-H atom pairs on the defect sites. The sample was characterized by room temperature PL again after 14 months and the PL spectrum still display similar optical characteristic of a strong UV emission with insignificant defect peak. Low temperature photoluminescence also showed evidence of acceptor bound exciton emission. The presence of an N1s peak in the XPS spectrum of the surface modified ZnO nanowires indicated the successful incorporation of ammonia complexes into the nanowires. The fabrication of flexible devices was demonstrated via various methods of transferring and aligning as-synthesized ZnO nanowires onto plastic substrates. Typical rectification characteristic of a p-n junction was observed from the I-V curve of the p-n homojunction fabricated using the surface modified ZnO nanowires. The results obtained from the electrical devices and hydrogen gas sensor show that ammonia plasma treatment is a feasible way to tune the electrical conductivity of ZnO nanowires.

References

1 Wang H T, Kang B S, Ren F, Tien L C, Sadik P W, Norton D P, Pearton S J and Lin J 2005 *Appl. Phys. A* **81** 1117

2 Fan H J, Yang Y and Zacharias M 2009 *J. Mater. Chem.* **19** 885

3 Yuan G D, Zhang W J, Jie J S, Fan X, Tang J X, Shafiq I, Ye Z Z, Lee C S and Lee S T 2008 *Adv. Mater.* **20** 168

4 Li Y, Meng G W and Zhang L D 2000 *Appl. Phys. Lett.* **76** 2011

5 Li S Y, Lee C Y and Tseng T Y 2003 *J. Cryst. Growth.* **247** 357

6 Vayssieres L, Keis K and Lindquist S -E 2001 *J. Phys. Chem. B* **105** 3350

7 Wang J M and Gao L 2004 *Solid State Communications* **132** 269

8 Yang J H, Zheng J H, Zhai H J and Yang L L 2009 *Cryst. Res. Technol.* **44** (1) 87

9 Xiang B, Wang P, Zhang X, Dayeh S A, Aplin D P R, Soci C, Yu D and Wang D 2007 *Nano. Lett*. **7** 323

10 Wang C H, Wong A S W and Ho G W 2007 *Langmuir* **23** 11960

11 Ho G W and Wong A S W 2007 *Appl. Phys. A* **86** 457

12 Oztekin N, Alemdar A, Gungor N and Erim F B 2002 *Mater. Lett.* **55** 73

13 Degen A and Kosec M J 2000 *Eur. Ceram. Soc.* **20** 667

14 Xiao Z Y, Liu Y C, Zhang J Y, Zhao D X, Lu Y M, Shen D Z and Fan X W 2005 *Semicond. Sci. Technol.* **20** 796

15 Cao P, Zhao D X, Zhang J Y, Shen D Z, Lu Y M, Yao B, Li B H, Bai Y and Fan X W 2008 *Appl. Surf. Sci.* **254** 2900

16 Ahn K S, Yan Y F, Lee S H, Deutsch T, Turner J, Tracy C E, Perkins C L and Jassim M A 2007 *J. Electrochem. Soc.* **154** B956

17 Bian J M, Li X M, Gao X D, Yu W D and Chen L D 2004 *Appl. Phys. Lett.* **84** 541

18 Kang S J and Donnelly V M 2007 *Plasma Sources Sci. Technol.* **16** 265

19 Van de Walle C G 2000 *Phys. Rev. Lett.* **85** 1012

20 Jokela S J and McCluskey M D 2007 *Phys. Rev. B* **76** 193201

21Mensah S L, Kayastha V K, Ivanov I N, Geohegan D B and Yap Y K 2007 *Appl. Phys. Lett.* **90** 113108

22 Huang J Y, Ye Z Z, Chen H H, Zhao B H and Wang L 2003 *J. Mat. Sci. Lett*. **22** 249

23 Tang H P, Ye Z Z and He H P 2008 *Opt. Mater*. **30** 1422

24 Meyer B K, Alves H, Hofmann D M, Kriegseis W, Forster D, Bertram F, Christen J, Hoffmann A, Straßburg M, Dworzak M, Haboeck U and Rodina A V 2004 *Phys. Stat. Sol. (b).* **241** 231

25 Wang F, Seo J H, Bayerl D, Shi J, Mi H Y, Ma Z Q, Zhao D Y, Shuai Y C, Zhou W D and Wang X D 2011 *Nanotechnology* **22** 225602

26 Li P J, Liao Z M, Zhang X Z, Zhang X J, Zhu H C, Gao J Y, Laurent K, Wang Y L, Wang N and Yu D P 2009 *Nano Lett.* **7** 2513

27 Liu W, Xiu F X, Sun K, Xie Y H, Wang K L, Wang Y, Zou J, Yang Z and Liu J L 2010 *J. Am. Chem. Soc.* **132** 2498

28 Wang G P, Chu S, Zhan N, Zhou H M and Liu J L 2011 *Appl. Phys. A* **103** 951 2011

29Yuan G D, Zhang W J, Jie J S, Fan X, Zapien J A, Leung Y H, Luo L B, Wang P F, Lee C S and Lee S T 2008 *Nano Lett*. **8** 2591

30 Wang J X, Sun X W, Yang Y, Huang H, Lee Y C, Tan O K and Vayssieres L 2006 *Nanotechnology* **17** 4995

Chapter 4 ZnO Nanowires for Flexible Hydrogen Gas Sensor Applications

In this chapter, ZnO nanowires are hydrothermally synthesized on polyethylene terephthalate (PET) substrate for hydrogen gas sensing application. The gas sensing measurements are carried out at room temperature and a thin layer of platinum (Pt) is sputtered on the nanowires to improve the sensing performance, especially at low hydrogen concentrations. The robustness of the flexible device is also tested by bending the device repeatedly and carrying out hydrogen sensing measurements with a bent sample.

4.1 Introduction

With the increasing demand for renewable and clean sources of energy, hydrogen (H_2) is expected to become the "fuel of the future".[1] However, H_2 is an invisible and odourless gas which can cause explosions when its concentration in ambient air exceeds 4.65 %, thus it is important to detect H_2 leakage in the environment. Many research groups have been focusing on the development of nanoscale H_2 sensors that are compact, reliable and inexpensive. Recent efforts are focused on the improvement of H_2 gas sensitivity, selectivity and room temperature operation.[2-7] Commercial sensors based on metal oxide particles and thin films are usually operated at elevated temperatures of 200 to 400 ^{O}C to maximise sensitivity and enhance surface molecular desorption. However, operation at elevated temperatures may not be ideal in certain scenarios, such as in the presence of other combustible gases in air.[8] Morever, operating the sensors at high temperature can also result in structural instability which in turn causes electrical drift to grain coalescence, porosity modification and grain boundary occurrence. For these reasons, it is desirable for H_2 sensors to operate at room temperature.

H_2 gas sensors based on metal oxides such as ZnO, SnO_2 and In_2O_3 nanowires exhibit excellent response and recovery characteristics[9] and can potentially overcome obstacles of other type of sensors, such as sensitivity, selectivity, etc. Among the various nanomaterials, ZnO is one of the most promising and useful material for gas sensors, especially H_2 sensing.[2-7] This metal oxide is attractive for sensing applications because of its wide bandgap (3.37 eV), the availability of heterostructures, the ease of synthesizing nanostructures, and its biosafe characteristics.[10,11] However, the sensitivity of ZnO bulk material is lower compared to one-dimensional (1D) ZnO nanostructures. 1D nanostructures are ideal for gas sensors because of several advantages such as large surface area,[12-14] thermal and mechanical stability,[15] and compatibility with other nanodevices. The high aspect ratio ZnO nanowires provide flexibility and optical transparency, while the single crystalline structures hold an efficient pathway for charge carrier transport. These properties also make nanowires ideal for sensitive flexible sensors on plastic substrates.[16,17]

Traditional H_2 sensors are usually fabricated on inorganic substrates such as glass, quartz and silicon wafers.[18,19] The rigidity of these substrates might limit the use of these sensors in new applications such as portable devices, aerospace science and civil engineering that demand flexible, lightweight, and mechanical shock-resistive sensing elements.[20] In contrast, thin polymer sheets with electrical and chemical inertness provide an ideal class of substrates for fabricating H_2 sensors, which can be used in applications complementary to those of the conventional sensors. However, the fabrication steps can be quite complicated as it involves the placement of nanomaterials onto desired substrates, followed by lithography and metallization steps to produce the metal contacts to the ends of nanostructures.[13,14,21] Vertically

aligned nanowires offer an attractive alternative to these laterally deposited or networked nanowires sensors. The nanowires can be easily configured to vertical device platforms and provide potential for device scaling and integration of the largest number density in mono-layered structures.[22-24] In addition, the modification of metal oxide active layer by adding small amounts of noble metals has been reported to improve gas sensing performance.[25] The metal coating causes catalytic dissociation of H_2 to atomic hydrogen, which produces a sensor response through binding to surface atoms and altering the surface potential.[26] However, for widespread applications and large scale production of ZnO nanowires in sensors, an inexpensive and environmentally benign synthesis method is required.[27-29]

In this chapter, a flexible H_2 gas sensor is demonstrated by synthesizing vertically-aligned ZnO nanowires on PET substrates via the low cost and environmentally friendly hydrothermal growth method. The nanowires were capable of sensing H_2 gas at room temperature even at a low concentration of 50 ppm. Pt nanoparticles were deposited on the nanowires by sputtering, and the catalytic decomposition of the H_2 molecules by Pt resulted in enhanced sensitivity of the sensor and faster response and recovery times. H_2 sensing measurements were also carried out while bending the sensor, and the results obtained were similar to that of the original unbent sample. These results indicate that this is a feasible method of fabricating flexible nanowires sensor towards novel applications such as mechanically flexible or transparent light-weight sensors.[20]

4.2 Experimental procedures

ZnO nanowires were grown on PET substrates by the low temperature hydrothermal method. The PET substrates were cleaned by sonicating in isopropyl alcohol (IPA) (5 min) followed by ethanol (5 min), and then blown dry with a stream

of nitrogen gas. The PET substrates were then sputtered with 6 nm of ZnO as seed layer via radio-frequency (RF) magnetron sputtering (Denton Vacuum Discovery 18 system) at room temperature. The seeded substrates were then placed into a 25 ml growth solution consisting of zinc nitrate (25 mM), hexamethylenetetramine (HMT) (25 mM) and 0.05 g of polyethylenimine (PEI) in de-ionized (DI) water. The synthesis process was carried out at 90 °C for 6 hrs and the fabrication steps are illustrated in the schematic diagram in Fig. 4.1.

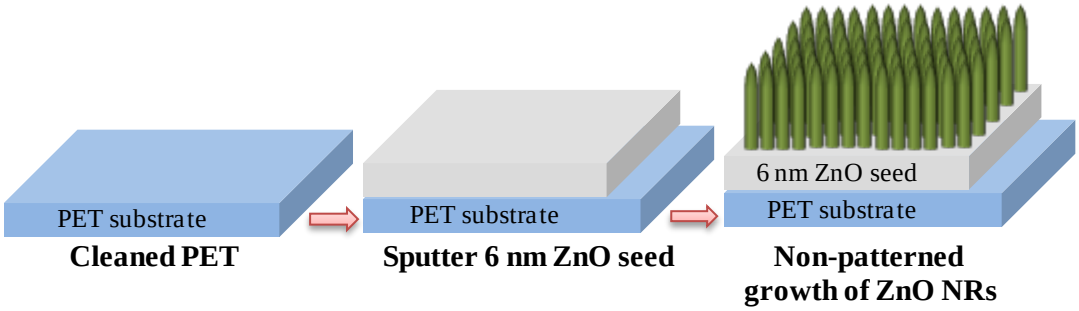

Figure 4.1. The schematic approach of growing ZnO nanowires on PET substrate.

The Pt catalysts were sputtered on the ZnO nanowires using the JEOL JFC-1600 Auto Fine Coater at a current of 30 mA for 40 s. This set of sputtering conditions produced a Pt thickness of about 10 nm. To fabricate the gas sensors, conductive silver (Ag) paste was used to attach copper wires to the film of nanowires (Fig. 4.2). The copper wires were then connected to the Keithley 4200-SCS semiconductor characterization system. Sensing measurements were carried out by biasing the device at 5 V and measuring the change in resistance of the device while alternating the environment in the sensing chamber between clean dry air (CDA) and H_2 gas at room temperature. Various concentrations of H_2 ambient were created by varying the flow of H_2 gas and CDA using Brooks Mass Flow Controllers.

Various characterization techniques were carried out on the samples. Scanning electron microscopy (SEM, JEOL FEG JSM 7001F) characterized the morphology of the synthesized products while the crystalline structure of the ZnO nanowires was

analyzed using X-ray diffraction (XRD, Philips X-ray diffractometer equipped with graphite-monochromated Cu Kα radiation at λ = 1.54Å) and transmissi on electron microscopy (TEM, Phillips FEG CM300). Room temperature optical properties were measured by the UV-VIS-NIR spectrophotometer (UV-vis, Shimadzu UV-3600) and micro-photoluminescence (PL) with He-Cd laser at 325 nm. The elements present in the ZnO nanowires sample sputtered with Pt were analyzed using Energy-dispersive X-ray spectroscopy (EDX, Oxford Instruments EDS system AZtecEnergy). The electrical properties of the samples were studied using a Keithley 4200-SCS semiconductor characterization system.

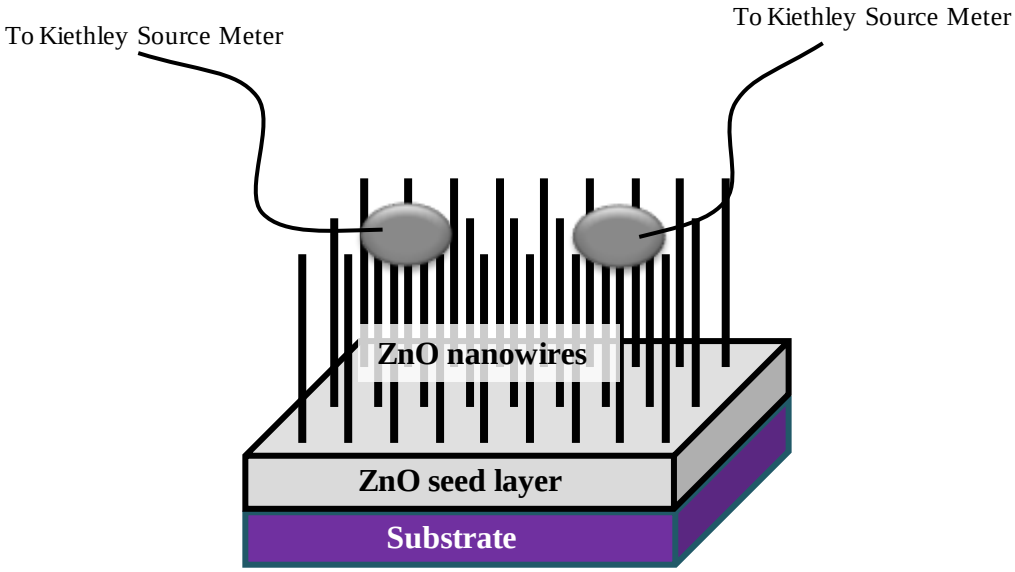

Figure 4.2. Schematic diagram of gas sensing device.

4.3 Results and discussion

4.3.1 Materials characterization

The SEM images of the ZnO nanowires on PET substrate are shown in Fig. 4.3. A uniform and high density growth of ZnO nanowires on PET substrate was achieved via this hydrothermal method (Fig. 4.3a and b). The average diameter of the ZnO nanowires is approximately 50 nm. The height of the ZnO nanowires is about 1.9 to 2 μm as shown in the cross-section view in Fig. 4.3c. Structural characterization of

the hydrothermally grown nanowires was also carried out via TEM. The HRTEM image (Fig. 4.3d) shows lattice fringes of an interplanar spacing ~ 0.52 nm, confirming that the ZnO nanowires are single crystalline with a preferential growth in the [0001] direction.

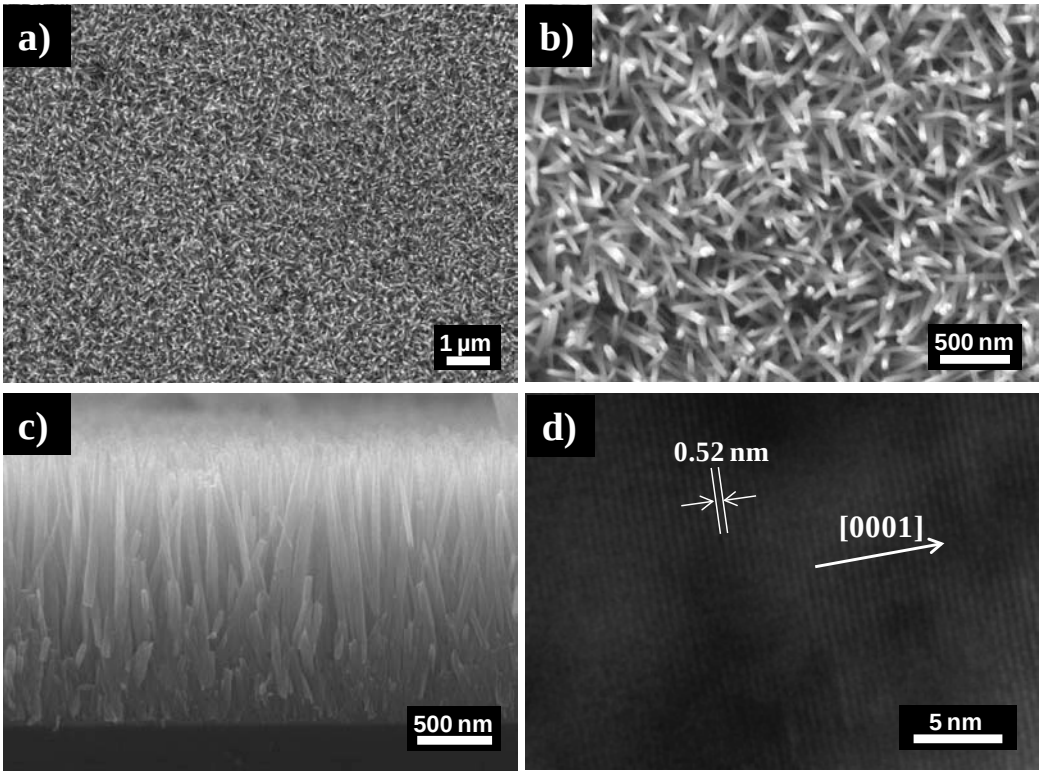

Figure 4.3. SEM images of ZnO nanowires synthesized on PET substrate. Top view images of (a) low and (b) high magnification and (c) cross-sectional SEM images of ZnO nanowires synthesized on PET substrate (d) HRTEM image of a nanowire showing the [0001] growth direction.

The XRD pattern of ZnO nanowires grown on PET is shown in Fig. 4.4. The diffraction pattern has a very pronounced PET (100) peak at 26°. Two other PET peaks namely, PET (12-2) at 46.6° and PET (2-30) at 52.9° (JCPDS Card No. 00-060-0989) are shown in the inset (a magnified view of the spectra in the range 30° to 60°). The only ZnO peak present is the prominent ZnO (002) peak which can be well indexed to the hexagonal phase of ZnO with lattice constants a = 0.3242 nm and c = 0.5194 nm (JCPDS Card No. 79-0205). The (002) peak indicates preferential growth

in the [0001] direction, and also the good crystal structure and phase purity of the product.

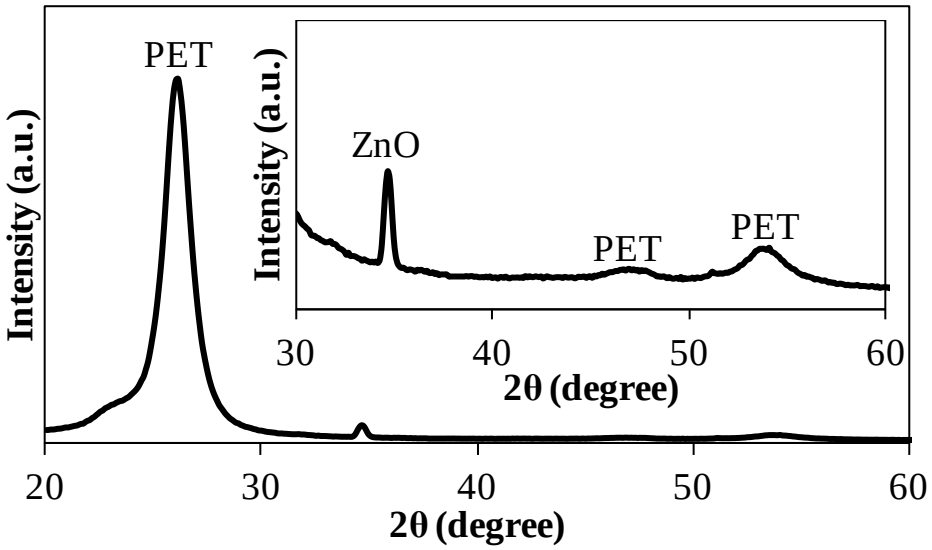

Figure 4.4. XRD pattern of ZnO nanowires grown on PET substrate.

Room temperature PL was carried out on ZnO nanowires synthesized on PET substrate (Fig. 4.5) to study the optical properties. A near band-edge emission peak at 380 nm and a broad yellow-orange emission band centered at 600 nm were observed in the sample. The yellow-orange emission defect peak observed in the spectrum is most likely due to the presence of intraband defect levels including oxygen vacancies.[30]

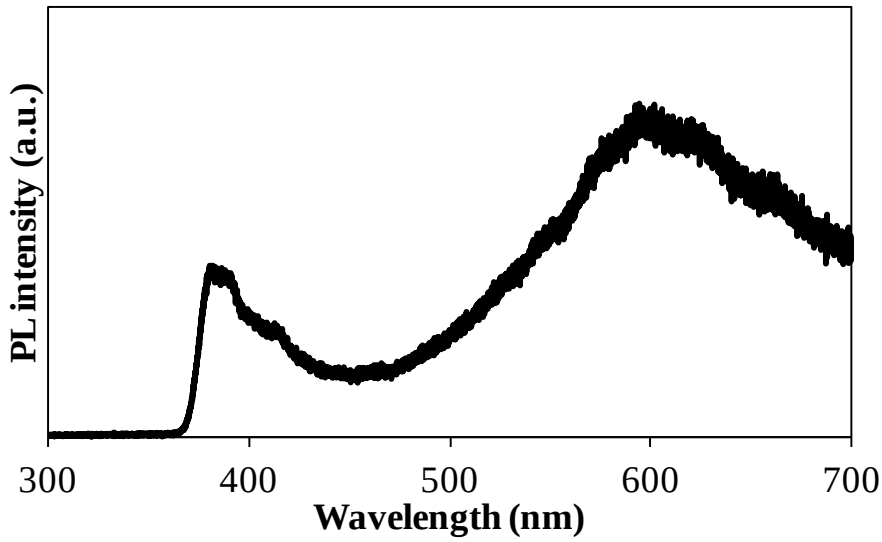

Figure 4.5. Room temperature photoluminescence of ZnO nanowires.

Room temperature UV-vis transmittance spectra of the samples were recorded by a UV-VIS-NIR spectrophotometer to determine the transparency of the synthesized products. Transmittance measurements were carried out on plain PET, PET synthesized with ZnO nanowires and ZnO nanowires sputtered with Pt (Pt-ZnO nanowires). As shown in Fig. 4.6, the transmittance of the plain PET is about 80 to 85 % in the visible range (400 to 700 nm) and ultraviolet (UV) light of wavelength less than 306 nm is absorbed by the PET.[31] With the growth of ZnO nanowires on the PET, the transmittance in the visible range decreased slightly to 70-85 %. The decrease in transmittance can be attributed to the absorbance and scattering of visible light by the nanowires. It is also noted that the transmittance of UV light was red-shifted to 360 nm instead of 306 nm observed in the PET substrate. The absorption of UV light of 360 nm and less is due to the presence of the ZnO nanowires.[32] After sputtering 10 nm of Pt on the ZnO nanowires synthesized on PET, the transmittance in the visible range decreased to 39 to 65 % and UV light of wavelength 360 nm and below is still absorbed due to the ZnO nanowires. A transmittance level of at least 39 % in the visible range for the Pt-ZnO nanowires on PET substrate makes it viable as a semi-transparent flexible gas sensing device. The inset of Fig. 4.6 shows the plain PET substrate (black outline), PET with ZnO nanowires (red outline) and nanowires sputtered with 10 nm Pt (extreme right) against a coloured background. It is evident from the photograph that the first two samples are highly transparent and the appearance of the coloured picture is hardly affected by the overlying samples. However, the deposition of Pt on the nanowires resulted in a slight "blackish" tint in the sample, causing it to be semi-transparent.

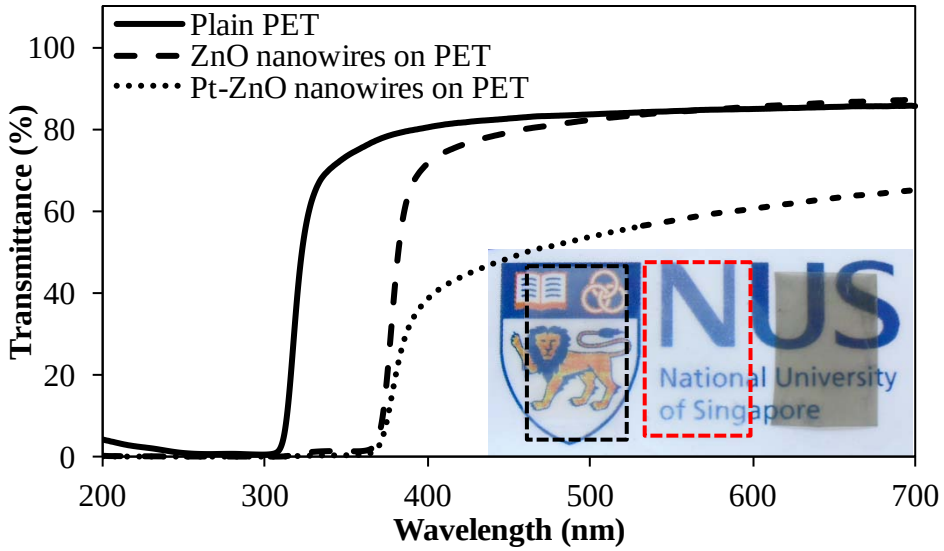

Figure 4.6. UV-vis transmittance spectra of plain PET substrate and ZnO nanowires synthesized on PET. Inset is a photograph illustrating the transparency of plain PET (black outline), ZnO nanowires grown on PET (red outline) and ZnO nanowires sputtered with Pt on PET.

4.3.2 Hydrogen gas sensing of intrinsic ZnO nanowires

The plain ZnO sample was used for H_2 sensing at various concentrations of H_2 from 400 parts-per-million (ppm) down to 50 ppm. The sample was placed in the gas sensing chamber where CDA was first flowed in to simulate ambient environment. After 100 s, the environment in the chamber was changed to a H_2 environment by flowing H_2 gas together with CDA into the chamber. The concentration of H_2 ambient in the sensing chamber can be controlled by varying the flowrate of H_2 gas and CDA. The sample was kept in the H_2 ambient for 200 s, after which the ambient was switched back to air by terminating the flow of H_2 but continuing the flow of CDA into the chamber to flush out the H_2 gas. The entire gas sensing experiment was carried out at room temperature without any heating of the ZnO nanowires sample. The sensitivity of the gas sensor is calculated by:

$$\text{Sensitivity (\%)} = |(R_{gas} - R_{air})/R_{air}| \times 100\% \quad (4.1)$$

where R_{gas} is the lowest resistance of the sample in the H_2 ambient and R_{air} is the resistance of the sample in air ambient just before introduction of H_2 gas.[33] From Fig. 4.7, it can be seen that the sensitivity of the sensor increases with the concentration of H_2. The sensitivity recorded is 38 % at 400 ppm, 27 % at 300 ppm, 26 % at 200 ppm, 20 % at 100 ppm and 7% at 50 ppm. When the ambient was changed to air after 300 s, the plain ZnO sample recovers back towards its original state but the recovery took more than 200 s.

When ZnO nanowires are left in air ambient, oxygen molecules adsorb onto the surface of the nanowires. These adsorbed molecules draw electrons from the nanowires, resulting in an electron-depleted space charge region at the surface of the nanowires. This is indicated by a reduced conductivity of the ZnO sample.

$$O_2(g) + e^- \rightarrow O_2^-(ad) \qquad (4.2)$$

However, when ZnO is exposed to H_2, the H_2 molecules would react with the surface adsorbed oxygen and remove it, releasing the electrons back to the conduction band of the ZnO surface. This in turn leads to an increase in the conductivity of the nanowires.[34-37]

$$2H_2(g) + O_2^-(ad) \rightarrow 2H_2O + e^- \qquad (4.3)$$

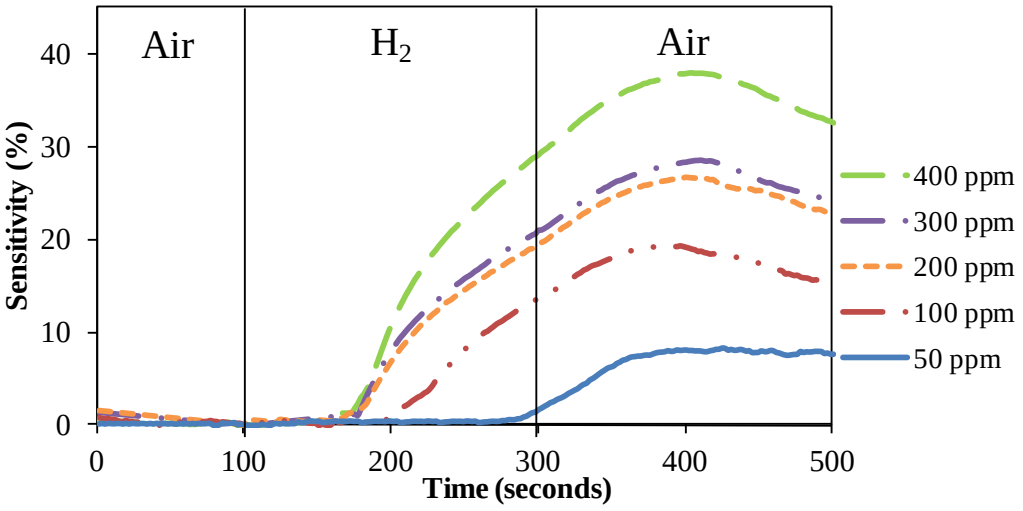

Figure 4.7. H_2 gas sensing results of intrinsic nanowires.

4.3.3 Hydrogen gas sensing of Pt-decorated ZnO nanowires

The addition of metal catalysts such as Pt and palladium (Pd) to metal oxide gas sensors is known to enhance the sensitivity due to the spillover effect.[38-42] For example, Wang et. al reported on the use of Pd nanoparticles for catalytic dissociation of H_2 to atomic H on ZnO.[40] The ZnO nanowires synthesized in this work were sputtered with Pt to enhance the gas sensing performance, and the presence of Pt on the ZnO nanowires was verified by EDX analysis as shown in Fig. 4.8. Prominent peaks of Zn $L\alpha_{1,2}$ at 1.01 keV, Zn $K\alpha_1$ at 8.63 keV and Zn $K\beta_1$ at 9.57 keV were clearly observed due to the ZnO nanowires. The Pt peak at 2.05 keV ascribed to the $M\alpha_1$ transition was also detected from the Pt deposited on the nanowires.

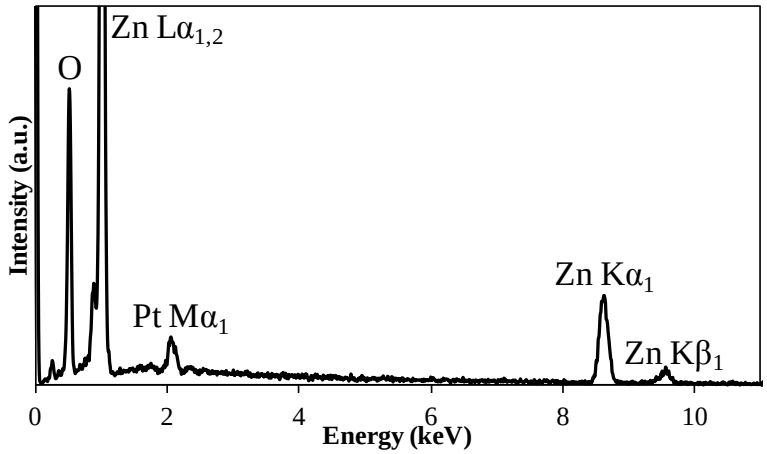

Figure 4.8. EDX spectrum of ZnO nanowires sputtered with Pt.

From the H_2 gas sensing results shown in Fig. 4.9, it is evident that the presence of Pt on the nanowires has improved the gas sensing performance. The Pt decorated device exhibited an enhanced sensitivity of 46 % at 400 ppm, 43 % at 300 ppm, 34 % at 200 ppm, 22 % at 100 ppm and 9 % at 50 ppm of H_2 gas. The sample also showed faster recovery than the plain ZnO nanowires sample with the sample displaying full recovery in 200 s after being exposed to 50 ppm of H_2 gas. The reason for the improved sensing performance is due to the dissociation of the H_2 molecules

by the Pt catalysts on the surface of the nanowires, allowing the sensing process to be more efficient.[41]

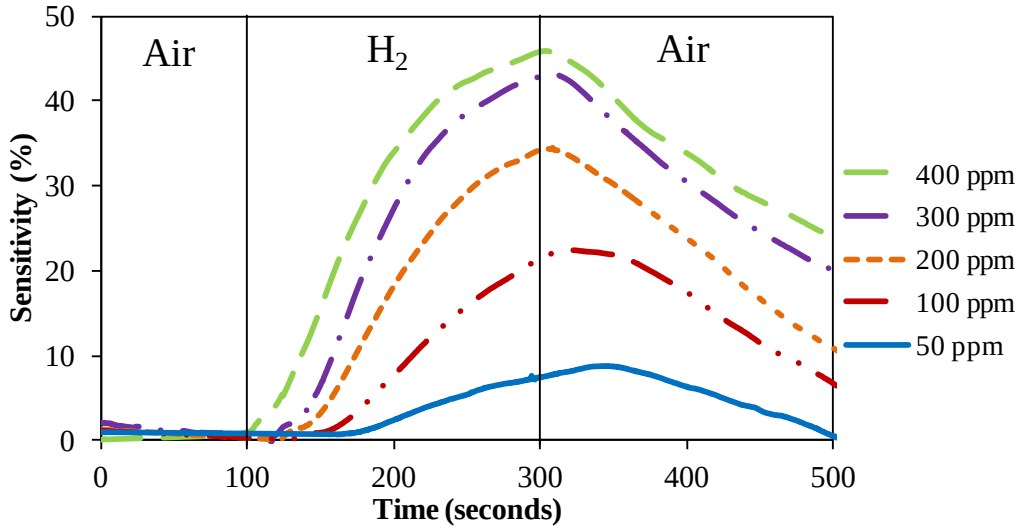

Figure 4.9. H_2 gas sensing results of ZnO nanowires sputtered with Pt.

The enhancement of gas sensing performance in the Pt decorated ZnO nanowires can be explained by the spillover model.[42] The spillover effect is reported to be most active in Pt and Pd metal catalysts. A schematic diagram of the spillover of H_2 from the catalyst onto the ZnO surface is shown in Fig. 4.10.

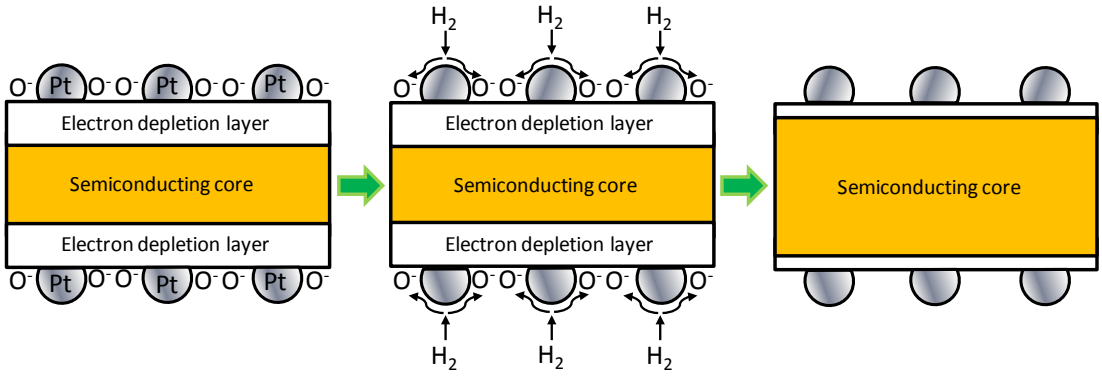

Figure 4.10. Schematic diagram on the spillover of H_2 from the catalyst onto the ZnO surface.

When the Pt decorated ZnO sample is placed in air ambient, O_2 molecules are dissociated on the metal catalyst and adsorbed on the surface of the nanowires.

$$2Pt + O_2 \rightarrow 2Pt{\cdot}O \qquad (4.4)$$

The adsorbed oxygen species then draw electrons from the conduction band of the nanowires to form O^-, resulting in an electron-depleted space charge region at the surface. This causes a decrease in the conductivity of the nanowires.

$$O + e^- \rightarrow O^- \tag{4.5}$$

When the ambient is switched to H_2, the incoming H_2 gas molecules are dissociated into atomic H on the metal catalyst surface.

$$2Pt + H_2 \rightarrow 2Pt{\cdot}H \tag{4.6}$$

The dissociated hydrogen then spillover or migrate onto the ZnO surface and enter a steady state reaction with the adsorbed O^-. The H atoms react with the surface adsorbed oxygen and remove it, releasing the electrons back to the conduction band of the ZnO surface and cause the conductivity of the nanowires to increase.

$$2H + O^- \rightarrow H_2O + e^- \tag{4.7}$$

The role of the Pt catalyst is to catalytically activate the dissociation of H_2 molecules into H atoms, which then spillover and adsorb onto the ZnO nanowires surface to facilitate the reduction of the adsorbed oxygen species, thereby increasing the rate of the redox reaction. This causes the Pt decorated ZnO nanowires to have a more efficient and sensitive H_2 sensing process compared to the pristine ZnO nanowires.

4.3.4 Discussion of hydrogen gas sensing results

A summary of the sensitivity of the plain ZnO and the Pt decorated samples for all concentrations of H_2 is shown in Table 4.1. There is an average of 30% improvement in the sensitivities of the samples sputtered with Pt compared to the plain ZnO samples.

Table 4.1. Sensitivity of pristine sample and Pt decorated sample.

H_2 concentration (ppm)	**Sensitivity (%)**	
	Plain ZnO	**Pt decorated ZnO**
400	38	46
300	28	43
200	26	34
100	19	22
50	7	9

However, besides sensitivity, the addition of Pt on the nanowires also improved the response time of the gas sensors as shown in Table 4.2. The response time is defined as the time taken to reach 90 % of the change in resistance after H_2 is introduced into the sensing chamber. For the plain ZnO nanowires, the response time was 240 s or more for all the H_2 concentrations, giving an average response time of 249 s. For the sample sputtered with Pt, the average response time was 171 s, with faster response times recorded at higher H_2 concentrations. The response time for Pt decorated samples decreased by 31 % on average as compared to plain ZnO samples. The catalytic dissociation of H_2 molecules by the Pt metal has produced a more responsive gas sensor with a more efficient sensing mechanism, resulting in a higher sensitivity towards H_2 gas.

The recovery time was also enhanced for the Pt decorated ZnO nanowires compared to plain ZnO sample. After switching from H_2 ambient (50 ppm) to air ambient, the Pt decorated sample has almost recovered fully after 200 s, while the plain ZnO sample only showed a small amount of recovery in the same amount of time. The improved recovery can be attributed to the catalytic dissociation of O_2 molecules on the Pt catalyst when the H_2 flow was terminated and the environment in the sensing chamber was reverted back to air.

Table 4.2. Response time of samples for various H_2 gas concentrations.

Concentration of H_2 (ppm)	Response time (seconds)	
	Plain	Pt decorated
400	240	140
300	248	153
200	246	163
100	241	188
50	271	213

4.3.5 Hydrogen gas sensing of bent sample

The ZnO nanowires on PET substrate is capable of functioning as a flexible gas sensor. The mechanical and electrical integrity of the nanostructures on PET substrate is demonstrated in Fig. 4.11. A photograph of a bent sample is shown in Fig. 4.11a. The sample is easily bendable and no cracking or delamination of the film of ZnO nanowires was observed when the sample was bent. Fig. 4.11b shows a schematic diagram illustrating the bending of the sample and θ is used to quantify the degree of bending. The PET with ZnO nanowires was bent repeatedly from θ = 90° to θ = 5° for 100 times and no cracking or delamination was observed in the film of ZnO nanowires after repeated bending. The excellent adhesion of the ZnO nanowires on the PET substrate under repeated bending indicates that the film of ZnO nanowires is mechanically robust, thus making it suitable for flexible device applications. The current-voltage (I-V) plots of the sample in flat and bent states are shown in Fig. 4.11c. An ohmic I-V curve was obtained for a flat sample. When the sample was bent, ohmic conductivity was still observed, indicating good electrical conductivity of the nanowires even in the bent state. The current exhibited a slight increase during tensile bending and a slight decrease during compressive bending. The slight change in current could be explained by the tighter or looser packing of the ZnO nanowires during bending, resulting in increased or decreased amounts of contact between the

nanowires network. When the sample was returned to the flat state, the conductivity recovers close to the original state. This shows that the electrical characteristics of the ZnO nanowires can be maintained despite bending.

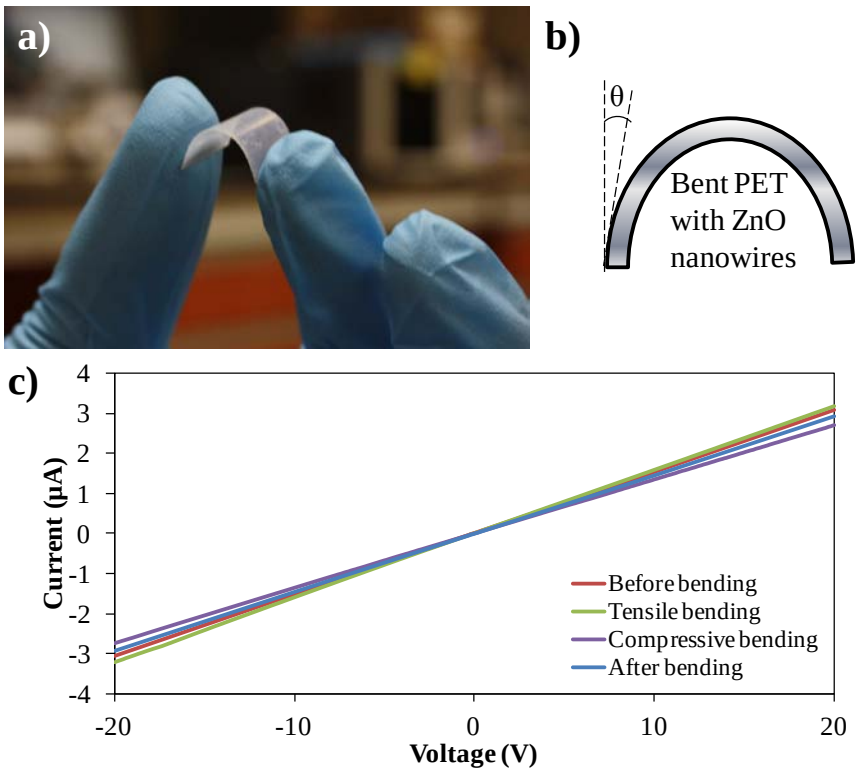

Figure 4.11. (a) Photograph of a bent sample. (b) Schematic diagram showing bending of the sample. (c) Current-voltage plot of flat and bent sample.

The H_2 gas sensing measurements were then carried out on a bent Pt decorated sample to determine how the sensing performance compares to that of a flat sample. Fig. 4.12 shows the result of the H_2 sensing results of the sample in both the flat and bent states. The bent sample exhibited a sensitivity of 45 % towards 400 ppm of H_2 gas which is similar to that of the flat sample. The response time of the bent sample was 142 s which is also about the same as that of the flat sample. From the results of the bent sample, it can be seen that the gas sensing performance is consistent and reproducible even when the sample is bent, thus indicating that the gas sensor can still be used effectively in a bent state.

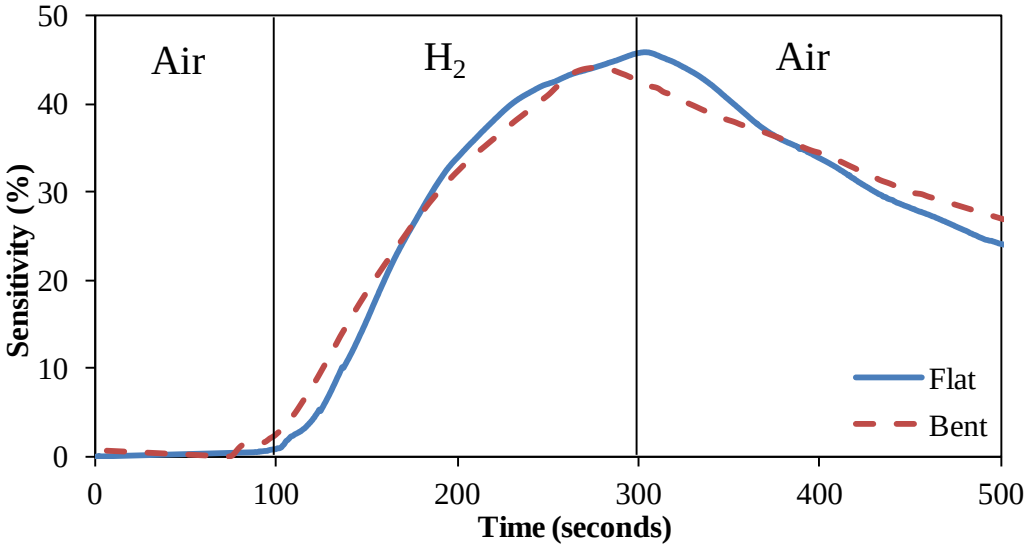

Figure 4.12. H_2 sensing at 400 ppm with flat and bent sample.

4.4 Conclusions

Uniform and high density growth of ZnO nanowires was successfully accomplished via hydrothermal method with good adhesion on flexible PET substrate. Enhanced sensitivity of H_2 sensing down to 50 ppm concentration at room temperature was demonstrated with Pt metal catalyst on ZnO nanowires. The response time and recovery time were substantially reduced by the presence of Pt on the ZnO nanowires, due to the catalytic dissociation of H_2 molecules on the Pt catalyst. When the sample was tested in a bent state, it was capable of producing sensing performance on par with a flat sample. On the whole, the Pt decorated ZnO nanowires gas sensor showed an improvement in the gas sensing performance and the nanowires grown on PET substrate proved to be robust and feasible for flexible device applications.

References

1 Basic research needs to assure a secure energy future, A Report from the Basic Energy Sciences Advisory Committee, February 2003. Available from (http://www.sc.doe.gov/bes/besac/Basic_Research_Needs_To_Assure_A_Secure_Energy_Future_FEB2003.pdf).

2 Kang B S, Heo Y W, Tien L C, Norton D P, Ren F, Gila B P and Pearton S J 2005 *Appl. Phys. A* **80** 1029

3 Favier F, Walter E C, Zach M P, Benter T and Penner R M 2001 *Science* **293** 2227

4 Yi G C, Wang C and Park W 2005 *Semicond. Sci. Technol.* **20** S22

5 Verhelst S and Sierens R 2001 *Int. J. Hydrogen Energy* **26** 987

6 Bevenot X, Trouillet A, Veillas C, Gagnaire H and Clement M 2000 *Sens. Actuators B Chem.* **67** 57

7 Rout C S, Raju A R, Govindaraj A and Rao C N R 2006 *Solid State Commun.* **138** (3) 136

8 Wang Y D, Ma C L, Wu X H, Sun X A and Li H D 2002 *Sens. Actuators B Chem.* **85** 270

9 Liao L, Lu H B, Li J C, He H, Wang D F, Fu D J, Liu C and Zhang W F 2007 *J. Phys. Chem. C* **111** (5) 1900

10 Keem K, Kim H, Kim G T, Lee J S, Min B, Cho K, Sung M Y and Kim S 2004 *Appl. Phys. Lett.* **84** 4376

11 Huang M H, Mao S, Feick H, Yan H, Wu Y, Kind H, Weber E, Russo R and Yang P 2001 *Science* **292** 1897

12 Ra H W, Choi K S, Kim J H, Hahn Y B and Im Y H 2008 *Small* **4** 1105

13 Kong J, Franklin N R, Zhou C, Chapline M G, Peng S, Cho K and Dai H 2000 *Science* **287** 622

14 Cui Y and Lieber C M 2001 *Science* **291** 851

15 Yonenaga I 2001 *Phys. B: Condens. Matter* **308–310** 1150

16 Zhou J, Gu Y, Fei P, Mai W, Gao Y, Yang R, Bao G and Wang Z L, 2008 *Nano Lett.* **8** 3035

17 Woo C S, Lim C H, Cho C W, Park B, Ju H, Min D H, Lee C J and Lee S B 2007 *Microelectron. Eng.* **84** 1610

18 Ibañez F J and Zamborini F P 2006 *Langmuir* **22** 9789

19 Zhao Z, Sevryugina Y, Carpenter M A, Welch D and Xia H 2004 *Anal. Chem.* **76** 6321

20 McAlpine M C, Ahmad H, Wang D W and Heath J R 2007 *Nature Mater.* **6** 379

21 Wan Q, Li Q H, Chen Y J, Wang T H, He X L, Li J P and Lin C L 2004 *Appl. Phys. Lett.* **84** 3654

22 Modi A, Koratkar N, Lass E, Wei B and Ajayan P M 2003 *Nature* **424** 171

23 Park W I, Yi G C, Kim J W and Park S M 2003 *Appl. Phys. Lett.* **82** 4358

24 Goldberger J, Hochbaum A I, Fan R and Yang P 2006 *Nano Lett.* **6** 973

25 Penza M, Cassano G, Rossi R, Alvisi M, Rizzo A, Signore M A, Dikonimos T, Serra E and Giorgi R 2007 *Appl. Phys. Lett.* **90** 173123

26 Tien L C, Wang H T, Kang B S, Ren F, Sadik P W, Norton D P, Pearton S J and Lin J 2005 *Electrochemical and Solid-State Letters,* **8 (**9) G230

27 Galoppini E, Rochford J, Chen H, Saraf G, Lu Y, Hagfeldt A and Boschloo G 2006 *J. Phys. Chem. B* **110** 16159

28 Du Pasquier A, Chen H and Lu Y 2006 *Appl. Phys. Lett.* **89** 253513

29 Shankar K S and Raychaudhuri A K 2005 *Mater. Sci. Eng. C* **25** 738

30 Mensah S L, Kayastha V K, Ivanov I N, Geohegan D B and Yap Y K 2007 *Appl. Phys. Lett.* **90** 113108

31 Fechine G J M, Rabello M S, Souto Maior R M and Catalani L H 2004 *Polymer* **45** 2303

32 Unalan H E, Hiralal P, Rupesinghe N, Dalal S, Milne W I and Amaratunga G A J 2008 *Nanotechnology* **19** 255608

33 Lim Z H, Chia Z X, Kevin M, Wong A S W and Ho G W 2010 *Sens. Actuators B* **151** 121

34 Lupan O, Ursaki V V, Chai G, Chow L, Emelchenko G A, Tiginyanu I M, Gruzintsev A N and Redkin A N 2010 *Sens. Actuators B* **144** 56

35 Wang J X, Sun X W, Yang Y, Huang H, Lee Y C, Tan O K and Vayssieres L 2006 *Nanotechnology* **17** 4995

36 Barsan N and Weidar U 2001 *J. Electroceram.* **7** 143

37 Lundstrom I 1981 *Sens. Actuators* **1** 403

38 Suzuki T, Yamazaki T, Takahashi K and Yokoi T 1989 *Journal of Materials Science Letters* **24** 2127

39 Kuriki S, Sano K, Konishi H and Matsumoto G 1987 *Electronics and Communications in Japan (Part II: Electronics)* **70** 54

40 Wang H T, Kang B S, Ren F, Tien L C, Sadik P W, Norton D P, Pearton S J and Lin J 2005 *Appl. Phys. Lett.* **86** 243503

41 Wang H T, Kang B S, Ren F, Tien L C, Sadik P W, Norton D P, Pearton S J and Lin J 2005 *Appl. Phys. A* **81** 1117

42 Morrison S R 1987 *Sensors and Actuators* **12** 425

Chapter 5 Patterned Growth of ZnO nanowires for Field Emission Applications

In this chapter, ZnO nanowires are synthesized on polyethylene terephthalate (PET) substrates by hydrothermal method for field emission application. Laser writing lithography is used to pattern the growth of the nanowires into periodic arrays of bundles with varying inter-bundle distances to investigate the screening effect on field emission properties. The visibly-transparent nanowires on PET substrate are also tested for superior structural integrity with ohmic electro-conductivity in a highly bent state.

5.1 Introduction

The excellent exhibition of unique electrical, optoelectronic and photochemical properties of ZnO nanomaterials has gained tremendous research interest in recent years. In particular, one dimensional (1D) ZnO nanostructures have been explored for applications such as ultraviolet (UV) laser,[1] field emission displays,[2] gas sensors[3] and dye sensitized solar cells.[4] Among these applications, the use of 1D ZnO nanostructures as electron field emitters is very appealing due to their high mechanical stability, high aspect ratio, and negative electron affinity in various vacuum environments.[5,6] Although carbon nanotubes (CNTs) have attracted much attention due to their low turn-on fields and large emission currents,[7] oxide emitters are more stable in harsh environment and controllable in electrical properties.[8] The field emission (FE) performance of various ZnO nanostructures such as nanowires,[9] nanoneedles,[10] 3D assembly of nanoneedles[11] have been reported and the results are comparable or superior to those of CNTs. Therefore, ZnO nanostructure is an appropriate alternative to CNT for field emission devices.

With the proliferation of portable display, communication and various state-of-the-art electronics products, the development of high performance transparent and conformal electronic devices is an important research focus. The accessibility to optically transparent and mechanically flexible electronic platforms is the essence of the next-generation display technologies, including other 'see-through' and conformable devices.[12] Polymer substrates such as PET are well-suited for use in conformal and highly transparent displays and organic electronic devices due to its light-weight, low cost, transparency, flexibility, thermal resistance and mechanical strength. As demonstrated in Chapter 4, the hydrothermal method can be used to synthesize ZnO nanowires on PET substrates because this route of synthesis is simple, low temperature, cost-effective and easily scalable to large area features. The controllable growth of 1D nanostructures on plastic substrates would open the door to many applications, including field emitting devices.

Besides growing ZnO nanowires on plastic substrates, there is also effort in trying to arrange them in a regular pattern to further enhance device performance. The patterning of the nanowires on substrates can be controlled by various techniques including optical lithography, soft lithography etc. However, conventional optical lithography patterning of nanostructures is commonly carried out on rigid substrates since it cannot be easily applied to a polymeric substrate. For the case of optical lithography, the challenges lie in the focusing of light on a transparent and non-rigid substrate, and the reactivity of the polymeric substrate towards the organic solvent used in the lithography process. Accordingly, the integration of vertically aligned nanostructures with patterned growth on a flexible platform for a transparent, conformable, shock-proof and lightweight product is a technological challenge. There are reported works that demonstrate patterning of micro/nanostructures on flexible

substrate mainly through soft lithography eg. microcontact and nanoimprinting.[13-15] Kang *et al.* and Wang *et al.* have presented patterned growth of ZnO nanorods that combines the direct patterning of ZnO nanoparticle seeds via microcontact printing on flexible PET and Si substrate respectively. Although the soft lithography patterning of nanostructures on flexible substrates have been demonstrated, to the best of our knowledge, there is limited work reported on laser writing based lithography towards patterned growth of nanowires on flexible substrate.

In this chapter, ZnO nanowires are grown on PET substrates for field emission purposes. The growth is patterned by laser writing into periodic arrays of circular bundles with varying inter-bundle distances to investigate the influence of screening effect on field emission properties. This will aid in the fabrication of field emitters with the optimal inter-bundle distance for best field emission performance. The visibly-transparent nanowires on the flexible PET substrate are also tested for superior mechanical integrity with electro-conductivity in a highly bent state.

5.2 Experimental procedures

The PET substrates were cleaned by sonicating in isopropyl alcohol (IPA) (5 min) followed by ethanol (5 min). The substrates were then blown dry with a stream of nitrogen gas. A thin layer (10 nm) of gold (Au) was then sputtered onto the PET substrates followed by a ZnO seed layer of 6 nm via radio-frequency (RF) magnetron sputtering (Denton Vacuum Discovery 18 system) at room temperature. The purpose of the Au layer is to provide a conductive layer for the application of an electric field across the nanowires to induce the emission of electrons. However, it has been noted that the patterning and growth of nanowires on PET is also feasible without the Au layer. The thickness of the Au layer was kept to 10 nm so that it is thin enough to allow some degree of transparency of the device but still ensure good conductivity

through the metal layer. The seeded substrates were then placed into a 25 ml growth solution containing 0.05 g of poly(ethyleneimine) solution (PEI), 25 mM of zinc nitrate hexahydrate and 25 mM of hexamethylenetetramine (HMT) in de-ionized (DI) water. The growth process was carried out at 90 °C for 6 hours. A thin strip of Au at the edge of the PET substrate was left bare without any ZnO seed layer to allow good contact between the copper tape and the Au layer during the field emission measurements.

For patterned growth of ZnO nanowires on PET, the seeded substrates were first spincoated with AZ1518 photoresist and soft-baked on a hotplate at 100 °C for 60 s. The photoresist was then patterned with a laser of wavelength 405 nm and laser power of 66 mW. The pattern is a periodic array of circles (1 μm in diameter) and a spacing of 2 μm to 8 μm between the adjacent circles. Development of the exposed photoresist was carried out in a diluted AZ developer (AZ 400K developer : DI water = 1 : 4) for 20 s, then rinsed in DI water and dried with a stream of compressed air. The patterned substrates were then placed in the same growth solution as mentioned above at 90 °C for 3 hrs. The fabrication steps are illustrated in the schematic diagram in Fig. 5.1.

Various characterization techniques were carried out on the samples. Scanning electron microscopy (SEM, JEOL FEG JSM 7001F) characterized the morphology of the synthesized products while the crystalline structure of the ZnO nanowires was analyzed using X-ray diffraction (XRD, Philips X-ray diffractometer equipped with graphite-monochromated Cu Kα radiation at $\lambda = 1.54$ Å) and transmission electron microscopy (TEM, Phillips FEG CM300). Room temperature optical properties were measured by the UV-VIS-NIR spectrophotometer (UV-vis, Shimadzu UV-3600) and micro-photoluminescence (PL) with He-Cd laser at 325 nm. The electrical properties

of the samples were studied by current-voltage (I-V) measurements carried out using a Keithley 4200-SCS semiconductor characterization system. The field emission properties of the synthesized products were measured using a two-parallel-plate configuration in a vacuum chamber with a base pressure of 2 x 10^{-6} Torr at room temperature. The sample was adhered onto a Cu substrate cathode by copper double-sided tape while indium tin oxide (ITO) glass was used as the anode. The distance between the electrodes was kept at 70 μm by a PET spacer with a circular hole of 0.28 cm^2. A Keithley 237 high voltage source measurement unit (SMU) was used to apply a voltage of 0-1100 V between the two electrodes and to measure the emission current at the same time.

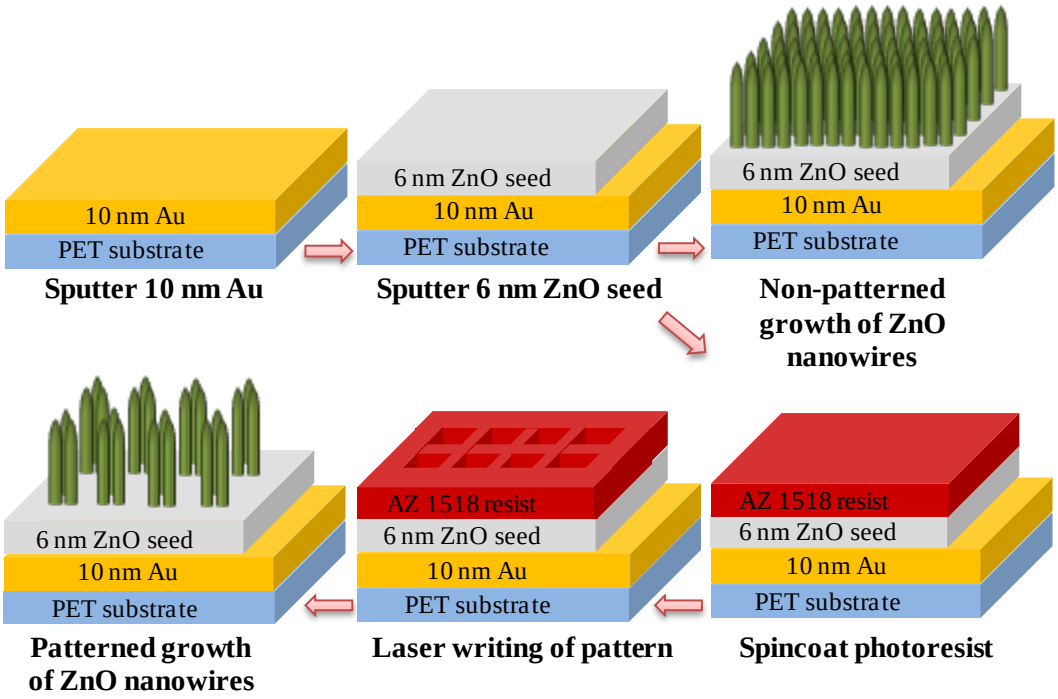

Figure 5.1. The schematic approach of growing ZnO nanowires on PET substrate with and without patterning.

5.3 Results and discussion

5.3.1 Materials characterization

The morphology of the synthesized ZnO nanowires on PET without patterning is shown in Fig. 5.2. The plan view SEM image (Fig. 5.2a) of the sample shows dense,

uniform growth across the entire substrate, while the 30° tilted view (Fig. 5.2b) shows well-aligned nanowires. The length of the nanowires is 2 μm with an average diameter of 50 nm. Structural characterization of the hydrothermally grown nanowires was carried out via TEM. Fig. 5.2c shows that the nanowires have a uniform diameter with a smooth surface. The HRTEM image (Fig. 5.2d) shows lattice fringes of an interplanar spacing ~ 0.52 nm, confirming that the ZnO nanowires are single crystalline with a preferential growth in the [0001] direction.[16] The corresponding selected area electron diffraction (SAED) pattern (inset of Fig. 5.2d) of the ZnO nanowire also implies that its growth is in the *c*-axis direction and suggests good crystallinity of the nanowire.

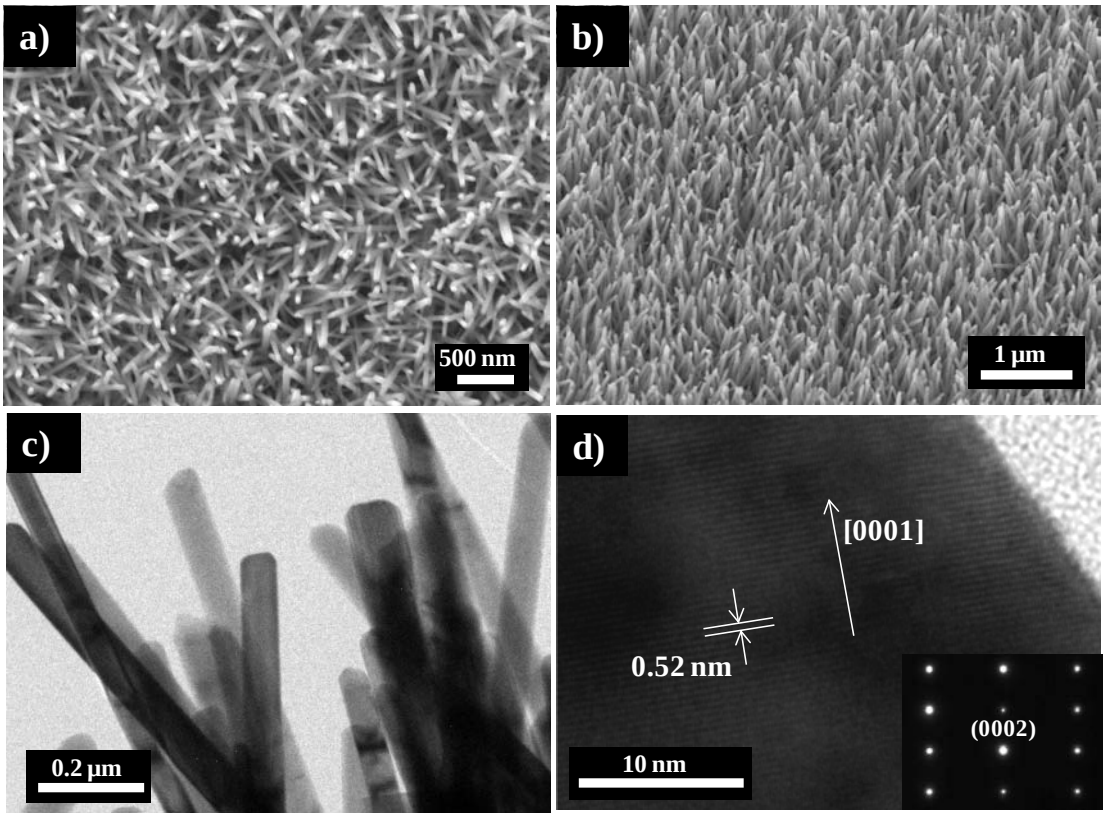

Figure 5.2. (a) Plan view SEM images of ZnO nanowires grown on PET substrate. (b) 30° titled view of ZnO nanowires. (c) TEM image of ZnO nanowires, and (d) HRTEM image of a nanowire showing the [0001] growth direction. The inset shows the corresponding selected area electron diffraction (SAED) pattern of the ZnO nanowire.

XRD spectra of Au-coated PET (Au/PET) and ZnO nanowires grown on Au-coated PET (ZnO nanowires/Au/PET) were obtained and shown in Fig. 5.3a. Both spectra have a very pronounced PET (100) peak at 26°. Other PET peaks present were the PET (12-2) at 46.6°and PET (2-30) at 52.9° (JCPDS Card No. 00-060-0989) as shown in the inset of Fig. 5.3a which shows a magnified view of the spectra in the range 30° to 60°. The only Au peak observed was the Au (111) peak at 38.2° (JCPDS Card No. 01-071-3755) which was found on both samples. The only peak that was present in the ZnO nanowires spectrum but not the Au/PET spectrum is the prominent ZnO (002) peak which can be well indexed to the hexagonal phase of ZnO with lattice constants a = 0.3242 nm and c = 0.5194 nm (JCPDS Card No. 79-0205). The (002) peak indicates preferential growth in the [0001] direction, and also the good crystal structure and phase purity of the product.

Room temperature PL was carried out on ZnO nanowires synthesized on both Si and PET substrates (Fig. 5.3b) to study the optical properties. Si substrate was included in this study to determine if the substrate affects the PL spectrum of the nanowires. A near band-edge emission peak at 380 nm and a broad yellow-orange emission band centered at 600 nm were observed in both samples. The yellow-orange emission defect peak observed in the spectra is most likely due to the presence of intraband defect levels including oxygen vacancies.[17] The intensities of the two peaks were noted to be similar for both samples. This similarity suggests that the optical properties of the ZnO nanowires grown on PET substrate do not differ from those grown on rigid substrates such as Si. Room temperature UV-vis transmittance spectra of the samples were recorded by a UV-VIS-NIR spectrophotometer to determine the transparency of the synthesized products.

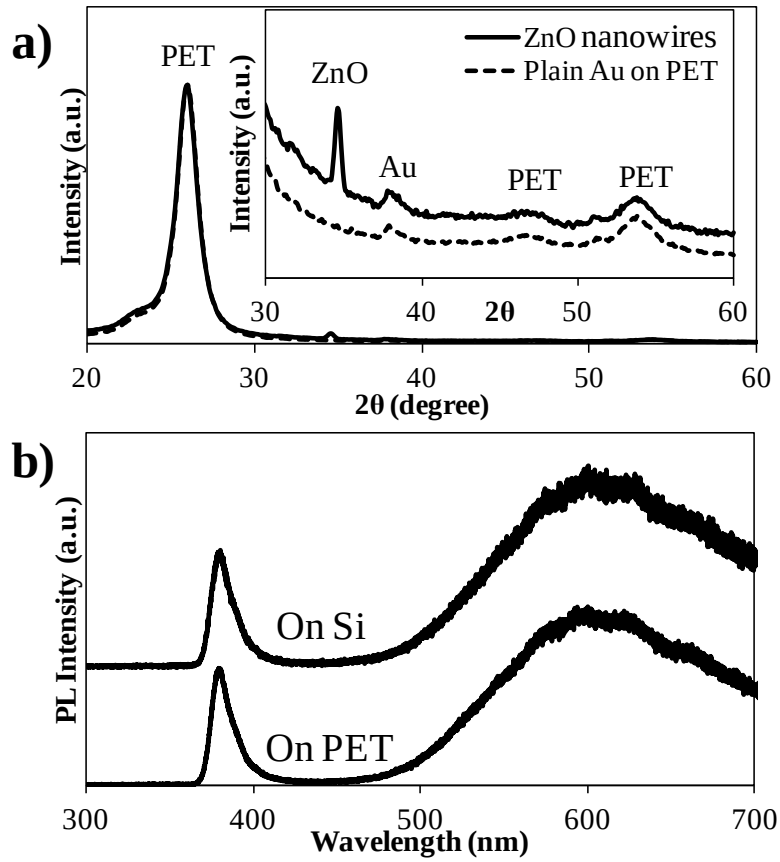

Figure 5.3. (a) XRD spectra of plain Au on PET and ZnO nanowires on Au-coated PET. (b) PL spectra of ZnO nanowires on Si and Au-coated PET substrates.

Transmittance measurements were carried out on plain PET, PET sputtered with 10 nm of Au (Au/PET) and ZnO nanowires grown on ZnO seeded Au/PET (ZnO nanowires/Au/PET). As shown in Fig. 5.4a, the transmittance of the plain PET is about 80 to 85 % in the visible range (400 to 700 nm) and ultraviolet (UV) light of wavelength less than 306 nm is absorbed by the PET.[18] After sputtering 10 nm Au on the PET, the transmittance level in the visible range exhibited a peak value of 57 % at 531 nm which decreased to 48 % at 700 nm. The pronounced absorption increasing at longer wavelengths could be attributed to the surface plasmon resonance of the Au layer.[19] UV light of wavelength less than 306 nm was also absorbed due to the PET substrate. The spectrum of the sample after synthesis of ZnO nanowires exhibited a peak transmittance of 58 % at 553 nm which was red-shifted from that of the Au/PET sample. The transmittance of wavelengths from 553 to 700 nm is quite similar to that

of the Au/PET sample. However, the transmittance of UV light was red-shifted to 360 nm instead of 306 nm observed in the previous two samples. The absorption of UV light of 360 nm and less is due to the presence of the ZnO nanowires.[20] A transmittance level of at least 40 % in the visible range for the PET substrate with ZnO nanowires makes it viable as a semi-transparent flexible field emission device. An optical photograph illustrating the transparency of the samples is shown in Fig. 5.4b. The plain PET substrate (outlined in red) is placed on the extreme left, the Au/PET sample is placed in the center and the Au/PET with ZnO nanowires is positioned on the right. From the photograph, it can be seen that despite having a darker shade, the ZnO nanowires sample is fairly "see through" or transparent.

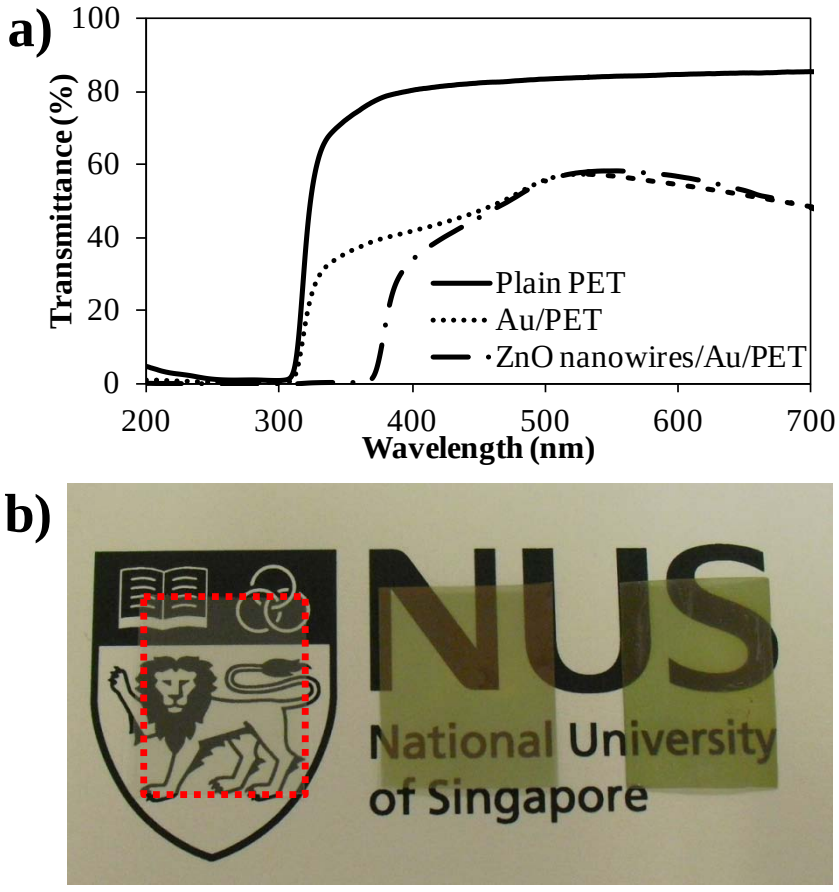

Figure 5.4. (a) UV-vis transmittance spectrum and (b) photograph showing transparency of (from left to right): plain PET substrate (red-dotted outline), sputtered Au (10 nm) on PET and ZnO nanowires synthesized on Au/PET.

Besides transparency, the mechanical and electrical integrity of the nanostructures on PET substrate is also of great concern. The homemade setup in Fig. 5.5a was used to bend the sample by various degree of bending quantified by the angle θ as shown in the Fig. 5.5a. From the SEM image (Fig. 5.5b inset), it can be observed that the film of ZnO nanowires grown on the PET substrate exhibits great flexibility and it conforms to the bending of the substrate without any delamination of the nanowires film from the substrate. SEM imaging was used to observe the state of the ZnO nanowires before and after cycling the bending of the sample at θ = 5° and 90° for 100 times. The SEM images showed that no cracks and delaminations were formed in the film of ZnO nanowires after bending it repeatedly many times. The excellent adhesion of the ZnO nanowires on the PET substrate under severe bending conditions suggests that the ZnO nanowires maintained mechanical robustness, thus making them suitable for flexible devices applications.

I-V measurement of the sample was carried out at various stages of bending to determine if the bending affects the electrical characteristics of the ZnO nanowires. From the I-V curves in Fig. 5.6 which show the results for compressive and tensile stress at θ = 5° respectively, it can be seen that the bending did not affect the ZnO nanowires. There was a slight decrease in current during and after compressive bending and slight increase in the current during and after tensile bending. This can be explained by the tighter packing of the ZnO nanowires during the tensile bending, resulting in more contacts between the nanowires network. When the bending is removed, conductivity falls and stabilises close to the original state. The structural integrity and electrical characteristics were maintained after the electromechanical testing.

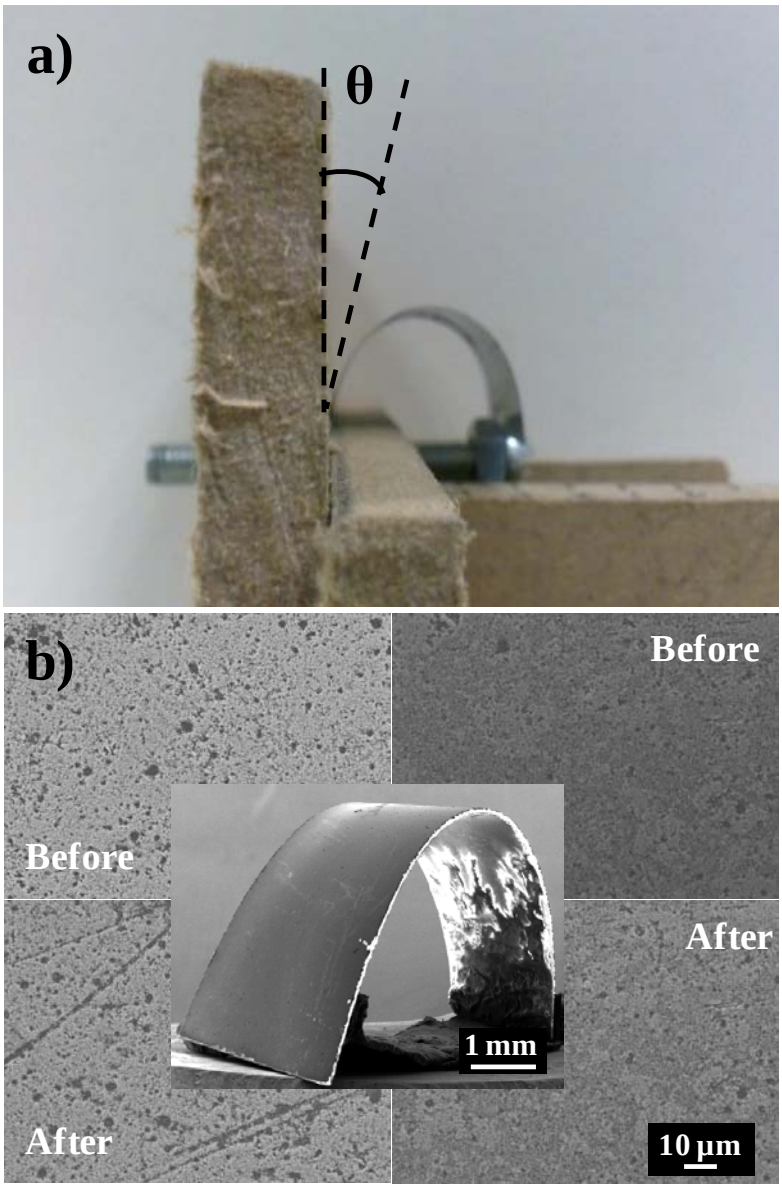

Figure 5.5. (a) Illustration of degree of bending. (b) SEM images of two areas on the sample before bending and after bending. Inset shows a bent flexible ZnO nanowires sample.

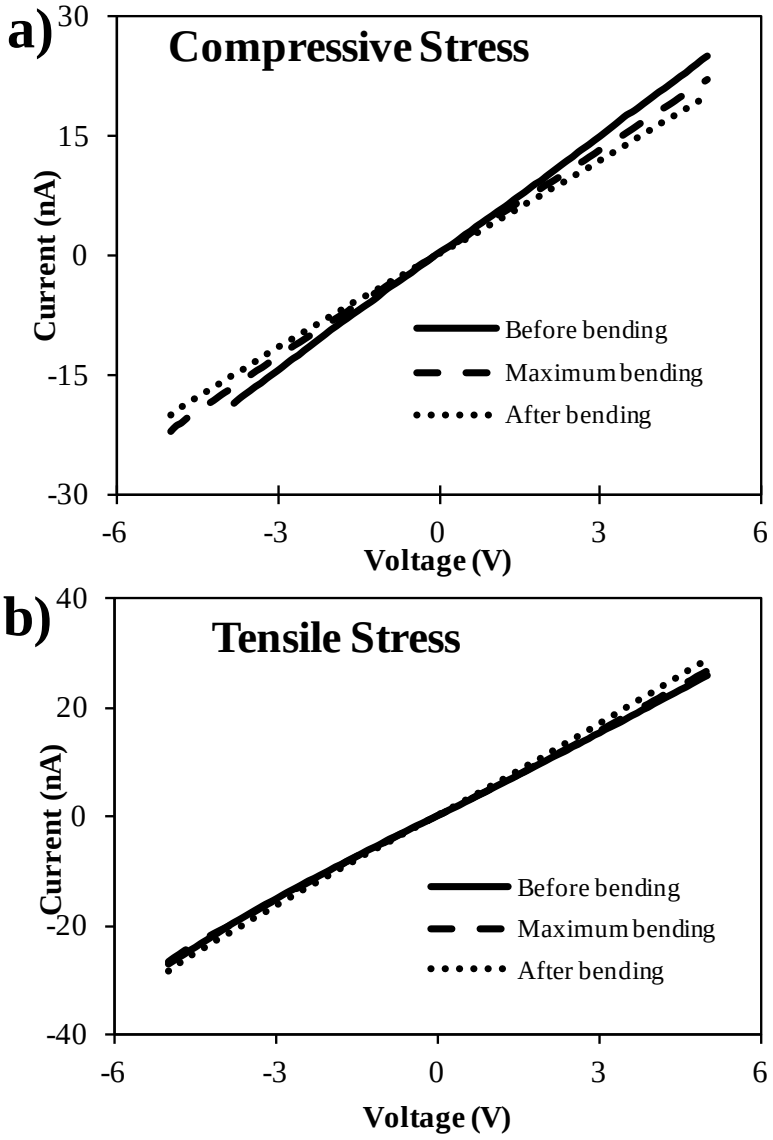

Figure 5.6. I-V curve of sample undergoing (a) compressive stress and (b) tensile stress. Maximum bending refers to $\theta = 5°$.

5.3.2 Patterned growth of ZnO nanowires

Patterned growth of ZnO nanowires on PET was achieved via direct laser writing. The periodic array of 1 μm circles with an array spacing of 2, 4, 6 and 8 μm was created by laser writing on the ZnO seeded Au/PET substrate spincoated with photoresist. Selective growth of ZnO nanowires was observed to occur only in the 1 μm circles and no nanowires were found in the spaces in-between. Patterned growth of ZnO nanowires in array patterns with varying array spacing is shown in Fig. 5.7.

The ZnO nanowires grew in bundles in the circles due to the difference between the size of the circular pattern and the diameter of the nanowires. The size of the circle is 1 μm while the diameter of the ZnO nanowires is between 80 to 600 nm. As a result, several nanowires could grow in the circle simultaneously, resulting in bundled growth of ZnO nanowires. Some of the nanowires were also observed to grow at a tilted angle relative to the substrate. This is because the height of the nanowires (2 to 3.3 μm) is greater than the thickness of the photoresist (1 to 2 μm). During the initial growth of the nanowires, they were confined to grow in the upward direction by the photoresist. However, when the nanowires grow above the photoresist, the growth direction is no longer confined to the circle, and this caused some of the nanowires to grow at a tilted angle, giving the bundles a flower-like appearance.

The average diameter and height of the ZnO nanowires are detailed in Table 5.1 together with the corresponding array spacing. It was observed that as the array spacing increases, the diameter and height of the nanowires tend to increase. This is because as the array spacing increases, the number of nucleation sites on the substrate decreases, thus more reactants are available per nucleation site.[21] As a result, the nanowires became larger in diameter and also grew taller.

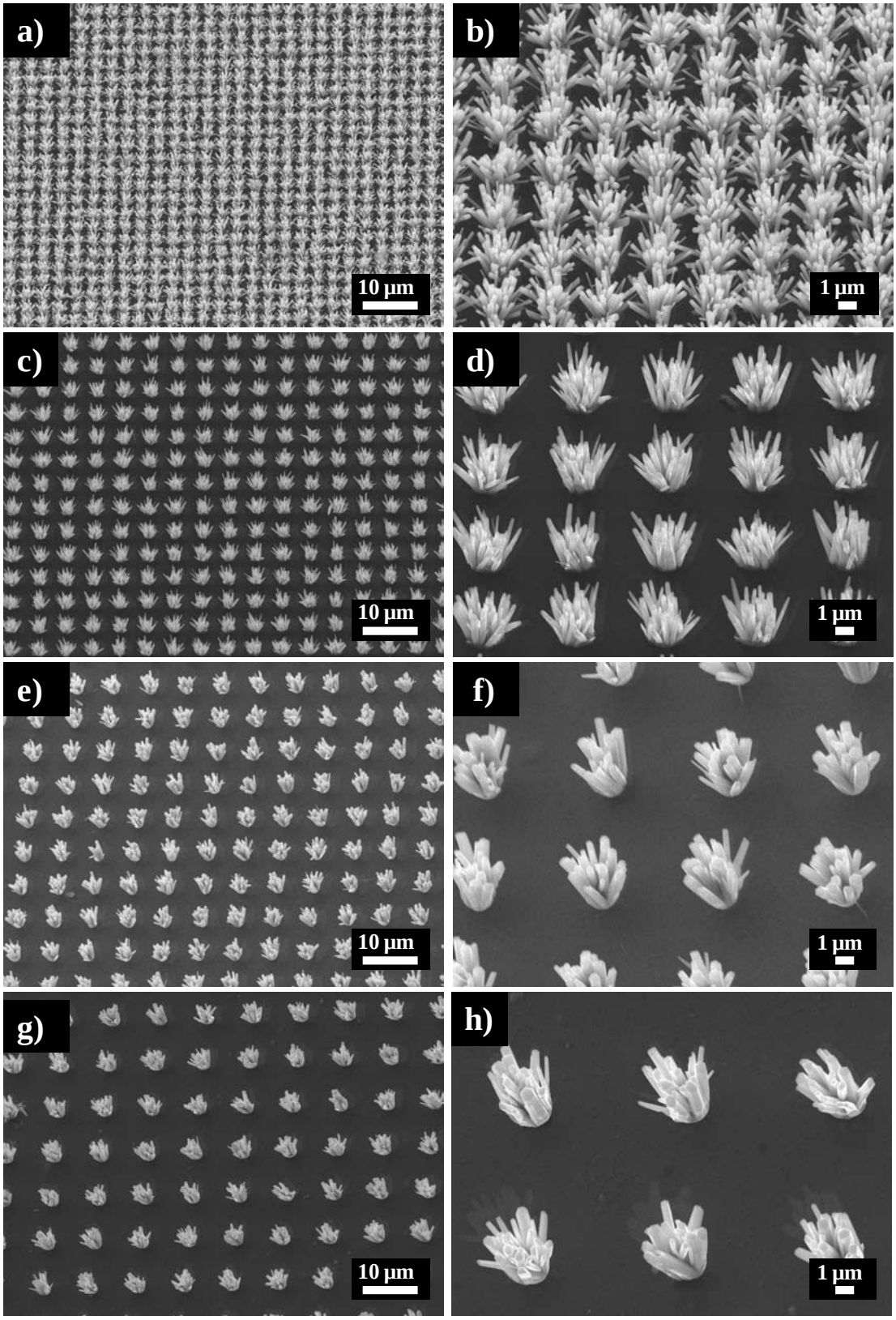

Figure 5.7. SEM images (30° tilted view) of magnification 1500x and 5000x for patterned growth with array spacing of (a, b) 2 µm, (c, d) 4 µm, (e, f) 6 µm, and (g, h) 8 µm.

5.3.3 Field emission measurements and screening effect

Field emission measurements were carried out on the patterned ZnO nanowires on PET substrate. The field emission characteristics are presented in Fig. 5.8 and Table 5.1. Fig. 5.8 shows the field emission measurement setup for the PET samples. It is noted that the spacer used is a PET sheet of thickness 70 µm. Strips of copper tapes were pasted on the ITO surface of the anode and the Au layer of the cathode, which were subsequently connected to the Keithley 237 high voltage SMU.

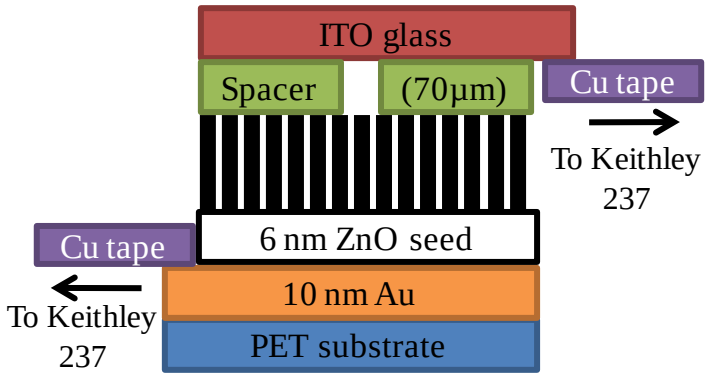

Figure 5.8. Schematic diagram of flexible field emitter device.

The plot of the emission current density J versus the applied field E from the samples is shown in Fig. 5.9a. The turn-on field (E_{on}) is defined as the applied electric field required to produce an emission current density of 0.1 µA/cm^2. The E_{on} of the ZnO nanowires grown on the non-patterned PET is 8.2 V/µm. The emission current–voltage characteristics were analyzed using the Fowler–Nordheim (F-N) equation:[22]

$$J = \frac{A\beta^2 E^2}{\emptyset} exp\left(\frac{-B\emptyset^{3/2}}{\beta E}\right) \quad (5.1)$$

where J is the current density (A/cm^2), E the applied field (V/µm), Φ the work function of the field emitter (5.3 eV for ZnO),[23] β the field enhancement factor, A = 1.56 x 10^{-10} (AeVV^{-2}) , and B = 6.83×10^9 Vm^{-1} eV$^{-3/2}$. The dependency of the emission current density on the applied field, plotted in ln(J/E^2) versus 1/E relationship is shown in Fig. 5.9b, where the slope of the fitted straight line corresponds to $B\Phi^{3/2}/\beta$. This indicates that the field emission of the ZnO nanowires

follows the F-N relationship,[24] and that the field emission mechanism is a barrier tunneling quantum mechanical process. From the F-N plots in Fig. 5.9b, the calculated field enhancement factor β for the non-patterned sample is 542. Despite the high aspect ratio of 80, the field emission property is poorer than that of the sample with 2 μm array spacing. The 2 μm sample has an aspect ratio of only 26 but produced an E_{on} of 5.7 V/μm and β of 2449. The difference in field emission performance is due to the screening effect from the dense growth of nanowires.[25] Although the non-patterned sample has a high aspect ratio, the closely pack nanowires resulted in a much stronger screening effect between the emitters compared to the 2 μm sample where the nanowires were spaced further apart. The sample with 4 μm array spacing has an aspect ratio of 24, which is similar to the 2 μm sample, but it shows a poorer field emission result with E_{on} of 7.7 V/μm and β of 986. The larger array spacing can aid in further reduction of the screening effect, but it also results in much fewer emitters available for field emission, hence, resulting in poorer field emission performance. The field emission performance deteriorates further for the 6 and 8 μm array spacing samples due to the lower aspect ratio and decreasing number of emitters available on the samples.

From Fig. 5.10, it is observed that the sample with array spacing of 2 μm produced the lowest turn-on field of 5.7 V/μm and the highest field enhancement factor β of 2449 among the samples investigated. This can be attributed to the screening effect being the weakest when the bundles are spaced 2 μm apart. The spacing/height ratio is 0.8 for the 2 μm sample as shown in Table 5.1. Several papers investigating the screening effect of 1-dimensional (1D) field emitters such as ZnO[26,27] and carbon nanotubes (CNTs)[28-30] suggested that the ideal spacing/height ratio which gives the least screening effect is between 1 to 2. The trend observed in

the field emission results of the samples with various array spacing shows that a spacing/height ratio of 0.8 (2 μm spacing sample) is ideal for minimal screening effect and gives the best field emission properties. This value of 0.8 is lower than the 1 to 2 reported in literature. However, it was also observed that the field emission result shows some degradation when the spacing/height ratio is increased to 1.5 (4 μm spacing sample). This suggests that a better field emission performance could be obtained if the spacing/height ratio is adjusted to a value between 0.8 and 1.5.

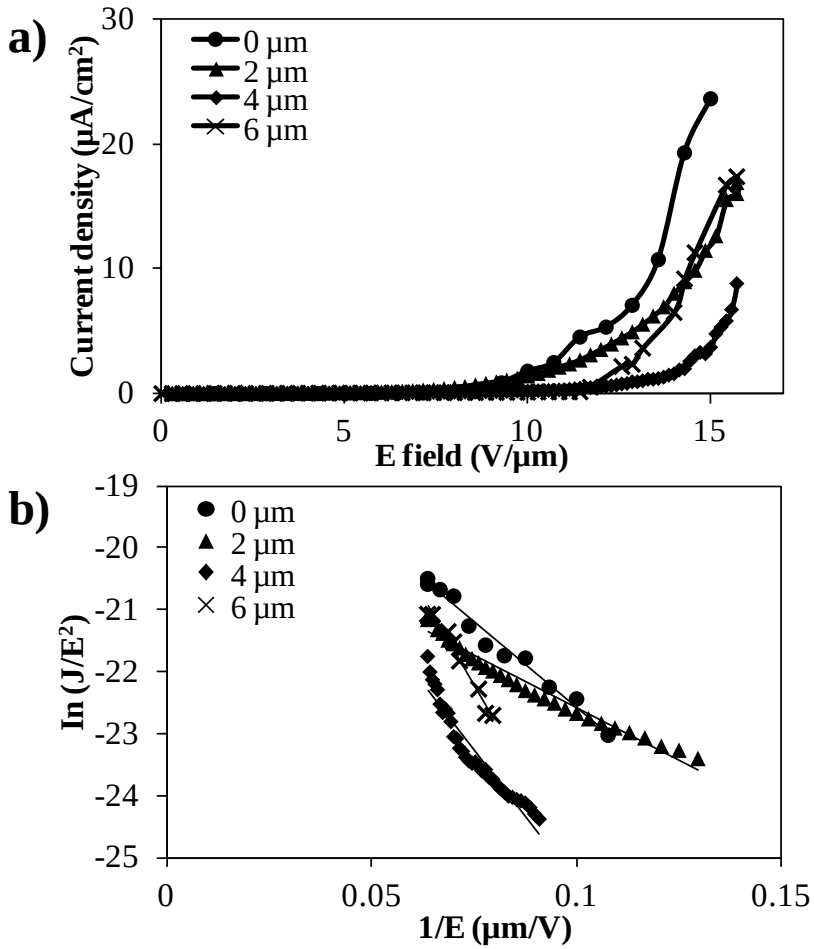

Figure 5.9. (a) J-E and (b) F–N plots of the ZnO nanowires with various array spacing.

Table 5.1: Summary of nanowires height and diameter, and field emission properties of non-patterned and patterned growth with various array spacing.

Array spacing (μm)	Average height (μm)	Average diameter (μm)	Aspect ratio	E_{on} (V/μm)	Calculated β	Spacing /height
0	2.0	0.05	80	8.5	1512	0.0
2	2.5	0.19	26	5.7	2449	0.8
4	2.7	0.22	24	7.7	986	1.5
6	3.1	0.55	11	9.1	742	1.9
8	3.3	0.66	10	Nil	Nil	2.3

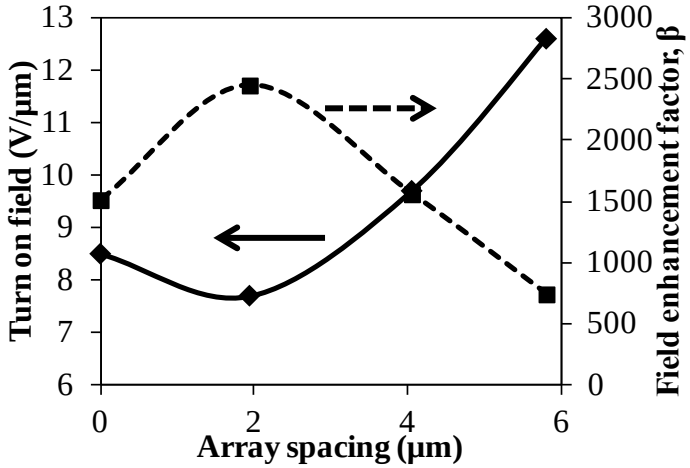

Figure 5.10. Relationship between array spacing and turn-on field and β.

5.4 Conclusions

ZnO nanowires were synthesized by the low temperature hydrothermal method on flexible PET substrates. The nanowires are single crystalline with wurtzite hexagonal phase and are preferentially oriented in the [0001] direction. The growth was patterned into periodic arrays of nanowire bundles by laser writing lithography. The inter-bundle distance was varied to investigate the screening effect on the field emission properties. The sample with an array spacing of 2 μm produced the lowest turn-on field of 5.7 V/μm and the highest field enhancement factor β of 2449 among the samples investigated. This can be attributed to the screening effect being the

weakest when the bundles are spaced 2 μm apart. The optically transparent nanowires on a PET platform exhibited superior structural integrity with ohmic electro-conductivity in a bent state. The feasibility of optically transparent and mechanically flexible electronic device could open the door to next-generation ‘see-through’, shock-proof and conformable display technologies.

References

1 Huang M H, Mao S, Feick H, Yan H, Wu Y, Kind H, Weber E, Russo R and Yang P 2001 *Science* **292** 1897

2 Gautam U K, Panchakarla L S, Dierre B, Fang X, Bando Y, Sekiguchi T, Govindaraj A, Golberg D and Rao C N 2009 *Adv. Funct. Mater.* **19** 131

3 Zeng Y, Zhang T, Wang L, Wang R, Fu W and Yang H 2009 *J. Phys. Chem. C* **113** 3442

4 Xu C, Shin P, Cao L and Gao D 2010 *J. Phys. Chem. C* **114** 125

5 Suh H W, Kim G Y, Jung Y S and Choi W K 2005 *J. Appl. Phys.* **97** 044305

6 Stoehr M, Juillaguet S, Kyaw T M and Wen J G 2005 *Phys. Status Solidi C* **2** 1314

7 Bonard J M, Kind H, Stockli T and Nilsson L O 2001 *Solid-State Electron.* **45** 893

8 Lee C J, Lee T J, Lyu S C, Zhang Y, Ruh H and Lee H J 2002 *Appl. Phys. Lett.* **81** 3648

9 Zhao Q, Xu X Y, Song X F, Zhang X Z, Yu D P, Li C P and Guo L 2006 *Appl. Phys. Lett.* **88** 033102

10 Yang H Y, Lau S P, Yu S F, Huang L, Tanemura M, Tanaka J, Okita T and Hng H H 2005 *Nanotechnology* **16** 1300

11 Maiti U N, Sen A, Mitra M K and Chattopadhyay K K 2010 *J. Nanosci. Nanotechnol.* **10** 4341

12 Ju S H, Facchetti A, Xuan Y, Liu J, Ishikawa F, Ye P D, Zhou C W, Marks T J and Janes D B 2007 *Nature Nanotech.* **2** 378

13 Kang H W, Lee J H, Yeo J, Rho Y S, Hwang J O, Kim S O, Hong S, Ko S H, Lee P, Han S Y and Sung H J 2011 *J. Phys. Chem. C* **115** 11435

14 Wang C H, Wong A S W and Ho G W 2007 *Langmuir*. **23** 11960

15 Kang M G and Guo L J 2007 *J. Vac. Sci. Technol. B* **25** 2637

16 Ku C H and Wu J J 2006 *J. Phys. Chem. B* **110** 12981

17 Mensah S L, Kayastha V K, Ivanov I N, Geohegan D B and Yap Y K 2007 *Appl. Phys. Lett.* **90** 113108

18 Fechine G J M, Rabello M S, Souto Maior R M and Catalani L H 2004 *Polymer* **45** 2303

19 Siegel J, Lyutakov O, Rybka V, Kolská Z and Švorčík V 2011 *Nanoscale Res. Lett.* **6** 96

20 Unalan H E, Hiralal P, Rupesinghe N, Dalal S, Milne W I and Amaratunga G A J 2008 *Nanotechnology* **19** 255608

21 Yang H S, Lee J S, Bae S M and Hwang J H 2009 *Curr. Appl. Phys.* **9** 797

22 Hughes W L and Wang Z L 2005 *Appl. Phys. Lett.* **86** 043106

23 Minami T, Miyata T and Yamamoto T 1998 *Surf. Coat. Technol.* **108** 583

24 Zhao Q, Zhang H Z, Zhu Y W, Feng S Q, Sun X C, Xu J and Yu D P 2005 *Appl. Phys. Lett.* **86** 203115

25 Qian X M, Liu H B, Guo Y B, Song Y L and Li Y L 2008 *Nanoscale Res. Lett.* **3** 303

26 Lee J H, Chung Y W, Hon M H and Leu I C 2009 *Appl. Phys. A* **97** 403

27 Li C, Yang Y, Sun X W, Lei W, Zhang X B, Wang B P, Wang J X, Tay B K, Ye J D, Lo G Q and Kwong D L 2007 *Nanotechnology* **18** 135604

28 Bonard J M, Weiss N, Kind H, Stöckli T, Forró L, Kern K and Châtelain A 2001 *Adv. Mater.* **13** 184

29 Nilsson L, Groening O, Emmenegger C, Kuettel O, Schaller E and Schlapbach L, Kind H, Bonard J M and Kern K 2000 *Appl. Phys. Lett.* **76** 2071

30 Suh J S, Jeong K S, Lee J S and Han I 2002 *Appl. Phys. Lett.* **80** 2392

Chapter 6 Conclusions and Future Directions

In this chapter, a summary of the findings in this doctoral dissertation, together with a few concluding remarks highlighting the implications of the findings, is first given. The chapter then ends with several recommendations for extension of the works reported in this thesis in possible future research directions.

6.1 Conclusions

ZnO films and nanowires were synthesized by the low temperature, low cost, scalable and substrate-independent hydrothermal method. The growth parameters were varied and the effect on the morphology and properties of the nanostructures were studied. ZnO films were grown on c-sapphire substrates and variation of the precursor concentration, trisodium citrate concentration and growth duration was carried out. It was observed that as the precursor concentration increased, both the diameter and height of the nanowires also increased, and began to approach a film-like morphology at a precursor concentration of 100 mM. Trisodium citrate was added to aid the formation of a smooth film and 0.97 mM of trisodium citrate was the minimum amount needed for the film to fully coalesce in a growth solution containing 50 mM of zinc nitrate. However, the height of the film was noted to decrease with increasing amounts of trisodium citrate. This is because the citrate anions adhere to the positively charged Zn-terminated (0001) plane, thus reducing the growth rate in the upward direction. When the growth duration was increased, the height of the film also increased, and a time of 1.5 hrs was sufficient for the film to fully coalesce.

ZnO nanowires were grown on rigid (Si) and flexible (PET) substrates by the hydrothermal method. Variation of the precursor concentration, amount of PEI added and growth duration was carried out. The results revealed that increasing the precursor concentration caused both the diameter and height of the nanowires to

increase. However, when the concentration was 100 mM, the large diameter nanowires were observed to coalesce and form a film-like morphology. Adding PEI to the solution helped to reduce the diameter of the nanowires but when more than 0.5 g of PEI was added, no growth occurred on the substrates. The height of the nanowires increased when the growth duration was increased, but the diameter stayed within the range of 30 to 40 nm.

The hydrothermal films and nanowires were then subjected to ammonia plasma treatment without deliberate heating to modify the electrical properties of the nanostructures towards p-type conductivity. The treatment duration of the ZnO films was varied from 30 to 180 s to investigate how the plasma treatment duration affects the characteristics of the film. The electrical properties of the ZnO films were observed to be effectively tuned by surface modification using NH_3 plasma and the XRD results showed that the plasma treatment did not degrade the crystallinity of the films. The reduction in the amount of defects present in the film as observed in the room temperature PL spectrum was due to the incorporation of the N-H complexes from the NH_3 plasma into the films. Hall measurements of the modified ZnO films revealed p-type conductivity with resistivity ranging from 0.57 to 95.52 Ω cm, carrier concentration ranging from 1.13 X 10^{17} to 1.95 X 10^{18} cm^{-3} and mobility from 0.3 to 5.67 cm^2/Vs. This change from n-type to p-type conductivity can be attributed to the incorporation of N-related radicals from the NH_3 plasma into the surface of the ZnO films. The ZnO film treated with NH_3 plasma for 90 s displayed the best electrical properties with the lowest resistivity (0.57 Ω cm), highest mobility (5.67 cm^2/Vs) and carrier concentration (1.95 X 10^{18} cm^{-3}). The presence of a N1s peak in the XPS spectrum of the surface modified ZnO film indicated the successful incorporation of

N complexes into the film. The results obtained shows that NH_3 plasma treatment is a feasible way to tune the electrical conductivity of ZnO films.

When the ZnO nanowires were treated with ammonia plasma, the nanowires also exhibited p-type conductivity with an average resistivity of 6.04 Ω cm, average carrier concentration of 1.42 X 10^{17} cm^{-3} and average mobility of 7.34 cm^2/Vs. The N1s peak was also detected in the XPS spectrum and it was deconvoluted to show the presence of N-Zn and N-H bonds in the treated nanowires, indicating the incorporation of N into the ZnO nanowires to form acceptors. Significant quenching of the visible emission in the room temperature PL spectrum was observed after NH_3 plasma modification, indicating a reduction in the amount of defects in the nanowires due to the occupation of N-H atom pairs on the defect sites. The sample was characterized by room temperature PL again after 14 months and the PL spectrum still displayed similar optical characteristic of a strong UV emission with insignificant defect peak. Low temperature PL carried out at 5 K revealed an acceptor bound exciton peak at 372.5 nm which indicated the presence of acceptors in the treated nanowires. The I-V curve of the treated nanowires on a n-type ZnO layer showed an apparent rectifying behaviour of the p-n junction and the turn-on voltage appeared at ~ 3.3 V under forward bias. Hydrogen gas sensors were fabricated from the plasma treated ZnO nanowires and they exhibited p-type behaviour towards hydrogen gas of various concentrations. The sensor showed a sensitivity of 15 % at 500 ppm of hydrogen and it increased to 27 % at a hydrogen concentration of 2500 ppm. The NH_3 modified nanowires were tested again after 14 months and the same p-type behaviour with no apparent degradation in the gas sensing performance was observed. C-V measurements carried out on the MOS capacitor fabricated from the NH_3 treated ZnO nanowires also revealed p-type conductivity.

Flexible hydrogen gas sensors and field emitters were then fabricated by synthesizing ZnO nanowires directly on PET substrates. The growth of the nanowires was uniform and dense with good adhesion on the flexible PET substrate. The hydrogen sensor was tested in hydrogen ambient of concentrations 50 to 400 ppm at room temperature, and the corresponding sensitivities obtained were 7 to 38 %. Pt catalyst was sputtered on the nanowires to enhance the sensing performance through catalytic decomposition of the hydrogen molecules. The Pt decorated samples showed improved sensitivities of 9 to 46 % corresponding to 50 to 400 ppm hydrogen ambient and also faster response and recovery. The gas sensor was still capable of sensing when it was bent and the performance was similar to that of a flat sample. The ZnO nanowires grown on PET substrate proved to be robust and feasible for flexible device applications.

The field emission properties of ZnO nanowires on PET substrates were also investigated. Laser writing on photoresist was used to pattern the growth of ZnO nanowires bundles in a periodic array with variation of the array spacing to investigate the influence of screening effect on the field emission properties. The array spacing was varied from 0 to 8 μm, and the screening effect was weakest when the array spacing was 2 μm. The corresponding spacing/height ratio at an array spacing of 2 μm was 0.8, and the nanowires exhibited a turn-on field of 5.7 V/μm and field enhancement factor β of 2449. The optically transparent nanowires on PET platform exhibited superior structural integrity with ohmic electro-conductivity in a bent state. The feasibility of such an optically transparent and mechanically flexible electronic device could open the door to next-generation ‘see-through’, shock-proof and conformable display technologies.

The ability to control the physical, chemical and electrical properties of the hydrothermally grown ZnO films and nanowires has been shown in this thesis. Together with the demonstration of flexible devices applications, the works featured in this thesis can help to bring this versatile material another step further in being practically applied in various sensory and electrical devices. Some of the work that lies ahead will be outlined briefly in the next section where we will provide some recommendations for future work.

6.2 Future directions

The ammonia plasma treatment on the hydrothermal ZnO nanowires and films proved to be successful in tuning the intrinsically n-type metal oxide into p-type conductivity. However, more characterizations can be carried out on the plasma treated samples to have a better understanding of the surface modification process. For example, Time of Flight Secondary Ion Mass Spectrometry (TOF-SIMS) can be used to identify the elements present in the plasma treated ZnO samples and also to obtain a depth profiling of the samples. This will give a clearer picture on the quantity of N-related complexes present in the treated ZnO samples and also how deep the complexes diffuse into the samples. Nuclear magnetic resonance (NMR) measurements can also be carried out on the plasma treated ZnO samples to detect the presence of nitrogen and determine the coordination arrangements and site occupancy within the different binding sites of the sample. It can clearly distinguish between different N environments and can effectively determine the relative amounts of N dopants incorporated.

To further prove the feasibility of this simple and versatile treatment method for p-type device applications, LEDs can be fabricated from the p-type ZnO nanowires and films. Electroluminescence (EL) measurements can then be carried out

on these LEDs to characterize the performance of the LEDs and the electrical properties of the p-type ZnO nanostructures.

The utility of the flexible gas sensors fabricated from the nanowires can be extended to sense gases other than hydrogen. For example, volatile organic compound (VOC) vapours are primary sources of environmental pollutants in indoor air and are considered seriously harmful to the human body.[1] There are notable correlations between VOC emissions and different kinds of cancers.[2] Therefore, it is important to develop sensors that can detect the vapours and provide timely information to the occupants regarding the presence and concentration of the VOCs. It will be ideal for the sensor to function at room temperature because some of the vapours could be combustible in air at elevated temperatures. It is also useful for the gas sensor to be flexible because it will allow easy placement of the sensor on any location and surface in the building. Other metal catalysts such as palladium (Pd) can also be deposited on the nanowires and the effect on the sensitivity towards various gases including hydrogen can be investigated.

A fully flexible field emission device or display can be fabricated from the ZnO nanowires on the Au-coated PET substrates. The top anode will be a piece of ITO coated PET instead of ITO coated glass. In this way, the ITO coating provides a transparent conducting layer on the PET where the emitted electrons can be collected and the flexible anode makes the entire device fully flexible. A layer of coloured phosphors will have to be coated on the ITO so that the bombardment of the emitted electrons will produce a coloured image. The field emission device can then become a lightweight electronic display device which is optically transparent, shock-proof and mechanically flexible.

References

1 Franciosoa L, Forleoa A, Taurinoa A M, Siciliano P, Lorenzelli L, Guarnieri V, Adami A and Agnusdei G 2008 *Sens. Actuators B Chem.* **134** 660

2 Boeglin M L, Wessels D and Henshel D 2006 *Environ Res.* **100** 242

Appendix A: List of Publications

A1: Journal publications

Work related to PhD research:

1. W. L. Ong, Q. X. Low, W. Huang, J. A. van Kan and G W Ho, "Patterned growth of vertically-aligned ZnO nanorods on a flexible platform for feasible transparent and conformable electronics applications", *J. Mater. Chem*. 22 (2012) 8518-8524.

2. W. L. Ong, C. Zhang and G. W. Ho, "Ammonia plasma modification towards a rapid and low temperature approach for tuning electrical conductivity of ZnO nanowires on flexible substrates", *Nanoscale* 3 (2011) 4206-4214.

3. W. L. Ong, X. D. Lim, C. H. Sow, C. Zhang and G. W. Ho, "Synthesis and field emission properties of well-aligned ZnO nanowires on buffer layer", *Thin Solid Films* 518 (2010) e139–e142.

Collaborative work:

1. M. Kevin, W. L. Ong, G. H. Lee and G. W. Ho, "Formation of hybrid structures: copper oxide nanocrystals templated on ultralong copper nanowires for open network sensing at room temperature", *Nanotechnology* 22 (2011) 235701.

2. W. X. Hu, Wiria, W. L. Ong and G. W. Ho, "High yield shape control of monodispersed Au nanostructures with 3D self-assembly ordering", *Colloids and Surfaces A: Physicochemical and Engineering Aspects* 358 (2010) 108-114.

3. S. C. Yeow, W. L. Ong, A. S. W. Wong and G. W. Ho, "Template-free synthesis and gas sensing properties of well-controlled porous tin oxide nanospheres", *Sensors and Actuators B* 143 (2009) 295–301.

A2: Conference papers

1. W. L. Ong and G. W. Ho, "Sensors based on microfluidically assembled ZnO nanowires", International Conference on Materials for Advanced Technologies (ICMAT) 2011, Singapore, Oral Presentation.

2. W. L. Ong and G. W. Ho, "Field emission performance of ZnO nanostructures of various morphologies", International Conference on Materials for Advanced Technologies (ICMAT) 2011, Singapore, Poster Presentation.

3. W. L. Ong and G. W. Ho, "Oxide nanostructures for field emission and nanoelectronics applications", 4th MRS-S Conference on Advanced Materials 2010, Poster Presentation.

4. W. L. Ong, K. Moe, G. H. Lee and G. W. Ho, "pH sensor based on thermally oxidized Cupric oxide nanowires, MRS-S Trilateral Conference on Advances in Nanoscience: Energy, Water and Healthcare 2010, Singapore, Poster Presentation.

5. W. L. Ong, A. S. W. Wong and G. W. Ho, "Structural and optical properties of well-aligned ZnO nanowires grown on buffer layer for photonic applications", International Conference on Materials for Advanced Technologies (ICMAT) 2009, Singapore, Oral Presentation.

6. W. L. Ong, X. D. Lim, C. H. Sow and G. W. Ho, "Synthesis and Field Emission Properties of Well-Aligned ZnO Nanowires on Buffer Layer", International Conference on Materials for Advanced Technologies (ICMAT) 2009, Singapore, Poster Presentation.